(1) The Relationship of Protein Expression and Cell Division, (2) 3D Imaging of Cells Using Digital Holography, and (3) General Chemistry Enrollment at University of Michigan

by

Rebecca L. Matz

A dissertation submitted in partial fulfillment
of the requirements for the degree of
Doctor of Philosophy
(Chemistry)
in the University of Michigan
2012

Doctoral Committee:

Professor Mark M. Banaszak Holl, Chair
Professor James R. Baker, Jr.
Professor Carol A. Fierke
Emeritus Professor Joseph S. Krajcik
Professor Bradford G. Orr

(District 203 photos)

NNHS chemistry teacher Lee Marek tests the composition of some mole-shaped cookies, with his class.

For my mom and dad

Acknowledgements

Above all, I am indebted to Mark Banaszak Holl for being a supportive, patient, and wise advisor. This work and my development as a scientist would not have been possible without him. His group is successful in large part because Mark obviously prioritizes his students and makes serious effort to be available and approachable. Amidst a multitude of important responsibilities, he always made time to meet with me, even for lengthy periods of time. This has not gone unnoticed. I also appreciate Mark's optimistic perspective; many times I brought "bad" data to his office only to have him show me the interesting scientific questions buried within. Mark has clearly had my best interests in mind throughout this journey, and I am thankful for his advocacy for women's and family issues at University of Michigan. I would be remiss if I didn't mention that Mark showed me how to eat lobster at a Gordon Conference in New Hampshire.

I'm thankful to Joe Krajcik for being my M.S. advisor in Education and for serving on my doctoral committee. Joe was an invaluable connection between the School of Education and the College of Literature, Sciences, and the Arts, and helped me learn the language of Education. Along with Joe Krajcik, Brian Coppola introduced me to the world of Chemistry Education. Having been in the right place at the right time, I benefitted from many years of Joe and Brian's labor in developing the M.S. program in Post-Secondary Science Education, the IDEA Institute, and the nascent faculty observation program in the Chemistry Department. With these two scholars, I learned how very difficult it is to do good educational research, and it was a privilege to learn from their years of experience and friendship.

I'm very grateful to Brad Orr for numerous helpful comments in the Friday morning group meetings, for serving on my doctoral committee, and for developing the

Nanobiology Certificate Program. Brad has brought a valuable perspective to this dissertation and has been unfailingly encouraging throughout the Ph.D. journey. I've enjoyed being a part of his partnership with Mark. Carol Fierke also served on my doctoral committee and offered helpful comments, suggestions, and perspective on these projects. Ed Rothman, formerly the Director of Michigan's Center for Statistical Consultation and Research, was indispensible as my unofficial statistics instructor. Ed was optimistic and helpful, and I always left our meetings feeling encouraged. In particular, I enjoyed Ed's wise stories about the limits of statistics.

I thank Jim Baker for serving on my doctoral committee and leading the development of the Michigan Nanotechnology Institute for Medicine and Biological Sciences (MNIMBS), which has been a cornerstone for my interdisciplinary graduate education. Numerous MNIMBS members have helped me in my research and added to the quality of my days in the lab: Wendy Banka, Igor Belyakov, Anna Bielinska, Ankur Desai, Sarah Emery, Yongyi Fan, CJ Gasper, Sascha Goonewardena, Elliott Hill, Baohua Huang, Dmitry Isakov, Katarzyna Janczak, Jeff Landers, Istvan Majoros, Paul Makidon, Catherine Mullen, Andrzej Myc, Doug Smith, Thommey Thomas, Claire Verweij, Suhe Wang, Pam Wong, Yuehua Zhang, as well as several students (notably, Shelly Leung). Alina Kotlyar has the heart of a teacher and has been my mom-away-from-home. Jola Kukowska-Latallo was extremely patient with my numerous questions and never refused to open her door when I knocked. Thankfully, Mike Parise tirelessly keeps the lab running.

I'm grateful to various support staff at University of Michigan. In particular, the Chemistry Department's business and student support offices helped me with all of the details and deadlines from recruitment through graduation, and no doctoral student would ever graduate without the services of the library staff. Dave Adams, the Manager of Michigan's Flow Cytometry Core, was my first flow cytometry teacher and was immensely patient with my naïve questions. Additionally, Tom Lanigan, Supervisor of Michigan's Vector Core, was a patient teacher.

For helpful group meetings, discussions, and advice, I thank group members past and present: Kevin Anderson, Meagan Cauble, Jiumei Chen, Seok-ki Choi, Casey

Dougherty, Blake Erickson, Ming Fang, Ajdin Kavara, Chris Kelly, Roya Lahiji, Dan McNerny, Doug Mullen, Rahul Rattan, Ahleah Rohr, Rong Qi, Anisha Shakya, Justin Silpe, Kumar Sinniah, Madhuresh Sumit, Devon Triplett, Sriram Vaidyanathan, Mallory van Dongen-Sohmer, and Randon Walker. Joey Wallace and Lisa Prevette were especially good role models, and Jimmy Li, Matt Lozier, and Erika Price were undergraduate research assistants who helped me learn differences between teaching in a classroom and teaching in a laboratory. Pascale Leroueil was a valuable unofficial mentor who was oftentimes able to help me see the bigger picture.

I credit Lee Marek, former Science Department faculty at Naperville North High School, with sparking my interest in science generally and chemistry specifically. Mr. Marek's enthusiasm for science and his students in AP Chemistry is the reason why I chose to major in Chemistry at the University of Illinois. I thank Scott Silverman, Professor of Chemistry at University of Illinois, for letting me make a lot of mistakes in his lab, and for his encouragement, attention to detail, and sense of humor. Additionally, Dana Baum was a patient mentor at Illinois.

I would not have made it through grad school without the fellowship and support of some very good friends: Mark and Cat Gordon, T Skujins, Katherine Swart, and Rachel Barnard, among others. They celebrated the peaks with me and empathized in the valleys. More broadly, Graduate Christian Fellowship, the Chemistry Prayer group, and Huron Hills Church have sustained me. Additionally, my family has been unflagging in their support of my journey at Michigan: Mom, Dad, Scott, Christina, and more. My mom and dad always believed I could get through whatever challenge I was facing, and I was refreshed by our numerous weekends together in Ann Arbor.

Finally, Josh is the best husband I could have asked for. Countless times he sacrificed for the sake of my work and accommodated an unpredictable lab schedule, dropping me off at school before the busses began to run or coming back in the evenings with me while I ran flow samples. He is my best friend; without him I would not have made it. And Emma is our sweet cupcake; she gives me the greatest smiles and has made this last year of school so fun.

Soli Deo Gloria

Acknowledgements Specific to Chapter 1: I thank Rahul Rattan and Drs. Thommey Thomas, Andrzej Myc, Anna Bielinska, and Lisa Prevette for helpful discussions and advice. I also thank University of Michigan's Microarray Core Group for conducting quality control assays on the total RNA samples as well as for performing the PCR arrays, Gayle Carroll for doing the Kinetic-QCL™ assay, and Catherine Mullen for performing the QUANTI-Blue™ assay. This project was funded in part with Federal funds from the National Institutes of Health, under award EB005028-01A2.

Acknowledgements Specific to Chapter 2: This work was a collaborative effort between Zhan Chen's and Mark Banaszak Holl's groups in University of Michigan's Chemistry Department. The digital holography methods and techniques were driven by Alex Khmaladze, then a postdoctoral research fellow in the Chen group.

Acknowledgements Specific to Chapter 3: The Center for Research on Learning and Teaching at University of Michigan provided partial support of this research in 2010 through an Investigating Student Learning grant, and I specifically thank Mary Wright and Brian Coppola for their generous assistance. I was greatly helped by personal communications with Nancy Kerner, Lee Marek, Jadwiga Sipowska, and Peggy Zitek. The U.S. Department of Education Graduate Assistantships in Areas of National Need grant #P200A070426 also provided me fellowship support during 2008 and 2009.

Table of Contents

List of Figures

List of Tables

List of Abbreviations

7AAD	7-Aminoactinomycin D
AAU	Association of American Universities
ACI	American Competitiveness Initiative
AFM	Atomic force microscopy
AVD	Apoptotic volume decrease
BS	Beamsplitter
cDNA	Complementary DNA
CFP	Cyan fluorescent protein
CMV	Cytomegalovirus
DHM	Digital holographic microscopy
EF1α	Elongation factor-1 alpha
FACS	Fluorescence-activated cell sorting
GFP	Green fluorescent protein
GPA	Grade point average
NLS	Nuclear localization signal
NPC	Nuclear pore complex
OUA	Office of Undergraduate Admissions
PBS	Phosphate buffered saline
PCAST	President's Council of Advisors on Science and Technology
pDNA	Plasmid DNA
PEG	Poly(ethylene glycol)
PEI	Poly(ethylenimine)
SA-β-gal	Senescence-associated β-galactosidase
SFM	Serum-free medium
ssDNA	Salmon sperm DNA
STEM	Science, technology, engineering, and mathematics
STS	Staurosporine
US	United States
WOBJ	Water immersion microscope objective

Abstract

(1) The Relationship of Protein Expression and Cell Division,
(2) 3D Imaging of Cells Using Digital Holography, and
(3) General Chemistry Enrollment at University of Michigan

by

Rebecca L. Matz

Chair: Mark M. Banaszak Holl

Chapter 1: The role of cell division in protein expression is important to understand in order to guide the development of better nonviral gene delivery materials that can transport DNA to the nucleus with high efficiency for a variety of cell types, particularly when nondividing cells are targets of gene therapy. We evaluated the relationship between cell division and protein expression when using commercial poly(ethylenimine) (PEI)-based polyplexes. The membrane dye PKH26 was used to assess cell division, and cyan fluorescent protein (CFP) was used to monitor protein expression. When analyzed at the whole population level, a greater number of cells divided than expressed protein, regardless of the level of protein expression observed, giving apparent consistency with the hypothesis that protein expression requires cells to pass through mitosis in order for the transgene to overcome the nuclear membrane. However, when the polyplex-exposed population was evaluated for the amount of division in the protein-expressing subpopulation, it was observed that substantial amounts of expression had occurred in the absence of division. Indeed, in HeLa S3 cells, this represented the majority of expressing cells.

Of interest, the doubling time for both cell lines was slowed by ~2-fold upon exposure to polyplexes. This change was not altered by the origin of the plasmid DNA (pDNA) transgene promoter (viral vs nonviral). Gene expression arrays in polyplex-exposed HeLa S3 cells showed upregulation of cell cycle arrest genes and downregulation of genes related to mitosis. Chemokine, interleukin, and toll-like receptor genes were also upregulated, suggesting activation of proinflammatory pathways. In summary, we find evidence that a cell division-independent expression pathway exists, and that polyplex exposure slows cell division and increases inflammatory response.

Chapter 2: Cell volume changes play important roles in processes associated with normal cell activities as well as disease states. Consequently, there is considerable need to accurately measure volumes of individual cells and cell populations over time. In this study, we monitored cell volume changes in real time during apoptosis using digital holographic microscopy (DHM). The results showed that after exposure to 1 mM staurosporine for four hours, the volumes of KB cells were reduced by ~50-60%, which is consistent with previous results obtained using electronic cell sizing and atomic force microscopy. In comparison with other techniques, DHM is advantageous because it employs noninvasive detection, has high time resolution and real time measurement capability, and can simultaneously probe the time-dependent volume changes of individual cells and cell populations.

Chapter 3: At the collegiate level, science laboratories and their corresponding lectures are often offered as separate courses, and students may not be required to concurrently enroll in both. We examined the impact of concurrent versus nonconcurrent enrollment on 9,438 students' withdrawal rates from and final grades in the general chemistry lecture at the University of Michigan at Ann Arbor using multiple linear and binary logistic regression analyses, respectively, at a significance level of 0.05. We found that concurrent enrollment in the lecture and laboratory positively impacts (1) the odds of retention in the lecture by a factor of 2.2 times on average and (2) the final grades in the

lecture course by up to 0.19 grade points on a 4.0 scale for the students that scored the lowest on university-level mathematics and chemistry placement exams.

Chapter 1

Polyplex Exposure Inhibits Cell Cycle, Increases Inflammatory Response, and Can Cause Protein Expression Without Cell Division[1]

1.1 Introduction

Nonviral gene delivery methods have been investigated as potential therapeutics for genetic diseases and disorders for decades. The role of cell division in protein expression is important to understand in order to guide the development of better nonviral gene delivery materials. Microinjection experiments have repeatedly confirmed that transgenes must reach the nucleus to generate a gene product,[1-5] indicating that the nuclear membrane is a major barrier to gene expression. Some studies have shown that nuclear uptake of plasmid DNA (pDNA) is strongly dependent on cell division[4,6-11] with seminal work having been done by Mario Capecchi more than 30 years ago.[1] Other research has shown that cell division is not required for nuclear uptake of pDNA[12-16] with most studies exploiting nuclear localization signals (NLS) for transport through nuclear pore complexes.[17] Indeed, Zanta *et al.* have shown that a single NLS is able to translocate pDNA to the nucleus.[18]

Much of this previous research employed microinjection or synchronization methods. Cooper has raised concerns that chemically synchronized cells do not reflect specific cell ages that are representative of the normal cell cycle.[19] Additionally, microarray analysis of gene expression patterns has cast doubt that a conventional double thymidine block is able to synchronize cells.[20] The drawbacks to microinjection experiments are that relatively low numbers of cells can be analyzed (usually on the

[1]Portions of this chapter have been submitted for publication: Matz, R. L.; Erickson, B.; Kukowska-Latallo, J. K.; Baker, J. R., Jr.; Orr, B. G.; Banaszak Holl, M. M. Polyplex Exposure Inhibits Cell Cycle, Increases Inflammatory Response, and Can Cause Protein Expression Without Cell Division. *Mol. Pharmaceutics* **2012**.

order of tens to hundreds), the average volume injected into each cell can vary substantially,[21] and material intended for the nucleus can be deposited into the cytoplasm. The limitations of synchronization and microinjection techniques indicate a need for a complementary method that can analyze the relationship of cell division and gene expression.

We designed a flow cytometry experiment to test the relationship of protein expression and cell division. This method utilizes large numbers of cells without perturbing the cell cycle with physical or chemical methods. The lipophilic dye PKH26 was used to assess division because it evenly stains the cell membrane and is divided approximately equally between daughter cells upon mitosis.[22-24] Protein expression was monitored by fluorescence of cyan fluorescent protein (CFP). Polyplexes were formed between pDNA and jetPEI™, a potent poly(ethylenimine) (PEI)-derivative transfection reagent, and delivered to HeLa S3 and 293A cells. As an early clone of the parent HeLa cell line,[25] HeLa S3 cells were used because they are established and commonly used. 293A cells were used because they produce high levels of transgene expression as the parent line was transformed with sheared human adenovirus type 5 DNA.[26] Our experiment was designed to test whether or not cell division was required for protein expression.

This chapter continues with detailed experimental procedures. Next, the results of the flow cytometry experiments are provided, showing that the number of polyplex-exposed cells that has divided is consistently greater than that expressing protein. This result provides apparent consistency with a model where cells divide in the course of gene expression because enough division has occurred to account for the entire expressing population. However, when we analyzed the amount of division in only the protein-expressing cells, we obtained evidence for expression occurring in the absence of cell division. This result substantiates a division-independent pathway. In the course of these experiments, we also discovered that exposure to polyplexes slowed the doubling time of both HeLa S3 and 293A cells by ~1.2 to 2.5 times. Gene expression arrays suggest that the cells are arrested in the G_1 phase of the cell cycle and that polyplex exposure induces innate inflammatory gene expression. Together, these

results demonstrate the need for development of nonviral gene delivery particles that mitigate the induction of inflammatory responses and alteration of the cell cycle progression. Finally, future work is proposed, and the appendix provides tables and figures that supplement the main conclusions of the chapter.

As the lead researcher on this project, I guided the experimental design, carried out the experiments, analyzed and interpreted the data, presented the work in various contexts, and wrote the entirety of the manuscript for publication. Blake Erickson wrote the custom MATLAB code used for compensating the flow cytometry data, and Brad Orr provided mathematical guidance and oversight for this process. Jola Kukowska-Latallo and Jim Baker provided important advice and expertise regarding experimental design. Mark Banaszak Holl provided overall guidance for the project.

1.2 Experimental Methods

1.2.1 Cell Culture

HeLa S3 (human epithelial; Cat. No. CCL-2.2™) and 293A (human epithelial; Cat. No. R705-07) cells were purchased from ATCC® (Manassas, VA) and Life Technologies (Carlsbad, CA), respectively. HeLa S3 cells are a derivative of the parent HeLa line (Cat. No. CCL-2™; ATCC®), and 293A cells are a subclone of HEK 293 cells (Cat. No. CRL-1573™; ATCC®). Each line tested negative for mycoplasma contamination (Cat. No. 6601; Takara Bio; Kyoto, Japan), was expanded, and then cryopreserved in liquid nitrogen. HeLa S3 and 293A cells were cultured in F-12K medium (Cat. No. 30-2004; ATCC®) and Dulbecco's modified Eagle's medium (D-MEM) with high glucose (Cat. No. 11995; Life Technologies), respectively. The media were supplemented with 10% fetal bovine serum (Cat. No. SH30910.03; Thermo Fisher Scientific; Waltham, MA) and 100 units/mL penicillin and 100 µg/mL streptomycin (Cat. No. 15140; Life Technologies). The 293A media was additionally supplemented with 100 µM MEM nonessential amino acids solution (Cat. No. 11140; Life Technologies). Cells were maintained at 37 °C with 5% CO_2 in a humidified atmosphere and subcultured by trypsinization (Cat. No. 25200; Life Technologies).

1.2.2 PKH26 Staining

Cells were stained with PKH26 (Cat. No. PKH26GL; Sigma-Aldrich; Saint Louis, MO) according to the manufacturer's protocol with final staining concentrations of 2 µM PKH26 and 1 × 10^7 cells/mL. After staining, 293A cell viability, as measured by exclusion of trypan blue stain (Cat. No. 15250; Life Technologies) and percent recovery, averaged 91 ± 3% and 72 ± 16%, respectively. Control cells that were not stained with PKH26 were still subjected to the staining conditions, albeit with no PKH26 dye present, and showed similar viability (94 ± 3%) and recovery (84 ± 17%) as the stained cells. Similar percentages were also obtained for stained and control HeLa S3 cells. Cells were seeded at 80,000 cells/well in 12-well tissue culture-treated plates (Cat. No. 353043; Becton, Dickinson and Company; Franklin Lakes, NJ) in 800 µL complete medium, and incubated at 37 °C with 5% CO_2 for 5 to 6 h prior to transfection.

1.2.3 DNA Preparation

The pDNAs used were 4.1 kb CFP-encoding pDNA (pAmCyan1-C1; Cat. No. 632441; Clontech; Mountain View, CA), 5.1 kb blank pDNA that encoded no fluorescent reporter protein (gWIZ™-blank; Cat. No. 5008; Aldevron; Fargo, ND), and 5.8 kb green fluorescent protein (GFP)-encoding pDNA (gWIZ™-GFP; Cat. No. 5006; Aldevron). These pDNAs were all under the control of the CMV immediate-early promoter ($P_{CMV\ IE}$). A fourth pDNA, 5.5 kb in size and GFP-encoding, was custom synthesized by Aldevron to be the same as gWIZ™-GFP except that it contained the human elongation factor-1 alpha (EF1α) nonviral transgene promoter from pEF1α-AcGFP1-C1 (Cat. No. 631974; Clontech) instead of the CMV promoter. All components of the gWIZ™-GFP-EF1α pDNA were nonviral in origin. All pDNAs were amplified after transformation of DH5α™ *Escherichia coli* cells (Cat. No. 18265; Life Technologies) according to the manufacturer's protocol, and LB Broth (Cat. No. 12780; Life Technologies) supplemented with 50 µg/mL kanamycin (Cat. No. K0254; Sigma-Aldrich) was used as the medium. The pDNAs were purified from the cells with a Qiagen EndoFree® Plasmid Mega Kit (Cat. No. 12381; Venlo, Netherlands) according to the manufacturer's instructions. A fifth DNA sample was sheared salmon sperm DNA (ssDNA; Cat. No.

AM9680; Applied Biosystems; Foster City, CA) which was also taken through the Qiagen EndoFree® purification for consistency with the pDNA samples. All DNA samples were nonpyrogenic according to a Kinetic-QCL™ assay (BioWhittaker, Inc.; Walkersville, MD) and tested negative for RAW-Blue™ cell (Cat. No. raw-sp; InvivoGen; San Diego, CA) activation according to a QUANTI-Blue™ enzymatic assay (Cat. No. rep-qb1; InvivoGen).

1.2.4 Polyplex Formation

Polyplexes were formed in DNase/RNase-free water (Cat. No. 10977; Life Technologies) between jetPEI™ (Cat. No. 89129-940; VWR International; West Chester, PA) and each of the five DNA samples at an N/P (+/–) ratio of 10 where N represents the nitrogen residues in the cationic polymer and P represents the phosphate residues in the DNA backbone. An equal volume (20 µL) of jetPEI™ in water was added to 20 µL of 40 µg/mL DNA in water, and the resultant solution was incubated at room temperature for ~20 to 30 min. Cells plated in 12-well plates were transfected with 40 µL polyplex solution/well containing 0.8 µg DNA. For samples exposed to jetPEI™ only, the same amount of jetPEI™ per 40 µL of total solution was used, replacing the DNA with an equal volume of water.

1.2.5 Cell Transfection

Prior to transfection, the complete medium was aspirated from the PKH26-stained and control cells that had incubated at 37 °C with 5% CO_2 for 5 to 6 h. The cells were washed once with phosphate buffered saline (PBS; Cat. No. 10010; Life Technologies), and 800 µL of serum-free medium (SFM) was added back to each well. To transfect the cells, 40 µL of either the polyplex or polymer-only solution, was added to the appropriate wells, and the cells were incubated at 37 °C with 5% CO_2. After 3 h, the SFM was aspirated and replaced with 800 µL complete medium. The cells were again incubated at 37 °C with 5% CO_2 until the selected time point, whereupon the cells were harvested for analysis by flow cytometry. A given time point includes the 3 h incubation in SFM. A 24 h transfection or time point, for example, indicates cells that

were exposed to nanoparticles in SFM for 3 h and then incubated 21 h further in complete medium prior to harvesting.

1.2.6 Flow Cytometry

The transfected cells were harvested for analysis by flow cytometry by trypsinization with 200 µL trypsin/well after rinsing once with PBS. Complete medium (1 mL) was added to each well to inhibit the trypsin, and resultant suspensions were centrifuged for 5 min at 835 x g. Cell pellets were resuspended in 1 mL PBS, and 7-aminoactinomycin D (7AAD; Cat. No. A1310; Life Technologies) was added to a final concentration of1 µg/mL as a viability marker. 7AAD single dye controls were made by resuspending the cell pellet in 500 µL PBS, adding an equal volume of 200 proof ethanol (Cat. No. 2716; Decon Labs; King of Prussia, PA), and subsequently adding 7AAD to a final concentration of 5 µg/mL. According to the 7AAD protocol, all samples were incubated on ice for 30 min, centrifuged for 5 min at 835 x g, and resuspended in PBS. The cells were analyzed with an Epics XL-MCL Flow Cytometer (Beckman Coulter; Brea, CA), which contains a 15 mW 488 nm argon laser, collecting 10,000 events per sample. We analyzed three technical replicates per sample, and experiments were repeated at least three independent times. The excitation and emission maxima and fluorescence filter used for each dye in this experiment is shown in Table 1.1

Table 1.1: Excitation and emission maxima and filters used for fluorescent dyes.

Dye	Excitation maximum (nm)	Emission maximum (nm)	Fluorescence filter (nm)
CFP	458	489	525 ± 20 (FL1)
GFP[a]	475	510	525 ± 20 (FL1)
PKH26	551	567	575 ± 20 (FL2)
7AAD	543	655	675 ± 20 (FL4)

[a]All parameters in this table are the same regardless of the transgene promoter.

Because the overlap of three (or more) colors cannot be easily manually compensated due to their interdependence,[27] data analyses were performed using Weasel software (Version 2.7.4; Walter and Eliza Hall Institute; Melbourne, Australia) and a custom code written in MATLAB (Version 7.8.0.347; The MathWorks; Natick, MA) that follows standard compensation protocols.[28-31] Median (as opposed to mean) fluorescence intensity is used throughout

this manuscript because it is relatively insensitive to outliers in the data. Curves of best exponential fit were determined using Microsoft® Excel® for Mac (Redmond, WA). Exponential regression was identified as the best method for fitting the flow cytometry data because it is known that cells undergo exponential growth. The exponential fits were constrained to go through the datum at 0 h from cells only treated with PKH26 because the cells for all the different treatments were stained in a single reaction. It is noted that Microsoft® Excel® calculates coefficients of determination (R^2) based on a transformed regression model, meaning it evaluates R^2 for a linear regression on data plotted as ln(y) versus x. This practice can inflate R^2.

1.2.7 Cell Proliferation Assay

To test whether the proliferation rate of HeLa S3 cells changed upon staining with PKH26, cells were either stained with PKH26 or taken through the staining procedure albeit with no dye present, plated at 80,000 cells/well in 12-well plates with 800 µL complete medium, and incubated for 5 to 6 h at 37 °C with 5% CO_2 as described. Cells were harvested at various time points over ~2 days for flow cytometry also as previously described with the exception that 7AAD was not employed as a viability stain. The density of the cell suspensions were counted with a BD Accuri C6 Flow Cytometer® (Accuri Cytometers; Ann Arbor, MI) which reports the amount of cell suspension volume pulled for a given number of cells, and curves of best exponential fit were again determined using Microsoft® Excel®. The experiment was repeated three independent times.

1.2.8 Cellular Senescence Assay

HeLa S3 and 293A cells were plated in triplicate and transfected as described except that cells were not stained with PKH26 and the experiment was performed in 24-well tissue culture-treated plates (Cat. No. 353047; Becton, Dickinson and Company); all reagents and cell numbers were scaled down according to the growth area of the wells. Following exposure to jetPEI™ only or polyplexes formed between jetPEI™ and the five types of DNA, cells were tested for cellular senescence (Cat. No. KAA002; EMD

Millipore; Billerica, MA) per the manufacturer's instructions at 48 h. The positive control was cells that had been exposed to 50 nM doxorubicin hydrochloride (Cat. No. 2004; AvaChem Scientific; San Antonio, TX) from 3 days prior to transfection through the time point at which cells were assayed for senescence (i.e., for 5 days total). This procedure assesses the activity of senescence-associated β-galactosidase (SA-β-gal) that is identified by blue-green stained cells under light microscopy. Brightfield images were obtained with an Olympus iX70-S1F2 microscope (Olympus Corporation; Tokyo) fitted with an Olympus DP72 digital camera, and the percent of blue-green as compared to normal cells across six separate images for each sample was counted according to previously established protocols.[32,33]

1.2.9 Total RNA Extraction and PCR Arrays

HeLa S3 cells were plated in triplicate as described above except that cells were not stained with PKH26. (Control experiments showed that PKH26-staining did not affect the rate of proliferation—see Figure 1.S1.) The transfection experiment was performed in 6-well tissue culture-treated plates (Cat. No. 353046; Becton, Dickinson and Company) with all reagents and cell numbers scaled up according to the growth area of the wells. Again, cells were exposed to jetPEI™ only or to polyplexes made between jetPEI™ and either gWIZ™-GFP or gWIZ™-GFP-EF1α pDNA. At 4 and 24 h following transfection, total RNA from each sample was isolated using the Qiagen RNeasy Mini Kit (Cat. No. 74104). Cell lysates were homogenized using Qiagen QIAshredder spin columns (Cat. No. 79654) and on-column DNase digestions were performed with RNase-Free DNase (Cat. No. 79254; Qiagen). The experiment was repeated three independent times yielding three biological replicates for each sample (the one exception is described in the Figure 1.S6 caption), and all biological replicates were subjected to quality control procedures and analysis by PCR arrays at the same time.

RNA concentration and purity (260/280 ratio) was measured with a UV spectrophotometer (NanoDrop 2000; Thermo Fisher Scientific). Ribosomal RNA integrity was measured with an Agilent 2100 BioAnalyzer (Agilent Technologies; Santa

Clara, CA). The RT^2 First Strand Kit (Cat. No. 330401; Qiagen) was used according to the manufacturer's protocol (500 ng total RNA per sample) to synthesize the complementary DNA (cDNA) for the entire RNA sample. The cDNA samples were analyzed for changes in gene expression as compared to the untreated control by both Human Cell Cycle (Cat. No. PAHS-020E) and Inflammatory Response and Autoimmunity (Cat. No. PAHS-077E) RT^2 Profiler™ PCR arrays from Qiagen. We used an ABI 7900HT Fast Real-Time PCR System (Life Technologies; Carlsbad, CA) with a 384-well block module, the manufacturer's recommended thermal cycling conditions, and the Qiagen RT^2 SYBR® Green qPCR Mastermix (Cat. No. PA-112) for amplification of the cDNA. Each plate contained 4 x 96 genes with each set of 96 containing 84 pathway-related genes plus genomic DNA contamination, reverse transcription, and positive PCR controls, and 5 housekeeping genes (β_2 microglobulin, hypoxanthine phosphoribosyltransferase 1, ribosomal protein L13a, glyceraldehyde 3-phosphate dehydrogenase, and β-actin), all of which were used for normalization. The data were analyzed using the $2^{-\Delta\Delta CT}$ method, a common method for presenting relative levels of gene expression, and genes that exhibited greater than or equal to 2-fold up- or downregulation were considered different from the control. Statistical significance was determined using false discovery rate, where a *p*-value of 0.05 indicates at most 5% false positives.[34,35]

1.3 Results

1.3.1 Relationship of Cell Division and Protein Expression in HeLa S3 and 293A Cells

A two-color flow cytometry experiment was designed to quantify the relationship between cell division and protein expression for PEI-based polyplexes. The membrane dye PKH26 was used to assess division and fluorescence of CFP was used to monitor protein expression. PKH26-stained HeLa S3 and 293A cells were transfected for 3 h with polyplexes formed between CFP-encoding pDNA and jetPEI™. The dilution of PKH26 in treated and untreated samples was observed by flow cytometry over 2 days following transfection (Figure 1.1; see Figure 1.S2 for representative 293A data). For

both cell lines, fluorescent signal indicating protein expression was evident by ~12 h following transfection. As the timescale of fluorescent protein maturation is on the order of tens of minutes,[36] it was not considered in these analyses.

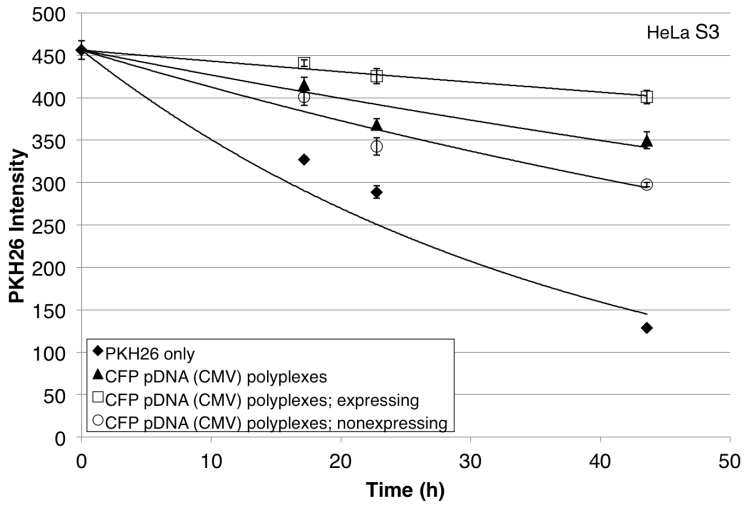

Figure 1.1: PKH26 intensity (arbitrary units) of representative HeLa S3 cells treated with polyplexes formed between jetPEI™ and CFP pDNA over 2 days following transfection as compared to control cells (PKH26 only). Cells expressing CFP (□) and those not expressing CFP (○) are subsets of the whole population (▲) that was treated with polyplexes. Cells were transfected for 3 h beginning at time = 0 h. Each point shows the mean ± SD of three technical replicates with curve of best exponential fit. All data are fit with PKH26 only data at 0 h.

We compared the number of polyplex-exposed cells that divided to the number that expressed protein. The number of cells that divided was measured by comparing the initial PKH26 intensity (at 0 h) to the final PKH26 intensity (at ~48 h), assuming an exponential decrease in PKH26 fluorescence upon division. The number of cells expressing CFP was measured by comparing CFP fluorescence intensity to that of the untreated (but still PKH26-stained) control (Figure 1.2). The untreated cells were used to determine the background level of fluorescence in the channel where CFP fluorescence was collected. In the treated samples, cells that fell outside of this background region were considered to be CFP-positive. Consistently, the number of cells that divided was greater than the number of cells that expressed CFP (Table 1.2). This held true regardless of the percent of cells expressing CFP (38 ± 9% for HeLa S3 and 84 ± 5% for 293A). For example, in HeLa S3 Experiment #1, out of 10,000 measured cells, 6000 ± 800 divided and 2400 ± 200 expressed CFP. Table 1.2 shows the results from the full sets of experiments in HeLa S3 and 293A cells; because the variability in the 293A data is low, we expect that the high variability in the HeLa S3

data reflects real biological (as opposed to technical) variability.

The polyplex-exposed population was subdivided into cells that expressed CFP and cells that did not express CFP. By comparing the initial PKH26 intensity to the final PKH26 intensity, we determined the number of cells that divided in the population expressing CFP (Table 1.2). For 293A cells, the majority of cells that expressed CFP had also divided (69% to 93% of expressing cells) whereas for HeLa S3 cells, the majority of cells that expressed protein had not divided (44% to 86% of expressing cells). Schematics of representative HeLa S3 and 293A experiments showing the relative numbers of divided versus not divided and expressing versus nonexpressing cells are shown in Figure 1.S3.

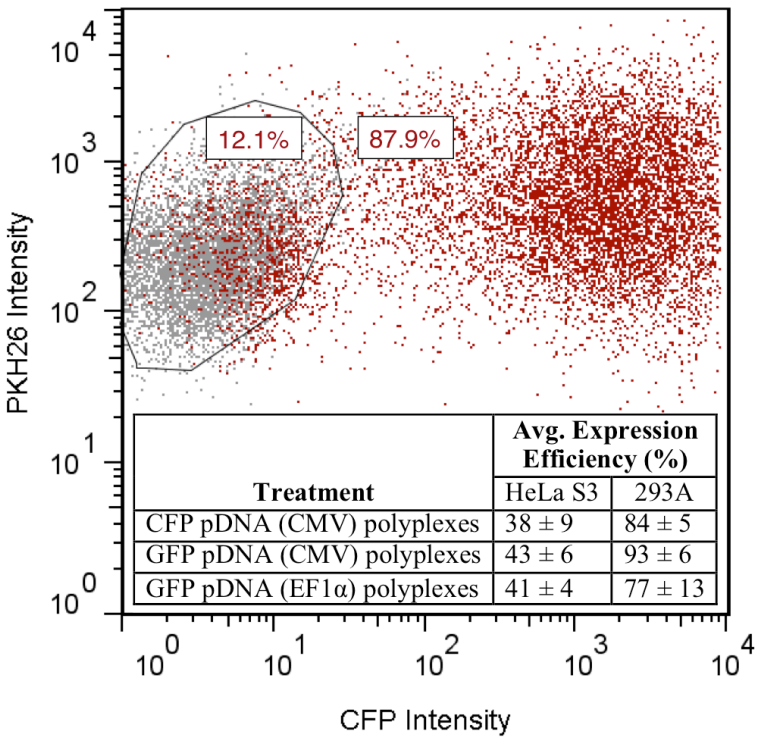

Treatment	Avg. Expression Efficiency (%)	
	HeLa S3	293A
CFP pDNA (CMV) polyplexes	38 ± 9	84 ± 5
GFP pDNA (CMV) polyplexes	43 ± 6	93 ± 6
GFP pDNA (EF1α) polyplexes	41 ± 4	77 ± 13

Figure 1.2: Scatterplot of flow cytometry data for representative 293A cells showing expression efficiency for CFP pDNA (CMV) polyplexes. The gate was drawn based on control cells (i.e., cells stained with PKH26 but not treated with polyplexes). The inset table shows the average percent of expression efficiency for all three protein-encoding polyplexes across all experiments at ~48 h following transfection. The scatterplot also qualitatively shows that cells exposed to CFP pDNA (CMV) polyplexes (red) have higher PKH26 intensity than control cells (gray) at ~48 h following transfection.

1.3.2 Effect of Cationic Polymer- and Polyplex-Exposure on HeLa S3 and 293A Doubling Times

HeLa S3 and 293A cells exposed to polyplexes formed with any of the five types of DNA divided ~1.2 to 2.5 times more slowly than control cells, but cells exposed to

Table 1.2: Breakdown of the number of cells for each experiment that have divided and/or expressed CFP ~48 h following transfection.

Cell Line	Expt #	All Cells						Cells Expressing CFP[a]		
		# of Cells Analyzed		# Divided[b]		# Expressing CFP[c]		# Divided[d]		Fraction Divided
		Avg[e]	SD	Avg[e]	SD	Avg[e]	SD	Avg[e]	SD	Avg
HeLa S3	1	10000	0	6000	800	2400	200	1100	100	0.47
	2[f]	-	-	-	-	-	-	-	-	-
	3	10000	0	4400	300	4300	100	900	100	0.21
	4	10000	0	8200	200	2400	100	1300	100	0.56
	5	10000	0	6400	100	4800	200	700	200	0.14
293A	1	10000	0	9800	700	8100	100	7500	500	0.93
	2	10000	0	8500	200	7700	0	5300	200	0.69
	3	10000	0	9000	2100	7900	100	6300	1600	0.80
	4[f]	-	-	-	-	-	-	-	-	-
	5	10000	0	9200	1500	7400	0	6000	1100	0.81
	6	10000	0	9500	900	8300	100	7600	700	0.91
	7[g]	7000	2700	6100	700	5600	100	4400	400	0.79

[a]Cells expressing CFP is a subset of all cells; the subpopulation is determined by flow cytometry. [b]Calculated based on the measured PKH26 intensity of all cells and the number of cells analyzed. [c]Measured based on the amount of CFP fluorescence over the untreated control. [d]Calculated based on the measured PKH26 intensity of cells expressing CFP and the number of all cells expressing CFP. [e]Avg is an average of three technical replicates. [f]HeLa S3 Expt #2 was not included because the percent CFP expression was a statistical outlier. 293A Expt #4 was not included because the doubling time of polyplex-exposed cells was a statistical outlier. [g]Occassionally we were unable to collect 10,000 cells for all three technical replicates.

only the cationic polymer, jetPEI™, divided at a similar rate as control cells (Figure 1.3). For both cell lines, these effects were consistently observed over multiple independent experiments, each sample being tested at least three independent times. The doubling times of the samples were extracted from curves of best exponential fit, the averages of which are shown in Figure 1.3b and Table 1.S1. Figure 1.S4a shows representative data for the dilution of PKH26 in HeLa S3 cells over time. Figure 1.S4b shows the average doubling times (from Figure 1.3b) of untreated and CFP polyplex-treated HeLa S3 cells in terms of PKH26 intensity over time, illustrating that even when the error on the doubling times is considered, polyplex-exposed cells exhibit a substantially slowed doubling time.

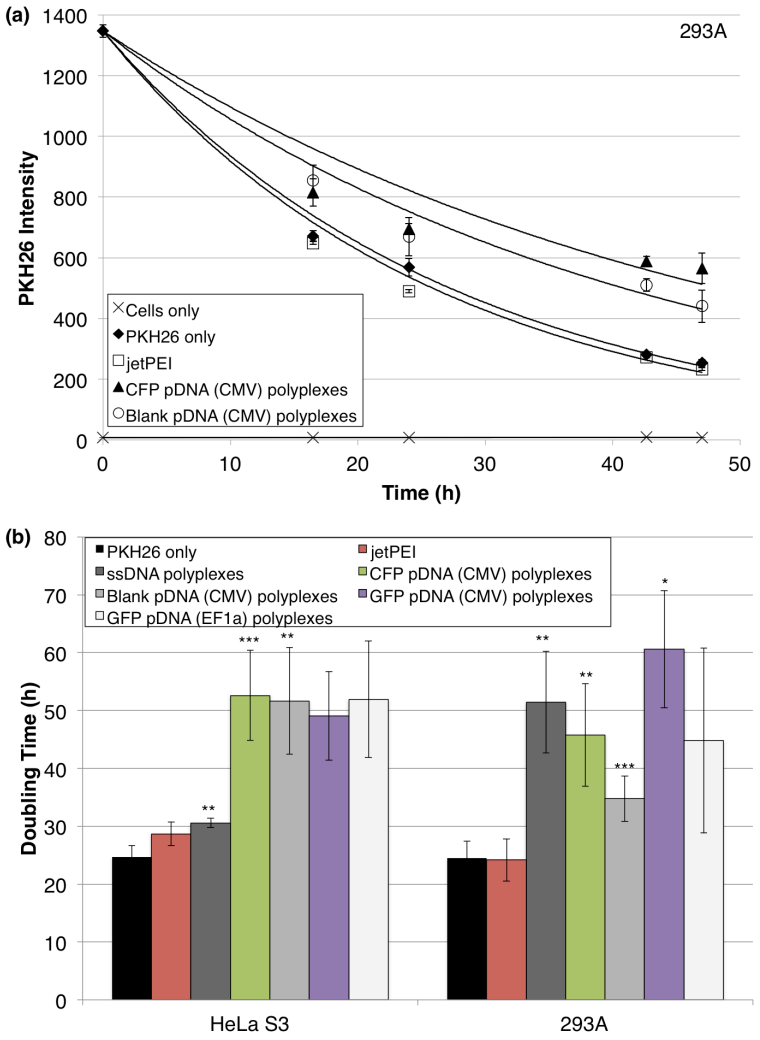

Figure 1.3: As measured by PKH26 intensity, cells treated with polyplexes formed between jetPEI^{TM} and any of five types of DNA divide more slowly than control cells (PKH26 only) over 2 days following transfection. Cells treated with polymer alone (jetPEI^{TM} only) are not different than the control. (a) Representative data for 293A cells. The cells were transfected for 3 h beginning at time = 0 h. Each point shows the mean ± SD of three technical replicates with curve of best exponential fit except for the cells only sample, which has a linear line of best fit. All data are fit with PKH26 only data at 0 h except for the cells only sample. (b) Summary of five and seven independent experiments with HeLa S3 and 293A cells, respectively. All samples were tested in three or more independent experiments even with statistical outliers having been removed. ANOVA shows that there are statistical differences in the mean doubling times for the different treatments within each cell line (for HeLa S3 cells, $F(6, 20) = 15.6$, $p < 0.05$, $\omega = 0.87$, and for 293A cells, $F(6, 29) = 16.9$, $p < 0.05$, $\omega = 0.85$). Differences were determined according to the *post hoc* Games-Howell test, with equal variance not assumed ($p < 0.05$ for the Levene statistic). * $p < 0.10$, ** $p < 0.05$, *** $p < 0.01$.

1.3.3 Senescence-Associated β-Galactosidase Assay on HeLa S3 and 293A Cells

The semiquantitative senescence-associated β-galactosidase (SA-β-gal) assay detects the level of the lysosomal hydrolase β-galactosidase that is increased insenescent cells over quiescent or normally proliferating cells. At pH 6.0, the β-galactosidase cleaves X-gal in senescent cells, leading to formation of a perinuclear blue-green precipitate that is observable by light microscopy.[32,37] In both polymer- and polyplex-treated HeLa S3 and 293A cells, senescence was not observed 48 h post-transfection over that of background levels observed in normally proliferating cells (Figure 1.S5).

1.3.4 Gene Expression in HeLa S3 Cells Related to the Cell Cycle and Inflammatory Response and Autoimmunity by Targeted PCR Arrays

The changes in expression of 84 cell cycle-related genes and 84 inflammatory response and autoimmunity-related genes were observed in polymer- and polyplex-exposed cells. The goal of the array study was to probe possible mechanisms by which polyplex exposure slowed HeLa S3 cell division, and to investigate differential responses based on the viral versus nonviral nature of the transgene promoter. Overall, the changes in gene expression were similar for both kinds of polyplexes (i.e., differences due to the viral vs nonviral nature of the transgene promoter were not observed). For the majority of affected genes at 24 h following transfection on both types of arrays, the polyplex-exposed samples were similarly up- or downregulated and the polymer-only sample was unchanged as compared to the untreated control.

The genes upregulated by the largest magnitude on the cell cycle array were *CDKN1A*, *CHEK2*, *DIRAS3*, *GADD45A*, *HERC5*, and *SERTAD1* (Table 1.3). These genes were upregulated 24 h following transfection in both polyplex-exposed samples but were unchanged in the polymer-only sample, with the exception of *GADD45A* which was upregulated 4-fold in the polymer-only sample. Four of these genes (*CDKN1A*, *CHEK2*, *DIRAS3*, and *GADD45A*) have been shown to function in cell cycle arrest or inhibition pathways, generally in response to stress stimuli such as DNA damage. The

Table 1.3: Changes in expression of selected genes related to the cell cycle pathway in jetPEI™ or polyplex-exposed HeLa S3 cells.

				Fold Change in Gene Expression[b]					
				jetPEI™		GFP (CMV) polyplexes		GFP (EF1α) polyplexes	
	GeneBank	Symbol	Description[a]	4h	24h	4h	24h	4h	24h
Upregulated	NM_000389	CDKN1A	Cyclin-dependent kinase inhibitor 1A (p21, Cip1)	**2.5**	1.4	**2.2**	**2.1**	**2.5**	**2.6**
	NM_007194	CHEK2	CHK2 checkpoint homolog (S. pombe)	-1.2	-1.3	1.0	**2.2**	1.0	**2.4**
	NM_004675	DIRAS3	DIRAS family, GTP-binding RAS-like 3	1.1	-2.8	**2.7**	**4.2**	**3.5**	**5.5**
	NM_001924	GADD45A	Growth arrest and DNA-damage-inducible, alpha	**2.5**	**4.0**	1.6	**3.6**	1.5	**3.8**
	NM_016323	HERC5	Hect domain and RLD 5	-1.1	1.4	**5.3**	**25.8**	**4.8**	**27.9**
	NM_013376	SERTAD1	SERTA domain containing 1	**4.1**	1.7	**3.5**	**2.8**	**4.1**	**2.8**
Downregulated	NM_031966	CCNB1	Cyclin B1	-1.3	-1.1	-1.3	**-2.1**	-1.2	**-2.1**
	NM_001761	CCNF	Cyclin F	**-2.8**	-1.1	**-2.3**	**-2.0**	**-2.8**	**-2.0**
	NM_003885	CDK5R1	Cyclin-dependent kinase 5, regulatory subunit 1 (p35)	1.6	-1.1	**2.0**	**-2.2**	**2.2**	-1.6
	NM_005192	CDKN3	Cyclin-dependent kinase inhibitor 3	-1.3	-1.1	-1.3	**-2.3**	-1.2	**-2.3**
	NM_002266	KPNA2	Karyopherin alpha 2 (RAG cohort 1, importin alpha 1)	-1.2	-1.5	-1.0	**-2.3**	-1.1	**-2.1**
	NM_002358	MAD2L1	MAD2 mitotic arrest deficient-like 1 (yeast)	-1.1	-1.2	-1.1	**-2.2**	1.0	**-2.3**
	NM_005590	MRE11A	MRE11 meiotic recombination 11 homolog A (S. cerevisiae)	-1.6	-1.5	-1.3	**-2.6**	-1.1	**-3.1**
	NM_007111	TFDP1	Transcription factor Dp-1	-1.2	-1.2	-1.3	**-2.1**	-1.2	**-2.2**

[a]The gene descriptions are reproduced from the array product information from Qiagen. [b]Green and red shading indicate fold-changes of ≥ 2 and ≤ 2, respectively, with $p \leq 0.05$.

genes downregulated by the largest magnitude on the cell cycle array were *CCNB1*, *CCNF*, *CDK5R1*, *CDKN3*, *KPNA2*, *MAD2L1*, *MRE11A*, and *TFDP1* (Table 1.3). At 24 h following transfection, these genes were generally downregulated between 2- and 3-fold in both polyplex-exposed samples but were unchanged in the polymer-only sample. These genes are all related to normal proliferation pathways except for *CDKN3*, which encodes a cyclin-dependent kinase inhibitor.[38] Figures 1.4a and 1.4b show scatterplots comparing the gene regulation of the jetPEI™ and GFP pDNA (CMV) polyplex

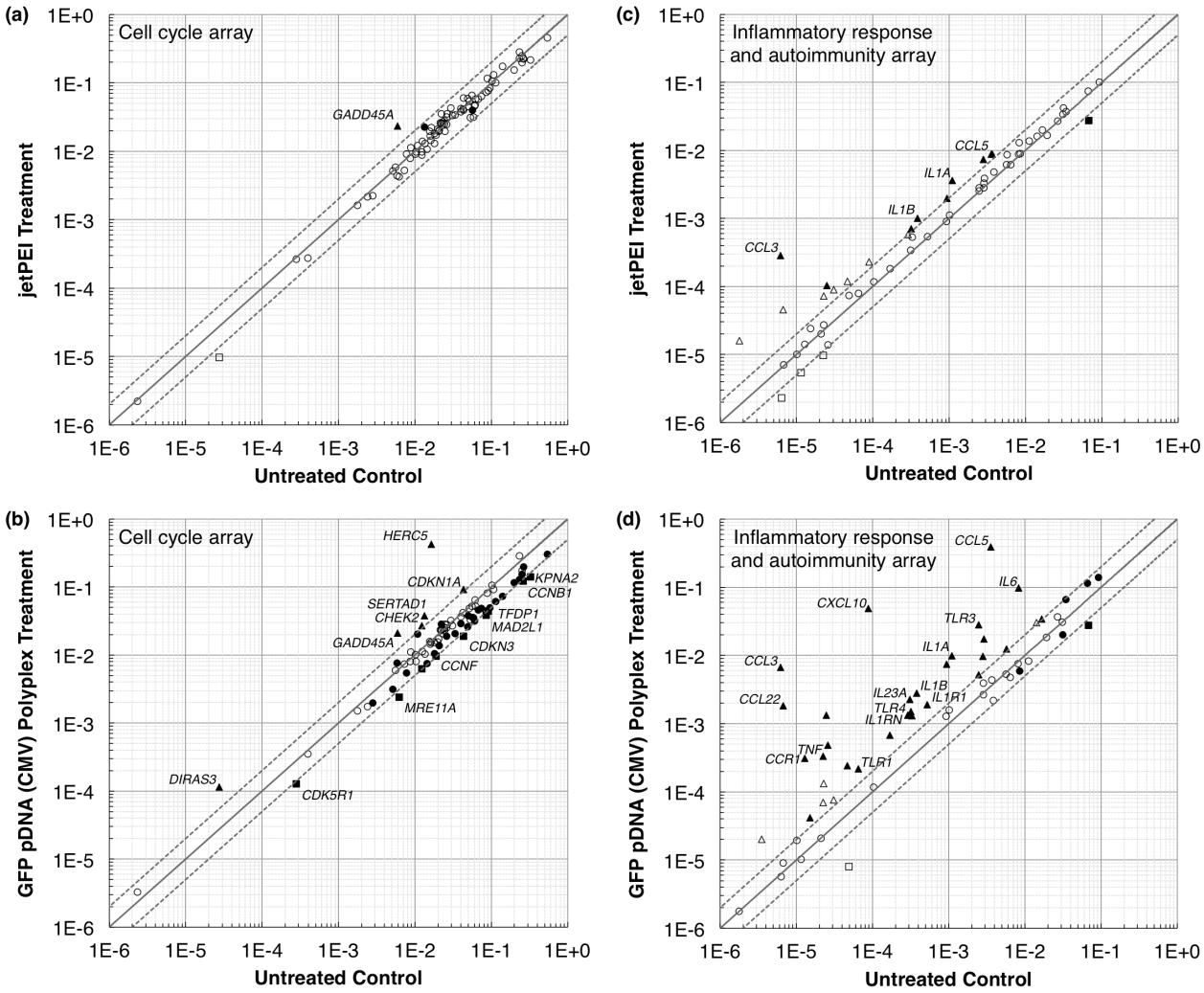

Figure 1.4: Scatterplots (arbitrary units) showing the relative number of up- (▲) and downregulated (■) genes for the jetPEI™ and GFP pDNA (CMV) polyplex treatments compared to the untreated control at 24 h following transfection. (a) and (b) Cell cycle array. (c) and (d) Inflammatory response and autoimmunity array. The centerline indicates a fold change ($2^{-\Delta\Delta Ct}$) of 1, meaning the gene expression is no different in the treated sample as compared to the control. The upper and lower dashed lines indicate fold changes of 2 in gene expression. Circles indicate genes with fold changes ≤ 2. Comparing to the untreated control, filled symbols indicate regulation that is significantly different ($p \leq 0.05$), and open symbols indicate regulation that is not significantly different. Only the significantly up- or downregulated genes shown in Tables 1.3 and 1.4 are labeled in this figure.

treatments to the untreated control at 24 h. Figure 1.S6 shows scatterplots of the 4 h treatments as well as the 24 h treatment with GFP pDNA (EF1α) polyplexes, and Table 1.S2 shows the full cell cycle array results.

We observed substantial upregulation of chemokine, interleukin, and toll-like receptor (TLR) genes on the inflammatory response and autoimmunity array (Table 1.4). The chemokine ligand genes (*CCL22*, *CCL3*, *CCL5*, and *CXCL10*) in the polyplex-exposed samples exhibited the highest magnitude upregulation, up to 1000-fold over the negative control. *TNF* and a number of interleukin genes (e.g., *IL1A*, *IL1B*, *IL1R1*, *IL1RN*, *IL23A*, and *IL6*), a class of cytokines that act as key regulators of the inflammatory response, were also highly upregulated in polyplex-exposed samples in comparison to the polymer-only treatment. Some genes encoding TLRs (*TLR1*, *TLR3*, *TLR4*, and *TLR5*), membrane-spanning proteins that activate inflammatory responses,[39] were additionally strongly affected by the polyplex treatments. Table 1.S3 shows the full inflammatory response and autoimmunity array results. Figures 1.4c and 1.4d show selected scatterplots for the 24 h time point comparing the gene regulation of the

Table 1.4: Changes in expression of selected genes related to inflammatory response and autoimmunity in jetPEI™ or polyplex-exposed HeLa S3 cells.

			Fold Change in Gene Expression[b]					
			jetPEI™		GFP (CMV) polyplexes		GFP (EF1α) polyplexes	
GeneBank	**Symbol**	**Description**[a]	4h	24h	4h	24h	4h	24h
NM_002990	CCL22	Chemokine (C-C motif) ligand 22	3.6	6.8	5.4	**272.8**	4.3	**213.1**
NM_002983	CCL3	Chemokine (C-C motif) ligand 3	-1.2	**46.5**	-1.1	**1084.1**	1.9	**989.4**
NM_002985	CCL5	Chemokine (C-C motif) ligand 5	1.1	**2.4**	**4.5**	**109.6**	**4.1**	**116.2**
NM_001295	CCR1	Chemokine (C-C motif) receptor 1	1.4	1.1	1.8	**24.2**	-2.0	**20.1**
NM_001565	CXCL10	Chemokine (C-X-C motif) ligand 10	-2.4	2.6	2.3	**553.0**	2.1	**652.0**
NM_000575	IL1A	Interleukin 1, alpha	**-2.1**	**3.3**	-1.0	**9.0**	1.1	**7.3**
NM_000576	IL1B	Interleukin 1, beta	-1.7	**2.6**	-1.2	**7.3**	-1.3	**6.3**
NM_000877	IL1R1	Interleukin 1 receptor, type I	**-6.8**	1.0	-3.4	**3.6**	**-5.8**	**3.1**
NM_000577	IL1RN	Interleukin 1 receptor antagonist	1.4	2.0	-1.1	**4.6**	1.0	**6.0**
NM_016584	IL23A	Interleukin 23, alpha subunit p19	-1.2	1.1	1.2	**7.2**	-1.6	**6.1**
NM_000600	IL6	Interleukin 6 (interferon, beta 2)	1.4	1.6	**7.5**	**11.8**	**7.1**	**12.4**
NM_003263	TLR1	Toll-like receptor 1	**-5.8**	1.2	-1.6	**3.4**	-2.4	**2.8**
NM_003265	TLR3	Toll-like receptor 3	**-2.2**	1.1	-1.9	**11.5**	-1.7	**10.8**
NM_138554	TLR4	Toll-like receptor 4	1.1	1.6	-1.2	**3.9**	-1.3	**4.3**
NM_003268	TLR5	Toll-like receptor 5	1.2	-6.5	1.5	5.8	1.5	**9.6**
NM_000594	TNF	Tumor necrosis factor (TNF superfamily, member 2)	**13.0**	1.2	**18.6**	**14.9**	**14.6**	**14.1**

[a]The gene descriptions are reproduced from the array product information from Qiagen.
[b]Green and red shading indicate fold-changes of ≥ 2 and ≤ 2, respectively, with $p \leq .05$.

jetPEI™ and GFP pDNA (CMV) polyplex treatments to the untreated control. Figure 1.S6 shows scatterplots of the 4 h treatments as well as the 24 h treatment with GFP pDNA (EF1α) polyplexes.

1.4 Discussion

1.4.1 Protein Expression Can Occur Without Cell Division

We developed a new approach to assess the relationship of cell division and protein expression. The results show that the number of divided cells is consistently higher than the number of protein-expressing cells, in apparent support of a model where division is required for gene expression. However, when we delineated the number of protein-expressing cells that divided, it became clear that a division-independent protein expression pathway was operative, regardless of the level of protein expression.

For 293A cells, the majority of cells that expressed protein also divided. Although this appears to support a division-dependent pathway for protein expression, we observed that 7% to 31% of protein-expressing cells had not divided. In HeLa S3 cells, 44 to 86% of protein-expressing cells had not divided, again showing that protein expression can occur without division, and consistent with a previous study that showed a lack of cell cycle dependence in HeLa cells for transfections with linear PEI.[40] Grandinetti *et al.* have also shown that linear PEI can induce nuclear membrane permeability, providing a possible route for nucleic acid entry into the nucleus.[41]

We acknowledge that in four of the six 293A experiments (#1, #3, #5, and #6), (a) the number of protein-expressing cells that did not divide is very close to (b) the standard deviation of the number of protein-expressing cells divided. This could mean that for these four experiments, there are actually no protein-expressing cells that have not divided. In all HeLa S3 experiments (and in experiments #2 and #7 in 293A cells), however, (a) is much greater than (b). Altogether, the data clearly show that protein expression can occur without cell division in HeLa S3 cells, and suggest that this is the case for 293A cells as well.

Our study improves understanding of transfection pathways by demonstrating that the apparent expression pathway is consistent with previous studies showing that cell division is required, but only when one cannot look at the different cell subpopulations. When using the quantitative methods employed here, which allow the division of protein-expressing cells to be analyzed, we find that protein expression can occur without division. Indeed, the apparent consistency for the overall cell population with a division-dependent pathway may arise from a coincidence of similar rates of protein expression and cell division.

1.4.2 Polyplex Exposure Slows the Doubling Time of HeLa S3 and 293A Cells

This study also improves current understanding of transfection by showing that transfection and subsequent protein expression slow cell division, which studies that employ nondividing cells could not detect. We employed a number of controls to determine the cause of the slowed division, such as a "blank" pDNA of comparable size to the CFP-encoding pDNA. The blank pDNA contains the same cytomegalovirus (CMV) transgene promoter but does not encode any fluorescent reporter protein. The slowed division of HeLa S3 and 293A cells is not attributable to toxicity of the generated fluorescent protein because when cells are exposed to blank pDNA polyplexes, division is slowed to a similar extent.

We also formed polyplexes with two pDNAs that encode GFP, one containing a viral transgene promoter (CMV) and the other of completely nonviral origin, containing the EF1α transgene promoter. These pDNAs were used because it has previously been shown that transfection can lead to upregulation of some cytokines (e.g., TNFα, IFNγ, and IL-10) that are able to differentially affect the activity of viral promoters such as CMV in comparison to nonviral promoters such as EF1α.[42-47] We had hypothesized that a pDNA lacking any viral origin would be unaffected by the cytokine upregulation, possibly yielding a normal doubling time. However, regardless of the type of DNA used in the polyplexes, division was consistently slowed.

We also find that the slowed division is not related to a cationic charge density effect of the free polymer, because cells exposed to only free polymer divide at a similar

rate as control cells. The amount of free polymer that cells are exposed to in the polymer-only treatments is the same as the total amount of polymer used in the polyplex formulations. The amount of excess free polymer in the polyplex formulations is necessarily less than that in the free polymer only case because the DNA in the polyplex formulations electrostatically binds some of the polymer.

In summary, we find that the generated protein product, the origin of the pDNA transgene promoter, and the cationic charge concentration do not cause the slowed cell division. As another control, we made polyplexes with sheared salmon sperm DNA (ssDNA), which is nonfunctional in terms of expression. Dynamic light scattering measurements of the hydrodynamic diameter of polyplexes formed with the pDNAs or the ssDNA show no appreciable differences (data not shown). Interestingly, exposure to polyplexes made with ssDNA slowed the doubling times of both cell lines, suggesting that a combination of the size and charge of the polyplexes, and perhaps simply the introduction of non-native DNA, was required to slow the doubling time. Particle size and surface properties have previously been found to affect cellular uptake and responses.[48,49] The slowed division appears to be a result of toxicity of the polyplexes on the cell, and this was further explored using gene expression arrays.

1.4.3 Cells Exposed to Polyplexes Do Not Enter Cellular Senescence

We investigated senescence, a postmitotic state where cells are no longer able to divide, as a possible mechanism by which the doubling times of polyplex-exposed HeLa S3 and 293A cells were slowed. Replicative senescence was not induced in any sample over the basal level observed in the control. Bringold and Serrano[50] have previously shown that *in vitro* upregulation of cyclin-dependent kinase inhibitors $p16^{INK4a}$, $p21^{Cip1}$, and $p27^{Kip1}$ can cause senescence; the PCR arrays described here show no change in gene expression for $p16^{INK4a}$ or $p27^{Kip1}$ in any sample at either time point. *CDKN1A*, which encodes $p21^{Cip1}$, was upregulated 2- to 3-fold at 24 h in the cells exposed to both types of polyplexes, but the gene encoding for p53 (another protein involved in the $p21^{Cip1}$ pathway) was unaffected. Additionally, the importance of $p21^{Cip1}$ for activating senescence is debated.[51] Together, these data indicate that entering

senescence is not a biological effect of exposure to the types of polyplexes used in this study.

1.4.4 Cell Cycle and Inflammatory Response PCR Arrays Suggest Pathways for Slowed HeLa S3 Cell Division

To further probe possible mechanisms by which cell division was being slowed, gene arrays were run on total RNA isolated from HeLa S3 cells that had been exposed to either jetPEI™ only, or to polyplexes formed between jetPEI™ and either gWIZ™-GFP or gWIZ™-GFP-EF1α pDNA. The isolated RNA was analyzed by both cell cycle and inflammatory response and autoimmunity PCR arrays for changes in gene expression relative to untreated controls. The inflammatory response and autoimmunity array was used because a preliminary study (data not shown) using the cell cycle array revealed that the hit of greatest magnitude fold change, *HERC5*, had some relationship in the literature to genes related to inflammatory response.

The cell cycle array shows that the upregulated genes are generally related to stress and cell cycle arrest, and the downregulated genes are generally related to normal pathways of proliferation. *SERTAD1* and *HERC5* are exceptions to this result that are also described here. The downregulated genes on the cell cycle array, specifically *CCNB1*, *CCNF*, and *MAD2L1*, suggest that normal progression through mitosis is being inhibited. *CCNB1* encodes cyclin B1, a G_2/M-specific regulatory protein that, once activated, is involved in several of the early events of mitosis;[52] *CCNB1* is downregulated 2-fold in both polyplex-exposed samples at 24 h. *CCNF* is another gene that is similarly downregulated and encodes a G_2/M-specific cyclin.[53] *MAD2L1* functions as a mitotic checkpoint gene as it encodes a protein that delays anaphase until the chromosomes have been properly aligned.[54] The downregulation of these three genes suggest that normal progression through mitosis is being inhibited. Interestingly, *KPNA2* encodes a protein that has been shown to interact with NLSs and may regulate transport of proteins across the nuclear membrane;[55] downregulation of *KPNA2* could represent a defense mechanism against foreign genetic material entering the nucleus.

The upregulation of *CDKN1A*, *CHEK2*, and *DIRAS3* in polyplex- but not polymer-exposed cells at 24 h specifically suggests arrest in the G_1 phase of the cell cycle. First, *CDKN1* encodes the $p21^{Cip1/Waf1}$ protein in mammalian cells and is upregulated 2- to 3-fold in polyplex-exposed cells. In response to DNA damage, $p21^{Cip1/Waf1}$ has been shown to inhibit G_1/S- and S-Cdks and therefore block cell cycle progression in the G_1 phase,[56] and overexpression of $p21^{Cip1/Waf1}$ has been shown to decrease mammalian cell proliferation.[57] Second, though it has also been linked to G_2 phase arrest,[58] *CHEK2* has been shown to function as a DNA damage checkpoint by stabilization of tumor suppressor protein p53, which leads to growth arrest at the G_1/S regulation point.[59] Third, expression of the ARHI protein, encoded by *DIRAS3* which is upregulated 4- to 6-fold in polyplex-exposed samples, has been associated with decreased proliferation in some cancerous cell types.[60] In this study, Rosen et al. reported that the ARHI acted by inducing $p21^{Cip1/Waf1}$ and downregulating Cyclin D1 activity; Cyclin D1 activates G_1-specific Cdks, suggesting that expression of ARHI can inhibit the cell cycle at the G_1 phase. Together, the upregulation of these three genes indicates that a key mechanism of slowed doubling time in polyplex-exposed cells may be arrest in the G_1 phase of the cell cycle.

The upregulation of *GADD45A* in polyplex-exposed samples at 24 h is a biologically interesting result in terms of cell cycle inhibition, although the polymer-only sample shows similar upregulation. *GADD45A* can be induced by DNA damage and cell growth arrest,[61] suggesting a mechanism by which growth may be arrested in the G_2/M cell cycle phase. Tumor suppressor protein p53 transcriptionally regulates production of GADD45A protein,[61,62] however, no significant changes in *TP53* were observed here at 24 h, consistent with p53 regulation primarily occurring through post-transcriptional mechanisms.[63] Subsequent research has shown that GADD45A protein interacts with the well-known cell cycle inhibitor $p21^{Cip1}$ that is also transcriptionally regulated by p53,[64] but that GADD45A protein is also able to arrest cell cycle progression independently of p21 by inhibiting Cdk1/Cyclin B1 kinase activity,[65,66] which normally regulates cell cycle progression from G_2 to M.[52] Additionally, *CCNB1*, which encodes Cyclin B1, is downregulated 2-fold in the polyplex-exposed samples at 24 h. Because

similar upregulation is observed in polymer-exposed samples at 24 h, the upregulation of *GADD45A* in polyplex-exposed samples may be irrelevant to the observed slowed division. Alternatively, it may be the case that upregulation of *GADD45A* is a contributing factor to the observed slowed division via inhibition of progression through the M phase and subsequent division, yet that it is not sufficient to cause the slowed division alone.

SERTAD1 is an upregulated gene in polyplex-exposed samples on the cell cycle array that does not represent a cell cycle inhibition pathway. *SERTAD1* encodes the Cdk4-binding protein $p34^{SEI-1}$, also known as TRIP-BR1, and is able to antagonize the function of the Cdk inhibitor protein $p16^{INK4a}$. $p16^{INK4a}$ is normally able to target monomeric Cdks 4 and 6 and inhibit binding to cyclins in response to DNA damage or other environmental inhibitory signals.[67] A subsequent study of $p34^{SEI-1}$ revealed that it was able to activate Cdk4 in a concentration-dependent manner.[68] The 3-fold upregulation of *SERTAD1* in polyplex-exposed samples at 24 h may indicate that the cells are attempting to recover functional growth mechanisms, though recovery of a normal doubling time after 24 h was not observed.

HERC5 is upregulated by the largest magnitude of any gene on the cell cycle array, with polyplex-exposed samples showing 26- to 28-fold upregulation at 24 h. *HERC5* upregulation is indicative of an inflammatory response as it has previously been induced by the proinflammatory cytokines tumor necrosis factor α (TNFα) and interleukin 1β (IL1β).[69] Indeed, *TNF* and *IL1B* are also strongly upregulated at 24 h in both polyplex-exposed samples, consistent with the characterization of *HERC5* as a late inflammatory response gene.[69] TNFα was previously shown to be upregulated in keratinocytes in response to polyplex exposure,[70] and activation of TNFα and IL1β has been shown to be effected through TLRs,[39] which are also strongly affected here by the polyplex and polymer treatments. Interestingly, *HERC5* has recently been shown to inhibit the replication of viral particles by blocking assembly,[71] and Gao et al.[72] observed a 5-fold decrease in *HERC5* by the same cell cycle array when human epidermal keratinocytes were treated with a fullerene derivative that induces cellular senescence. *HERC5* encodes a ubiquitin ligase member of the HERC protein family called CEB1[73].

This protein has been established as an active E3 enzyme required for posttranslational conjugation of ISG15, a ubiquitin-like protein, to target proteins, with ISG15 upregulation induced by interferons α and β during antiviral responses to infection.[74] More recently, interferon regulatory factor 3 (IRF3) was shown to be a target for ISG15 conjugation by HERC5 protein;[75] IRF3 is a tightly regulated transcription factor that has been shown to mediate antiviral responses.[76]

Upregulation of various chemokine ligand and receptor genes at 24 h also indicates a significant inflammatory response to the polyplexes and, in some cases, even to the polymer alone. Chemokines play a key role in inflammatory response by chemically attracting lymphocytes to the endothelial cells secreting the chemokines. Here, a number of chemokine ligand genes were strongly upregulated in the polyplex-exposed samples, with fold changes ranging from 110- to 1084-fold above the untreated control. *CCR1*, which encodes a chemokine receptor, was also upregulated 20- to 24-fold in polyplex-exposed samples; some chemokine receptors have previously been shown to be upregulated in murine kidney tissue following polyplex administration at the same N/P ratio (10) used in this study.[77] The chemokine ligand 10 gene (*CXCL10*) was also upregulated 553- to 652-fold in polyplex-exposed samples but unchanged in the polymer-only treatments.

Interleukins are another class of cytokines whose gene expression was strongly affected at 24 h by the polyplexes, including *IL6*, *IL1R1*, *IL1RN*, and *IL23A*. Upregulation of these interleukins was observed for both polyplex-exposed samples, whereas polymer-treated samples were either unchanged or minimally upregulated (~2-fold upregulation for *IL1RN*). Upregulation of interleukins *IL10* and *IL4* in murine spleen cells in response to polyplex treatment was previously observed.[70] These gene expression data, coupled with the chemokine ligand and receptor responses, suggest that the strong inflammatory response displayed in the polyplex-treated cells is a contributing factor to the observed slowed division.

It is well appreciated that the presence of free DNA in different cellular spaces, notably the cytosol that is normally void of DNA, has been shown to induce antiviral responses.[78-81] Even so, the purported benefits of nonviral over viral gene delivery

systems almost always include that nonviral systems are less immunogenic than viral systems,[82-88] with the chief drawback of nonviral systems being a lack of comparable transfection and expression efficiency. Indeed, nonviral carriers have been used to specifically deliver anti-inflammatory drugs.[89] Our data demonstrate that exposure to nonviral gene delivery nanoparticles induces an inflammatory response in terms of gene expression, though the severity of this response in comparison to a response induced by viral gene delivery agents is not established here. It is possible that the inflammatory responses identified here are primarily related to cytosolic free pDNA that has been released from the polycationic polymeric carrier. For this reason it may be most beneficial for *in vivo* and clinical applications to pursue polymeric vectors that minimally separate from the pDNA prior to nuclear entry.[90-92]

1.5 Conclusions and Future Work

In summary, when viewed at the whole population level, this study employing PEI/pDNA polyplexes in HeLa S3 and 293A cells appears to support a model where the pathway for protein expression requires cell division. However, when the division of only protein-expressing cells is considered, there is evidence that protein expression in some cells occurs without division. These experiments provide a complementary data set using independent methods to previous studies that showed that cell division is not required for protein expression.[12-16] Additionally, we have shown that exposure to polyplexes can cause up to a 2-fold decrease in the doubling time of HeLa S3 and 293A cells. Analysis of changes in gene expression suggests that polyplex exposure slows cell division by upregulation of pathways that arrest the cell cycle in G_1, and downregulation of pathways related to mitosis. Differences in proliferation rates upon exposure to polyplexes have not been apparent using other techniques and may affect data interpretation. The implications of nanoparticle exposure causing slowed cell division and inflammatory response should be considered in research that employs nanoscale drug or gene delivery vectors.

Future work in this area should employ protein-level immunostaining experiments to understand whether observed changes on the gene array are reflected at the protein

level. Although it is useful to understand the changes in mRNA expression of the cell cycle- and inflammatory response-related genes, many of these genes are known to function at the protein level, not at the mRNA level. Therefore, the effect of polyplex exposure on downstream protein expression should be determined. Indeed, TNFα and IFNγ have been shown to have antiproliferative effects on some human and murine cell lines.[93] Initially, the Western blotting technique can be used semi-quantitatively assess the differences in protein levels in cell extracts exposed to different polyplex treatments.

Finally, gene array experiments will complement the data presented here. First, it is important to perform gene arrays on 293A cells to be able to compare to the gene regulation already observed in polyplex-treated HeLa S3 cells. In particular, the blank pDNA polyplex and ssDNA polyplex treatments showed different magnitudes of slowed cell division across the two cell lines. A gene array comparing these two treatments across the two cell lines would yield insight as to whether the different doubling time magnitudes are related to different cellular pathways. Second, the gene regulation response specific to protein-expressing cells could be identified by performing gene array experiments on isolated expressing and nonexpressing subpopulations of polyplex-treated cells. Fluorescence-activated cell sorting (FACS) would be used to isolate these subpopulations. Along with the research that has already been done, these gene array experiments will provide insight into the cellular pathways that are most dramatically affected by polyplex exposure, and this understanding will guide the development of better nonviral gene delivery materials.

1.6 References

1. Capecchi, M. R. High efficiency transformation by direct microinjection of DNA into cultured mammalian cells. *Cell* **1980,** *22*, 479-488.

2. Dean, D. A.; Dean, B. S.; Muller, S.; Smith, L. C. Sequence Requirements for Plasmid Nuclear Import. *Exp. Cell Res.* **1999,** *253*, 713-722.

3. Zabner, J.; Fasbender, A. J.; Moninger, T.; Poellinger, K. A.; Welsh, M. J. Cellular and Molecular Barriers to Gene Transfer by a Cationic Lipid. *J. Biol. Chem.* **1995,** *270*, 18997-19007.

4. Dean, D. A.; Strong, D. D.; Zimmer, W. E. Nuclear entry of nonviral vectors. *Gene Ther.* **2005,** *12*, 881-890.

5. Escriou, V.; Ciolina, C.; Helbling-Leclerc, A.; Wils, P.; Scherman, D. Cationic lipid-mediated gene transfer: Analysis of cellular uptake and nuclear import of plasmid DNA. *Cell Biol. Toxicol.* **1998,** *14*, 95-104.

6. Lam, A. P.; Dean, D. A. Progress and prospects: nuclear import of nonviral vectors. *Gene Ther.* **2010,** *17*, 439-447.

7. Vaughan, E. E.; DeGiulio, J. V.; Dean, D. A. Intracellular trafficking of plasmids for gene therapy: Mechanisms of cytoplasmic movement and nuclear import. *Curr. Gene Ther.* **2006,** *6*, 671-681.

8. Brunner, S.; Sauer, T.; Carotta, S.; Cotten, M.; Saltik, M.; Wagner, E. Cell cycle dependence of gene transfer by lipoplex, polyplex and recombinant adenovirus. *Gene Ther.* **2000,** *7*, 401-407.

9. Grosse, S.; Thévenot, G.; Monsigny, M.; Fajac, I. Which mechanism for nuclear import of plasmid DNA complexed with polyethylenimine derivatives? *J. Gene Med.* **2006,** *8*, 845-851.

10. Mortimer, I.; Tam, P.; MacLachlan, I.; Graham, R. W.; Saravolac, E. G.; Joshi, P. B. Cationic lipid-mediated transfection of cells in culture requires mitotic activity. *Gene Ther.* **1999,** *6*, 403-411.

11. Tseng, W.-C.; Haselton, F. R.; Giorgio, T. D. Mitosis enhances transgene expression of plasmid delivered by cationic liposomes. *Biochimica et Biophysica Acta* **1999,** *1445*, 53-64.

12. Dean, D. A. Import of Plasmid DNA into the Nucleus Is Sequence Specific. *Exp. Cell Res.* **1997,** *230*, 293-302.

13. Dowty, M. E.; Williams, P.; Zhang, G.; Hagstrom, J. E.; Wolff, J. A. Plasmid DNA entry into postmitotic nuclei of primary rat myotubes. *Proc. Natl. Acad. Sci. U.S.A.* **1995,** *92*, 4572-4576.

14. Ludtke, J. J.; Sebestyen, M. G.; Wolff, J. A. The Effect of Cell Division on the Cellular Dynamics of Microinjected DNA and Dextran. *Mol. Ther.* **2002,** *5*, 579-588.

15. Pollard, H.; Remy, J.-S.; Loussouarn, G.; Demolombe, S.; Behr, J.-P.; Escande, D. Polyethylenimine but Not Cationic Lipids Promotes Transgene Delivery to the Nucleus in Mammalian Cells. *J. Biol. Chem.* **1998,** *273*, 7507-7511.

16. Wilson, G. L.; Dean, B. S.; Wang, G.; Dean, D. A. Nuclear Import of Plasmid DNA in Digitonin-permeabilized Cells Requires Both Cytoplasmic Factors and Specific DNA Sequences. *J. Biol. Chem.* **1999,** *274*, 22025-22032.

17. Bergen, J. M.; Pun, S. H. Peptide-Enhanced Nucleic Acid Delivery. *MRS Bull.* **2005,** *30*, 663-667.

18. Zanta, M. A.; Belguise-Valladier, P.; Behr, J.-P. Gene delivery: A single nuclear localization signal peptide is sufficient to carry DNA to the cell nucleus. *Proc. Natl. Acad. Sci. U.S.A.* **1999,** *96*, 91-96.

19. Cooper, S. Rethinking synchronization of mammalian cells for cell cycle analysis. *Cell. Mol. Life Sci.* **2003,** *60*, 1099-1106.

20. Shedden, K.; Cooper, S. Analysis of cell-cycle-specific gene expression in human cells as determined by microarrays and double-thymidine block synchronization. *Proc. Natl. Acad. Sci. U.S.A.* **2002,** *99*, 4379-4384.

21. Minaschek, G.; Bereiter-Hahn, J.; Bertholdt, G. Quantitation of the volume of liquid injected into cells by means of pressure. *Exp. Cell Res.* **1989,** *183*, 434-442.

22. Horan, P. K.; Slezak, S. E. Stable cell membrane labelling. *Nature* **1989,** *340*, 167-168.

23. Horan, P. K.; Jensen, B. D.; Slezak, S. E. Viable Cell Labelling. U.S. Patent 4,783,401, November 8, 1988.

24. Wallace, P. K.; Tario, J. D.; Fisher, J. L.; Wallace, S. S.; Ernstoff, M. S.; Muirhead, K. A. Tracking antigen-driven responses by flow cytometry: Monitoring proliferation by dye dilution. *Cytometry, Part A* **2008,** *73A*, 1019-1034.

25. Puck, T. T.; Marcus, P. I.; Cieciura, S. J. Clonal Growth of Mammalian Cells In Vitro. *J. Exp. Med.* **1956,** *103*, 273-283.

26. Graham, F. L.; Smiley, J.; Russell, W. C.; Nairn, R. Characteristics of a Human Cell Line Transformed by DNA from Human Adenovirus Type 5. *J. Gen. Virol.* **1977,** *36*, 59-72.

27. Roederer, M.; De Rosa, S.; Gerstein, R.; Anderson, M.; Bigos, M.; Stovel, R.; Nozaki, T.; Parks, D.; Herzenberg, L.; Herzenberg, L. 8 Color, 10-parameter flow cytometry to elucidate complex leukocyte heterogeneity. *Cytometry* **1997,** *29*, 328-339.

28. Roederer, M. Compensation in Flow Cytometry. In *Current Protocols in Cytometry;* John Wiley & Sons: Hoboken, NJ, 2002; pp 1:1.14.1-1.14.20.

29. Roederer, M. Spectral compensation for flow cytometry: Visualization artifacts, limitations, and caveats. *Cytometry* **2001,** *45*, 194-205.

30. Baumgarth, N.; Roederer, M. A practical approach to multicolor flow cytometry for immunophenotyping. *J. Immunol. Methods* **2000,** *243*, 77-97.

31. Tung, J. W.; Parks, D. R.; Moore, W. A.; Herzenberg, L. A.; Herzenberg, L. A. New approaches to fluorescence compensation and visualization of FACS data. *Clin. Immunol.* **2004,** *110*, 277-283.

32. Dimri, G. P.; Lee, X.; Basile, G.; Acosta, M.; Scott, G.; Roskelley, C.; Medrano, E. E.; Linskens, M.; Rubelj, I.; Pereira-Smith, O. A biomarker that identifies senescent human cells in culture and in aging skin in vivo. *Proc. Natl. Acad. Sci. U.S.A.* **1995,** *92*, 9363-9367.

33. Schwarze, S. R.; Fu, V. X.; Desotelle, J. A.; Kenowski, M. L.; Jarrard, D. F. The Identification of Senescence-Specific Genes during Induction of Senescence in Prostate Cancer Cells. *Neoplasia* **2005,** *7*, 816-823.

34. Benjamini, Y.; Hochberg, Y. Controlling the False Discovery Rate: A Practical and Powerful Approach to Multiple Testing. *J. Roy. Stat. Soc. B Met.* **1995,** *57*, 289-300.

35. Smyth, G. K. Linear Models and Empirical Bayes Methods for Assessing Differential Expression in Microarray Experiments. *Stat. Appl. Genet. Mol. Biol.* **2004,** *3*, 1-25.

36. Gordon, A.; Colman-Lerner, A.; Chin, T. E.; Benjamin, K. R.; Yu, R. C.; Brent, R. Single-cell quantification of molecules and rates using open-source microscope-based cytometry. *Nat. Methods* **2007,** *4*, 175-181.

37. Bandyopadhyay, D.; Gatza, C.; Donehower, L. A.; Medrano, E. E. Analysis of Cellular Senescence in Culture In Vivo: The Senescence-Associated β-Galactosidase Assay. In *Current Protocols in Cell Biology;* John Wiley & Sons: Hoboken, NJ, 2005; pp 18:18.9.1-18.9.9.

38. Gyuris, J.; Golemis, E.; Chertkov, H.; Brent, R. Cdi1, a human G1 and S phase protein phosphatase that associates with Cdk2. *Cell* **1993,** *75*, 791-803.

39. Akira, S.; Takeda, K.; Kaisho, T. Toll-like receptors: critical proteins linking innate and acquired immunity. *Nat. Immunol.* **2001,** *2*, 675-80.

40. Brunner, S.; Furtbauer, E.; Sauer, T.; Kursa, M.; Wagner, E. Overcoming the Nuclear Barrier: Cell Cycle Independent Nonviral Gene Transfer with Linear Polyethylenimine or Electroporation. *Mol. Ther.* **2002,** *5*, 80-86.

41. Grandinetti, G.; Smith, A. E.; Reineke, T. M. Membrane and Nuclear Permeabilization by Polymeric pDNA Vehicles: Efficient Method for Gene Delivery or Mechanism of Cytotoxicity? *Mol. Pharmaceutics* **2011,** *9*, 523-538.

42. Audouy, S. A. L.; de Leij, L. F. M. H.; Hoekstra, D.; Molema, G. In Vivo Characteristics of Cationic Liposomes as Delivery Vectors for Gene Therapy. *Pharm. Res.* **2002,** *19*, 1599-1605.

43. Gribaudo, G.; Ravaglia, S.; Gaboli, M.; Gariglio, M.; Cavallo, R.; Landolfo, S. Interferon-α Inhibits the Murine Cytomegalovirus Immediate-Early Gene Expression by Down-Regulating NF-κB Activity. *Virology* **1995,** *211*, 251-260.

44. Harms, J. S.; Splitter, G. A. Interferon-γ inhibits transgene expression driven by SV40 or CMV promoters but augments expression driven by the mammalian MHC I promoter. *Hum. Gene Ther.* **1995,** *6*, 1291-1297.

45. Qin, L.; Ding, Y.; Pahud, D. R.; Chang, E.; Imperiale, M. J.; Bromberg, J. S. Promoter attenuation in gene therapy: Interferon-γ and tumor necrosis factor-α inhibit transgene expression. *Hum. Gene Ther.* **1997,** *8*, 2019-2029.

46. Ritter, T.; Brandt, C.; Prösch, S.; Vergopoulos, A.; Vogt, K.; Kolls, J.; Volk, H.-D. Stimulatory and inhibitory action of cytokines on the regulation of hCMV-IE promoter activity in human endothelial cells. *Cytokine* **2000,** *12*, 1163-1170.

47. Teschendorf, C.; Warrington, K. H.; Siemann, D. W.; Muzyczka, N. Comparison of the EF-1 alpha and the CMV promoter for engineering stable tumor cell lines using recombinant adeno-associated virus. *Anticancer Res.* **2002,** *22*, 3325-30.

48. Kim, J. A.; Aberg, C.; Salvati, A.; Dawson, K. A. Role of cell cycle on the cellular uptake and dilution of nanoparticles in a cell population. *Nat. Nanotechnol.* **2012,** *7*, 62-68.

49. Jiang, W.; Kim, B. Y. S.; Rutka, J. T.; Chan, W. C. W. Nanoparticle-mediated cellular response is size-dependent. *Nat. Nanotechnol.* **2008,** *3*, 145-150.

50. Bringold, F.; Serrano, M. Tumor suppressors and oncogenes in cellular senescence. *Exp. Gerontol.* **2000,** *35*, 317-329.

51. Pantoja, C.; Serrano, M. Murine fibroblasts lacking p21 undergo senescence and are resistant to transformation by oncogenic Ras. *Oncogene* **1999,** *18*, 4974-4982.

52. Morgan, D. O. *The cell cycle: principles of control;* New Science Press: London, 2007.

53. Kong, M.; Barnes, E. A.; Ollendorff, V.; Donoghue, D. J. Cyclin F regulates the nuclear localization of cyclin B1 through a cyclin-cyclin interaction. *EMBO J.* **2000,** *19*, 1378-1388.

54. Li, Y.; Benezra, R. Identification of a Human Mitotic Checkpoint Gene: hsMAD2. *Science* **1996,** *274*, 246-248.

55. Braem, C. V.; Kas, K.; Meyen, E.; Debiec-Rychter, M.; Van de Ven, W. J. M.; Voz, M. L. Identification of a Karyopherin α2 Recognition Site in PLAG1, Which Functions As a Nuclear Localization Signal. *J. Biol. Chem.* **2002,** *277*, 19673-19678.

56. Harper, J. W.; Adami, G. R.; Wei, N.; Keyomarsi, K.; Elledge, S. J. The p21 Cdk-interacting protein Cip1 is a potent inhibitor of G1 cyclin-dependent kinases. *Cell* **1993,** *75*, 805-816.

57. Xiong, Y.; Hannon, G. J.; Zhang, H.; Casso, D.; Kobayashi, R.; Beach, D. p21 is a universal inhibitor of cyclin kinases. *Nature* **1993,** *366*, 701-704.

58. Matsuoka, S.; Huang, M.; Elledge, S. J. Linkage of ATM to Cell Cycle Regulation by the Chk2 Protein Kinase. *Science* **1998,** *282*, 1893-1897.

59. Chehab, N. H.; Malikzay, A.; Appel, M.; Halazonetis, T. D. Chk2/hCds1 functions as a DNA damage checkpoint in G1 by stabilizing p53. *Genes Dev.* **2000,** *14*, 278-288.

60. Rosen, D. G.; Wang, L.; Jain, A. N.; Lu, K. H.; Luo, R. Z.; Yu, Y.; Liu, J.; Bast, R. C. Expression of the Tumor Suppressor Gene ARHI in Epithelial Ovarian Cancer Is Associated with Increased Expression of p21WAF1/CIP1 and Prolonged Progression-Free Survival. *Clin. Cancer Res.* **2004,** *10*, 6559-6566.

61. Kastan, M. B.; Zhan, Q.; El-Deiry, W. S.; Carrier, F.; Jacks, T.; Walsh, W. V.; Plunkett, B. S.; Vogelstein, B.; Fornace, A. J. A mammalian cell cycle checkpoint pathway utilizing p53 and GADD45 is defective in ataxia-telangiectasia. *Cell* **1992,** *71*, 587-597.

62. Zhan, Q.; Bae, I.; Kastan, M. B.; Fornace, A. J. The p53-dependent γ-Ray Response of GADD45. *Cancer Res.* **1994,** *54*, 2755-2760.

63. Kastan, M. B.; Onyekwere, O.; Sidransky, D.; Vogelstein, B.; Craig, R. W. Participation of p53 Protein in the Cellular Response to DNA Damage. *Cancer Res.* **1991,** *51*, 6304-6311.

64. Kearsey, J. M.; Coates, P. J.; Prescott, A. R.; Warbrick, E.; Hall, P. A. Gadd45 is a nuclear cell cycle regulated protein which interacts with p21Cip1. *Oncogene* **1995,** *11*, 1675-1683.

65. Zhan, Q.; Antinore, M. J.; Wang, X. W.; Carrier, F.; Smith, M. L.; Harris, C. C.; Fornace, A. J. Association with Cdc2 and inhibition of Cdc2/Cyclin B1 kinase activity by the p53-regulated protein Gadd45. *Oncogene* **1999,** *18*, 2892-2900.

66. Zhao, H.; Jin, S.; Antinore, M. J.; Lung, F.-D. T.; Fan, F.; Blanck, P.; Roller, P.; Fornace, A. J.; Zhan, Q. The Central Region of Gadd45 Is Required for Its Interaction with p21/WAF1. *Exp. Cell Res.* **2000,** *258*, 92-100.

67. Sugimoto, M.; Nakamura, T.; Ohtani, N.; Hampson, L.; Hampson, I. N.; Shimamoto, A.; Furuichi, Y.; Okumura, K.; Niwa, S.; Taya, Y.; Hara, E. Regulation of CDK4 activity by a novel CDK4-binding protein, p34SEI-1. *Genes Dev.* **1999,** *13*, 3027-3033.

68. Li, J.; Melvin, W. S.; Tsai, M.-D.; Muscarella, P. The Nuclear Protein p34SEI-1 Regulates the Kinase Activity of Cyclin-Dependent Kinase 4 in a Concentration-Dependent Manner. *Biochemistry* **2004,** *43*, 4394-4399.

69. Kroismayr, R.; Baranyi, U.; Stehlik, C.; Dorfleutner, A.; Binder, B. R.; Lipp, J. HERC5, a HECT E3 ubiquitin ligase tightly regulated in LPS activated endothelial cells. *J. Cell Sci.* **2004,** *117*, 4749-4756.

70. Kawase, A.; Isaji, K.; Yamaoka, A.; Kobayashi, N.; Nishikawa, M.; Takakura, Y. Enhanced antigen-specific antibody production following polyplex-based DNA vaccination via the intradermal route in mice. *Vaccine* **2006,** *24*, 5535-5545.

71. Woods, M. W.; Kelly, J. N.; Hattlmann, C. J.; Tong, J. G. K.; Xu, L. S.; Coleman, M. D.; Quest, G. R.; Smiley, J. R.; Barr, S. D. Human HERC5 restricts an early state of HIV-1 assembly by a mechanism correlating with the ISGylation of Gag. *Retrovirology* **2011,** *8*, 1-17.

72. Gao, J.; Wang, H. L.; Shreve, A.; Iyer, R. Fullerene derivatives induce premature senescence: A new toxicity paradigm or novel biomedical applications. *Toxicol. Appl. Pharmacol.* **2010,** *244*, 130-143.

73. Mitsui, K.; Nakanishi, M.; Ohtsuka, S.; Norwood, T. H.; Okabayashi, K.; Miyamoto, C.; Tanaka, K.; Yoshimura, A.; Ohtsubo, M. A Novel Human Gene Encoding HECT Domain and RCC1-like Repeats Interacts with Cyclins and Is Potentially Regulated by the Tumor Suppressor Proteins. *Biochem. Biophys. Res. Commun.* **1999,** *266*, 115-122.

74. Dastur, A.; Beaudenon, S.; Kelley, M.; Krug, R. M.; Huibregtse, J. M. Herc5, an Interferon-induced HECT E3 Enzyme, Is Required for Conjugation of ISG15 in Human Cells. *J. Biol. Chem.* **2006,** *281*, 4334-4338.

75. Shi, H.-X.; Yang, K.; Liu, X.; Liu, X.-Y.; Wei, B.; Shan, Y.-F.; Zhu, L.-H.; Wang, C. Positive Regulation of Interferon Regulatory Factor 3 Activation by Herc5 via ISG15 Modification. *Mol. Cell. Biol.* **2010,** *30*, 2424-2436.

76. Collins, S. E.; Noyce, R. S.; Mossman, K. L. Innate Cellular Response to Virus Particle Entry Requires IRF3 but Not Virus Replication. *J. Virol.* **2004,** *78*, 1706-1717.

77. Jeong, G.-J.; Byun, H.-M.; Kim, J. M.; Yoon, H.; Choi, H.-G.; Kim, W.-K.; Kim, S.-J.; Oh, Y.-K. Biodistribution and tissue expression kinetics of plasmid DNA complexed with polyethylenimines of different molecular weight and structure. *J. Controlled Release* **2007,** *118*, 118-125.

78. Hornung, V.; Latz, E. Intracellular DNA recognition. *Nat. Rev. Immunol.* **2010,** *10*, 123-130.

79. Park, J.-H.; Chang, S.-H.; Kim, M.-C.; Shin, S.-H.; Youn, H.-J.; Kim, J.-K.; Jang, Y.-S.; Kim, C.-W. Up-regulation of the expression of major histocompatibility complex class I antigens by plasmid DNA transfection in non-hematopoietic cells. *FEBS Lett.* **1998,** *436*, 55-60.

80. Ishii, K. J.; Coban, C.; Kato, H.; Takahashi, K.; Torii, Y.; Takeshita, F.; Ludwig, H.; Sutter, G.; Suzuki, K.; Hemmi, H.; Sato, S.; Yamamoto, M.; Uematsu, S.; Kawai, T.; Takeuchi, O.; Akira, S. A Toll-like receptor-independent antiviral response induced by double-stranded B-form DNA. *Nat. Immunol.* **2006,** *7*, 40-48.

81. Stetson, D. B.; Medzhitov, R. Recognition of Cytosolic DNA Activates an IRF3-Dependent Innate Immune Response. *Immunity* **2006,** *24*, 93-103.

82. Thomas, M.; Klibanov, A. M. Non-viral gene therapy: polycation-mediated DNA delivery. *Appl. Microbiol. Biotechnol.* **2003,** *62*, 27-34-34.

83. Lechardeur, D.; Verkman, A. S.; Lukacs, G. L. Intracellular routing of plasmid DNA during non-viral gene transfer. *Adv. Drug Delivery Rev.* **2005,** *57*, 755-767.

84. Medina-Kauwe, L. K.; Xie, J.; Hamm-Alvarez, S. Intracellular trafficking of nonviral vectors. *Gene Ther.* **2005,** *12*, 1734-1751.

85. Nabel, G. J.; Nabel, E. G.; Yang, Z. Y.; Fox, B. A.; Plautz, G. E.; Gao, X.; Huang, L.; Shu, S.; Gordon, D.; Chang, A. E. Direct gene transfer with DNA-liposome complexes in melanoma: expression, biologic activity, and lack of toxicity in humans. *Proc. Natl. Acad. Sci. U.S.A.* **1993,** *90*, 11307-11311.

86. Khalil, I. A.; Kogure, K.; Akita, H.; Harashima, H. Uptake Pathways and Subsequent Intracellular Trafficking in Nonviral Gene Delivery. *Pharmacol. Rev.* **2006,** *58*, 32-45.

87. Glover, D. J.; Lipps, H. J.; Jans, D. A. Towards safe, non-viral therapeutic gene expression in humans. *Nat. Rev. Genet.* **2005,** *6*, 299-310.

88. Hsu, J.; Muro, S. Nanomedicine and Drug Delivery Strategies for Treatment of Genetic Diseases. In *Genetic Disease;* Plaseska-Karanfilska, D., Ed. InTech: Rijeka, Croatia, 2011; pp 241-266.

89. Moon, J. J.; Huang, B.; Irvine, D. J. Engineering Nano- and Microparticles to Tune Immunity. *Adv. Mater.* **2012,** *24*, 3724-3746.

90. Godbey, W. T.; Wu, K. K.; Mikos, A. G. Tracking the intracellular path of poly(ethylenimine)/DNA complexes for gene delivery. *Proc. Natl. Acad. Sci. U.S.A.* **1999,** *96*, 5177-5181.

91. Godbey, W. T.; Barry, M. A.; Saggau, P.; Wu, K. K.; Mikos, A. G. Poly(ethylenimine)-mediated transfection: A new paradigm for gene delivery. *J. Biomed. Mater. Res.* **2000,** *51*, 321-328.

92. Bieber, T.; Meissner, W.; Kostin, S.; Niemann, A.; Elsasser, H.-P. Intracellular route and transcriptional competence of polyethylenimine-DNA complexes. *J. Controlled Release* **2002,** *82*, 441-454.

93. Sugarman, B. J.; Aggarwal, B. B.; Hass, P. E.; Figari, I. S.; Palladino, M. A.; Shepard, H. M. Recombinant human tumor necrosis factor-alpha: effects on proliferation of normal and transformed cells in vitro. *Science* **1985,** *230*, 943-945.

1.7 Appendix

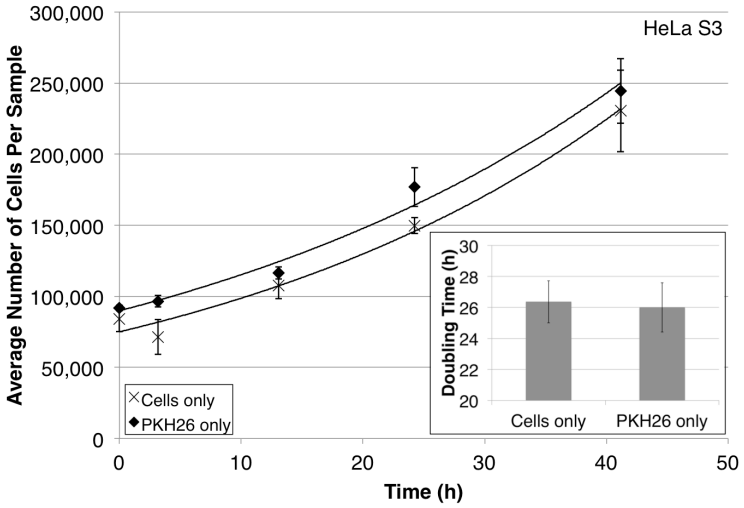

Figure 1.S1: Representative data showing that, as measured by density of cell suspensions, staining with PKH26 does not affect the proliferation rate of HeLa S3 cells as compared to control cells. Each point shows the mean ± SD of three technical replicates with curve of best exponential fit. The differences in absolute numbers of stained vs unstained cells is likely due to normal variation in cell counting prior to plating. The inset shows summary of data from three independent experiments. M = 26.0, SE = 0.79 for PKH26-stained cells as compared to M = 26.4, SE = 0.92 for control cells, $t(4) = 0.30$, $p > 0.05$.

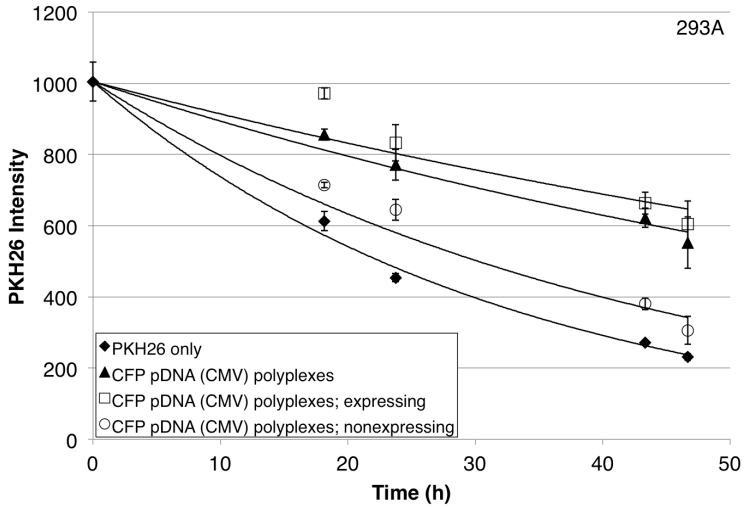

Figure 1.S2: PKH26 intensity of representative 293A cells treated with polyplexes formed between jetPEI^{TM} and CFP pDNA over 2 days following transfection as compared to control cells (PKH26 only). Cells expressing CFP (□) and those not expressing CFP (○) are subsets of the whole population (▲) that was treated with polyplexes. Cells were transfected for 3 h beginning at time = 0 h. Each point shows the mean ± SD of three technical replicates with curve of best exponential fit. All data are fit with PKH26 only data at 0 h.

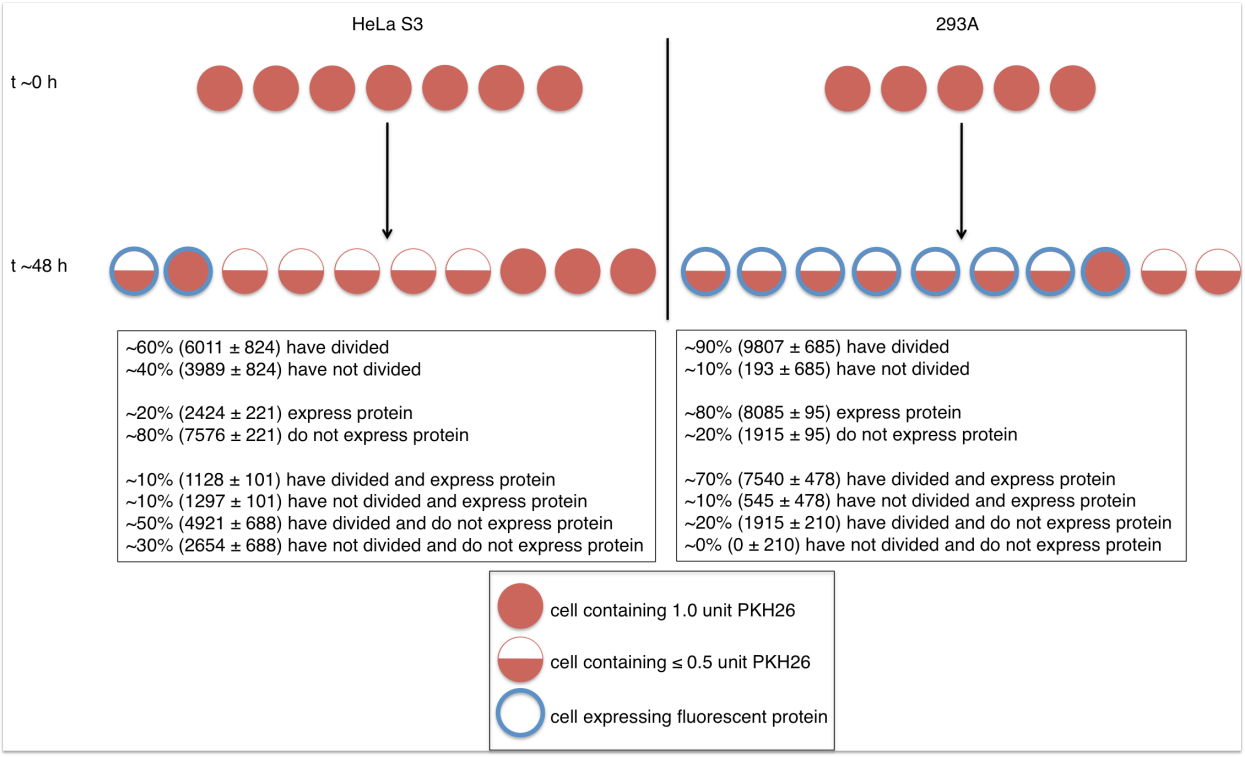

Figure 1.S3: Representative schemes showing the approximate breakdown of divided vs not divided and expressing vs not expressing cells ~48 h following transfection. Division is measured by dilution of the membrane-stable dye PKH26, and expression is measured by fluorescence of the plasmid-encoded protein. The percentages are taken from the data shown in Table 1.2 (HeLa S3, Expt #1; 293A, Expt #3).

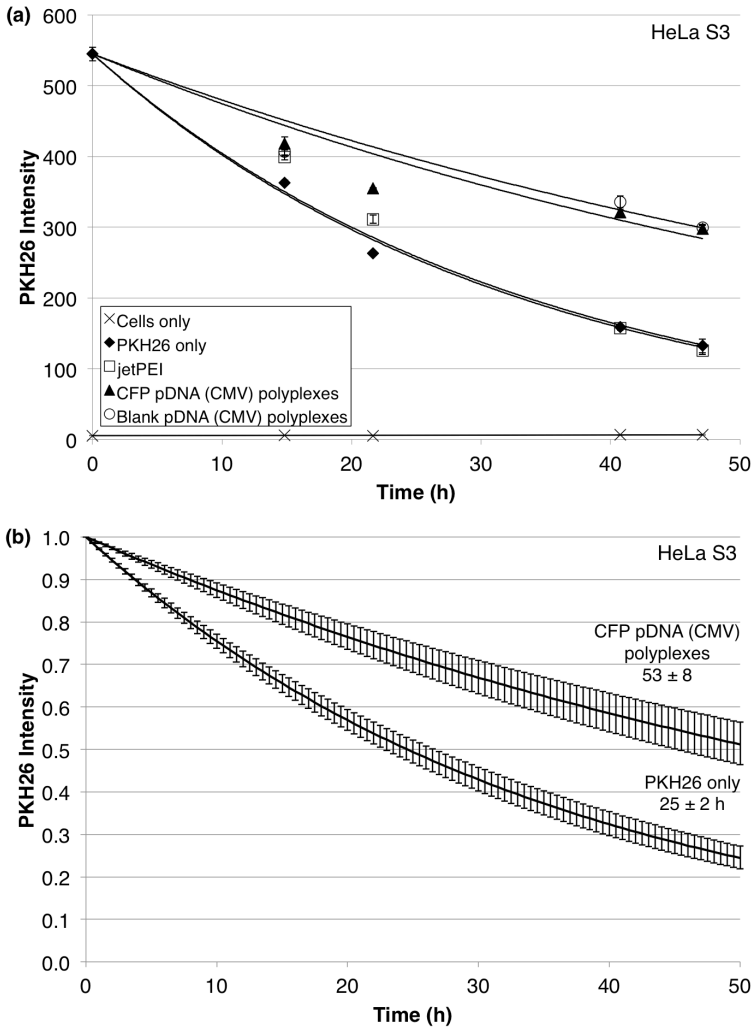

Figure 1.S4: (a) Representative data for HeLa S3 cells showing that exposure to polyplexes slows the doubling time. The cells were transfected for 3 h beginning at time = 0 h. Each point shows the mean ± SD of three technical replicates with curve of best exponential fit except for the cells only sample, which has a linear line of best fit. All data are fit with PKH26 only data at 0 h except for the cells only sample. (b) Average PKH26 intensity of untreated and CFP pDNA (CMV) polyplex-treated HeLa S3 cells over time based on the average doubling times shown in Figure 1.3b. The standard deviations reflect the standard deviations of the average doubling times.

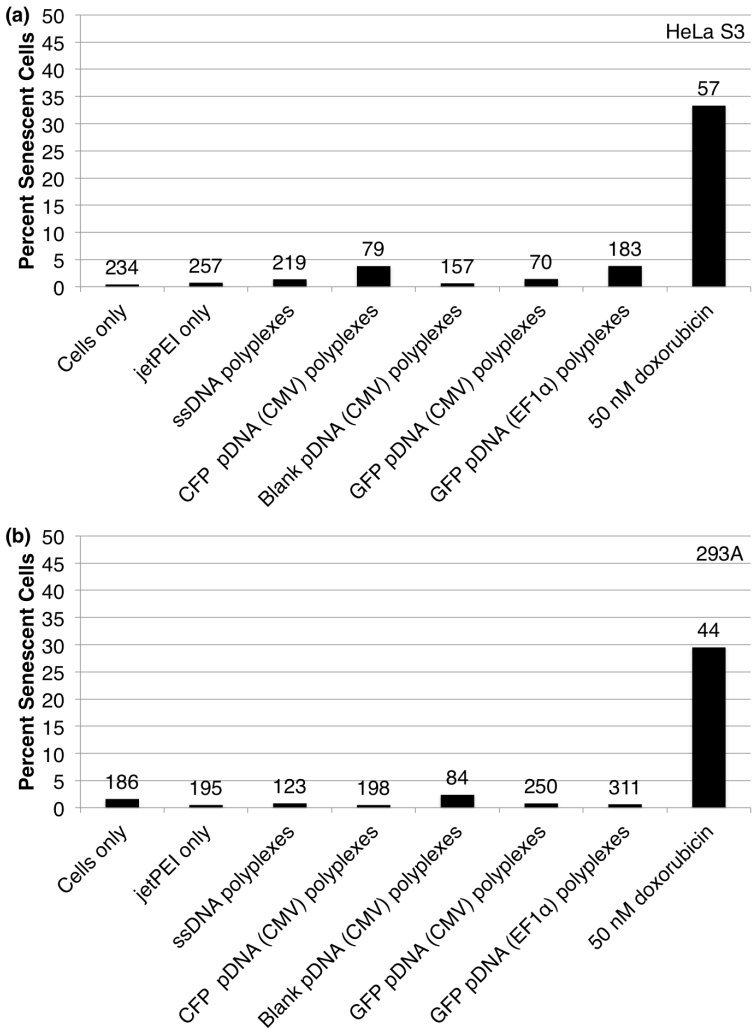

Figure 1.S5: HeLa S3 (a) and 293A (b) cells do not enter cellular senescence upon exposure to the polymer alone (jetPEI™ only) or any type of polyplex used in this study. Each data point is labeled with N, the number of cells counted for that sample. N for the doxorubicin case is lower than for the other treatments because there were fewer cells per image due to doxorubicin-induced toxicity. According to Fisher's exact test, no samples are more senescent than the cells only negative control, except for the 50 nM doxorubicin positive control. *** $p < 0.01$.

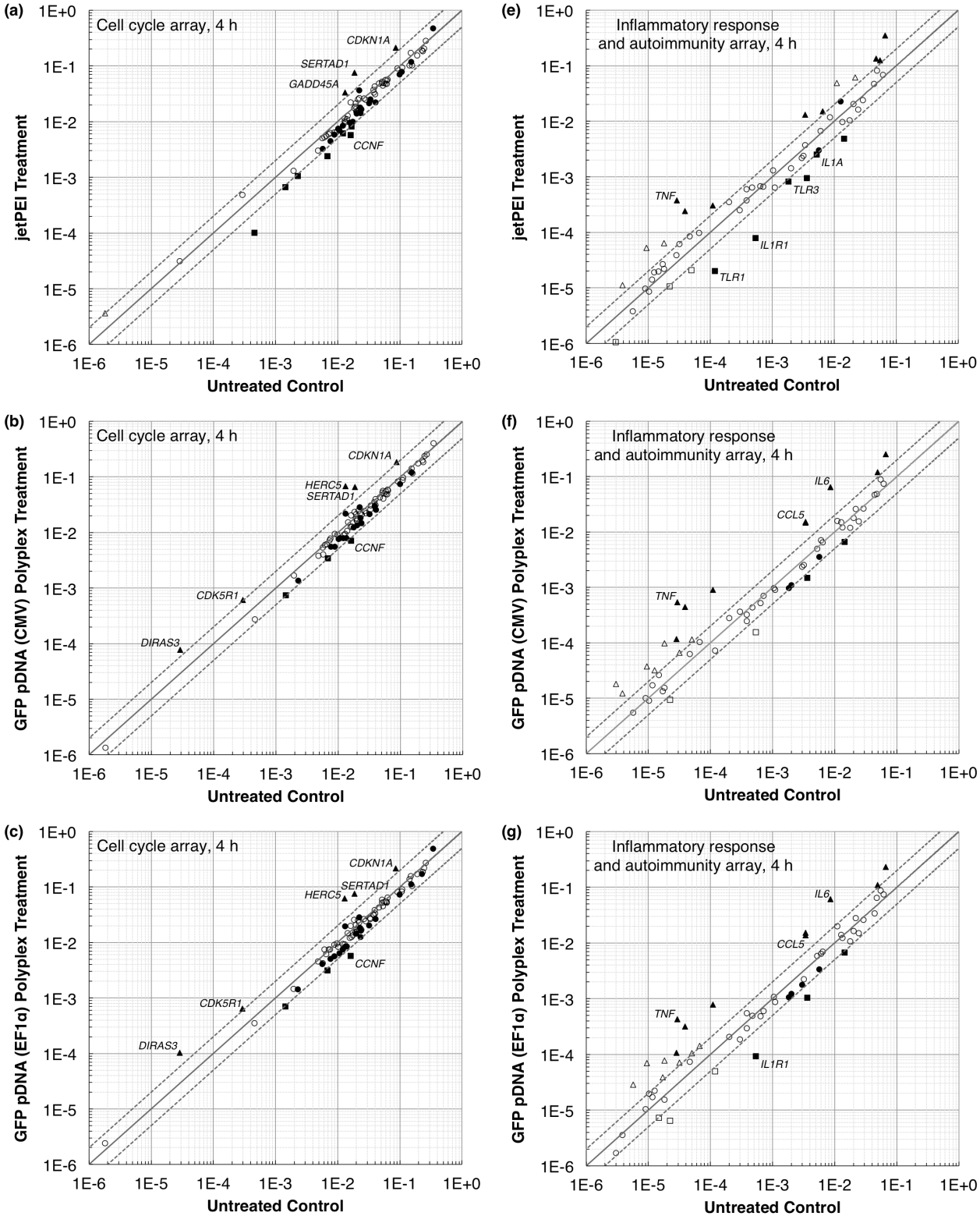
(a)
Cell cycle array, 4 h
CDKN1A
SERTAD1
GADD45A
CCNF
jetPEI Treatment
Untreated Control
(b)
Cell cycle array, 4 h
CDKN1A
HERC5
SERTAD1
CCNF
CDK5R1
DIRAS3
GFP pDNA (CMV) Polyplex Treatment
Untreated Control
(c)
Cell cycle array, 4 h
CDKN1A
SERTAD1
HERC5
CCNF
CDK5R1
DIRAS3
GFP pDNA (EF1α) Polyplex Treatment
Untreated Control
(e)
Inflammatory response
and autoimmunity array, 4 h
IL1A
TLR3
TNF
IL1R1
TLR1
jetPEI Treatment
Untreated Control
(f)
Inflammatory response
and autoimmunity array, 4 h
IL6
CCL5
TNF
GFP pDNA (CMV) Polyplex Treatment
Untreated Control
(g)
Inflammatory response
and autoimmunity array, 4 h
IL6
CCL5
TNF
IL1R1
GFP pDNA (EF1α) Polyplex Treatment
Untreated Control
1E+0
1E-1
1E-2
1E-3
1E-4
1E-5
1E-6

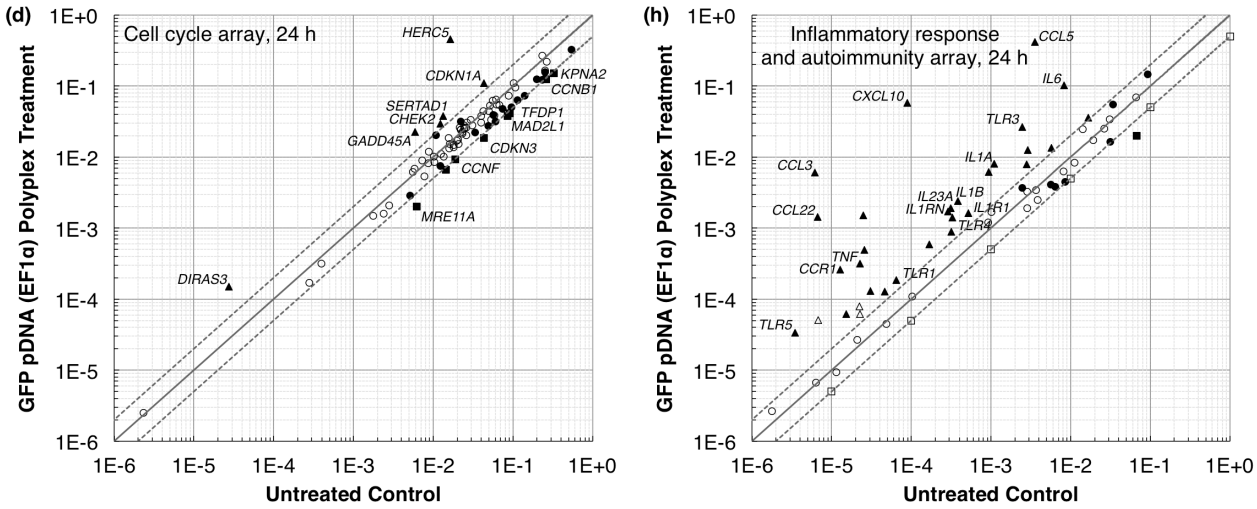

Figure 1.S6: Scatterplots (arbitrary units) showing the relative number of up- (▲) and downregulated (■) genes for the jetPEI™, GFP pDNA (CMV) polyplex, and GFP pDNA (EF1α) polyplex treatments compared to the untreated control at 4 h following transfection. The GFP pDNA (EF1α) polyplex treatment at 24 h is also shown. (a) – (d) Cell cycle array. (e) – (h) Inflammatory response and autoimmunity array. The centerline indicates a fold change ($2^{-\Delta\Delta Ct}$) of 1, meaning the gene expression is no different in the treated sample as compared to the control. The upper and lower dashed lines indicate fold changes of 2 in gene expression. Circles indicate genes with fold changes ≤ 2. Comparing to the untreated control, filled symbols indicate regulation that is significantly different ($p \leq 0.05$), and open symbols indicate regulation that is not significantly different. Only the significantly up- or downregulated genes shown in Tables 1.3 and 1.4 are labeled in this figure. Note that the cell cycle array data for the 24 h treatment with GFP pDNA (EF1α) polyplexes are based on only two biological replicates; the third had to be removed due to evident inhibition of the reverse transcription step.

Table 1.S1: Average doubling times of HeLa S3 and 293A cells exposed to jetPEI™ only, or polyplexes made between jetPEI™ and ssDNA or various pDNAs.

	Average Doubling Time (h)[a]	
Treatment	HeLa S3	293A
PKH26 only (neg. control)	25 ± 2	25 ± 3
jetPEI™ only	29 ± 2	24 ± 4
ssDNA polyplexes	31 ± 1 **	52 ± 9 **
CFP pDNA (CMV) polyplexes	53 ± 8 ***	46 ± 9 **
Blank pDNA (CMV) polyplexes	52 ± 9 **	35 ± 4 ***
GFP pDNA (CMV) polyplexes	49 ± 8	61 ± 10 *
GFP pDNA (EF1α) polyplexes	52 ± 10	45 ± 16

[a] * $p < 0.10$, ** $p < 0.05$, *** $p < 0.01$.

Table 1.S2: Changes in expression of all genes related to the cell cycle pathway in jetPEI™ or polyplex-exposed HeLa S3 cells.

			Fold Change in Gene Expression[b]					
			jetPEI™		GFP (CMV) polyplexes		GFP (EF1α) polyplexes	
GeneBank	Symbol	Description[a]	4h	24h	4h	24h	4h	24h
NM_005157	ABL1	C-abl oncogene 1, receptor tyrosine kinase	-1.4	1.2	-1.2	1.1	-1.3	1.2
NM_013366	ANAPC2	Anaphase promoting complex subunit 2	-1.6	-1.0	-1.3	-1.2	-1.3	-1.2
NM_013367	ANAPC4	Anaphase promoting complex subunit 4	-1.5	1.1	-1.3	-1.1	-1.7	-1.1
NM_000051	ATM	Ataxia telangiectasia mutated	**-2.1**	-1.3	-1.7	-1.4	-1.6	-1.4
NM_001184	ATR	Ataxia telangiectasia and Rad3 related	-1.7	-1.1	-1.4	-1.3	-1.5	-1.2
NM_004324	BAX	BCL2-associated X protein	-1.2	1.2	-1.3	-1.1	-1.2	1.1
NM_016567	BCCIP	BRCA2 and CDKN1A interacting protein	-1.2	1.3	-1.1	-1.9	-1.2	-1.9
NM_000633	BCL2	B-cell CLL/lymphoma 2	-1.5	-1.1	-1.2	-1.3	-1.3	-1.5
NM_001168	BIRC5	Baculoviral IAP repeat-containing 5	-1.1	1.0	-1.1	-1.6	-1.4	-1.8
NM_007294	BRCA1	Breast cancer 1, early onset	-1.7	1.3	-1.6	1.1	-1.9	1.2
NM_000059	BRCA2	Breast cancer 2, early onset	**-2.9**	-1.3	**-2.0**	1.3	**-2.2**	1.2
NM_031966	CCNB1	Cyclin B1	-1.3	-1.1	-1.3	**-2.1**	-1.2	**-2.1**
NM_004701	CCNB2	Cyclin B2	-1.4	-1.1	-1.3	-1.9	-1.4	-1.8
NM_005190	CCNC	Cyclin C	-1.1	1.1	-1.1	-1.1	-1.1	1.0
NM_053056	CCND1	Cyclin D1	-1.1	1.6	1.3	1.0	1.4	1.1
NM_001759	CCND2	Cyclin D2	2.0	-1.1	-1.4	1.4	1.3	1.1
NM_001238	CCNE1	Cyclin E1	1.4	1.0	1.3	-1.7	1.2	-1.3
NM_001761	CCNF	Cyclin F	**-2.8**	-1.1	**-2.3**	**-2.0**	**-2.8**	**-2.0**
NM_004060	CCNG1	Cyclin G1	-1.0	-1.4	-1.1	-1.6	-1.2	-1.4
NM_004354	CCNG2	Cyclin G2	-1.4	-1.4	-1.3	1.0	-1.2	1.2
NM_001239	CCNH	Cyclin H	-1.0	1.0	-1.1	-1.6	-1.0	-1.5
NM_001240	CCNT1	Cyclin T1	1.2	1.5	-1.0	1.1	1.0	1.1
NM_001241	CCNT2	Cyclin T2	-1.2	1.0	-1.0	1.1	1.2	1.1
NM_003903	CDC16	Cell division cycle 16 homolog (S. cerevisiae)	-1.5	1.1	-1.5	-1.1	-1.6	-1.1
NM_001786	CDC2	Cell division cycle 2, G1 to S and G2 to M	-1.4	-1.1	-1.2	-1.9	-1.3	-1.9
NM_001255	CDC20	Cell division cycle 20 homolog (S. cerevisiae)	-1.2	-1.0	-1.1	-1.6	-1.1	-1.6
NM_004359	CDC34	Cell division cycle 34 homolog (S. cerevisiae)	-1.0	1.2	-1.1	1.0	-1.3	1.2
NM_001798	CDK2	Cyclin-dependent kinase 2	1.0	-1.1	1.0	-1.3	1.0	-1.1
NM_000075	CDK4	Cyclin-dependent kinase 4	-1.3	-1.0	-1.2	-1.8	-1.3	-1.9
NM_003885	CDK5R1	Cyclin-dependent kinase 5, regulatory subunit 1 (p35)	1.6	-1.1	**2.0**	**-2.2**	**2.2**	-1.6
NM_016408	CDK5RAP1	CDK5 regulatory subunit associated protein 1	-1.2	-1.1	-1.1	-1.1	-1.1	-1.1
NM_001259	CDK6	Cyclin-dependent kinase 6	-1.1	1.2	1.1	-1.9	1.1	-1.8
NM_001799	CDK7	Cyclin-dependent kinase 7	1.2	1.1	1.2	1.1	1.2	1.1
NM_001260	CDK8	Cyclin-dependent kinase 8	-1.8	1.2	-1.4	-1.4	-1.3	-1.4
NM_000389	CDKN1A	Cyclin-dependent kinase inhibitor 1A (p21, Cip1)	**2.5**	1.4	**2.2**	**2.1**	**2.5**	**2.6**
NM_004064	CDKN1B	Cyclin-dependent kinase inhibitor 1B (p27, Kip1)	-1.4	1.1	-1.6	-1.3	-1.5	-1.2
NM_000077	CDKN2A	Cyclin-dependent kinase inhibitor 2A (melanoma, p16, inhibits CDK4)	-1.0	1.0	-1.1	1.0	-1.1	1.1
NM_004936	CDKN2B	Cyclin-dependent kinase inhibitor 2B (p15, inhibits CDK4)	1.7	1.2	1.3	-1.0	1.3	1.0
NM_005192	CDKN3	Cyclin-dependent kinase inhibitor 3	-1.3	-1.1	-1.3	**-2.3**	-1.2	**-2.3**
NM_001274	CHEK1	CHK1 checkpoint homolog (S. pombe)	-1.3	1.0	-1.3	-1.1	-1.3	1.1
NM_007194	CHEK2	CHK2 checkpoint homolog (S. pombe)	-1.2	-1.3	1.0	**2.2**	1.0	**2.4**
NM_001826	CKS1B	CDC28 protein kinase regulatory subunit 1B	1.1	1.2	-1.0	1.2	1.0	1.2
NM_001827	CKS2	CDC28 protein kinase regulatory subunit 2	1.4	-1.2	1.2	-1.8	1.4	-1.7
NM_003592	CUL1	Cullin 1	-1.3	1.1	-1.1	-1.4	-1.3	-1.3
NM_003591	CUL2	Cullin 2	-1.3	-1.0	-1.2	-1.4	-1.4	-1.3
NM_003590	CUL3	Cullin 3	**-4.5**	-1.4	-1.7	-1.1	-1.3	-1.3
NM_004399	DDX11	DEAD/H (Asp-Glu-Ala-Asp/His) box polypeptide 11	-1.4	1.1	-1.2	-1.1	-1.2	-1.1

		(CHL1-like helicase homolog, S. cerevisiae)						
NM_004675	DIRAS3	DIRAS family, GTP-binding RAS-like 3	1.1	-2.8	**2.7**	**4.2**	**3.5**	**5.5**
NM_004945	DNM2	Dynamin 2	-1.5	1.3	-1.1	1.3	-1.0	1.3
NM_001950	E2F4	E2F transcription factor 4, p107/p130-binding	-1.3	1.1	-1.3	-1.1	-1.7	-1.2
NM_001924	GADD45A	Growth arrest and DNA-damage-inducible, alpha	**2.5**	**4.0**	1.6	**3.6**	1.5	**3.8**
NM_005316	GTF2H1	General transcription factor IIH, polypeptide 1, 62kDa	-1.1	1.2	1.1	1.0	1.0	-1.0
NM_016426	GTSE1	G-2 and S-phase expressed 1	-1.3	-1.4	-1.4	**-2.***	-1.4	-1.6
NM_016323	HERC5	Hect domain and RLD 5	-1.1	1.4	**5.3**	**25.8**	**4.8**	**27.9**
NM_004507	HUS1	HUS1 checkpoint homolog (S. pombe)	-1.4	-1.0	-1.5	-1.5	-1.3	-1.4
NM_014708	KNTC1	Kinetochore associated 1	-1.4	-1.1	-1.4	-1.1	-1.3	-1.1
NM_002266	KPNA2	Karyopherin alpha 2 (RAG cohort 1, importin alpha 1)	-1.2	-1.5	-1.0	**-2.3**	-1.1	**-2.1**
NM_002358	MAD2L1	MAD2 mitotic arrest deficient-like 1 (yeast)	-1.1	-1.2	-1.1	**-2.2**	1.0	**-2.3**
NM_006341	MAD2L2	MAD2 mitotic arrest deficient-like 2 (yeast)	-1.3	-1.2	-1.3	-1.5	-1.2	-1.6
NM_004526	MCM2	Minichromosome maintenance complex component 2	-1.1	1.2	-1.1	-1.2	-1.1	-1.1
NM_002388	MCM3	Minichromosome maintenance complex component 3	-1.2	-1.2	-1.1	-1.3	-1.3	-1.2
NM_005914	MCM4	Minichromosome maintenance complex component 4	-1.2	-1.1	-1.2	-1.2	-1.1	-1.1
NM_006739	MCM5	Minichromosome maintenance complex component 5	1.1	-1.2	-1.1	-1.4	-1.1	-1.2
NM_002417	MKI67	Antigen identified by monoclonal antibody Ki-67	-1.5	1.3	-1.3	-1.1	-1.5	-1.2
NM_002431	MNAT1	Menage a trois homolog 1, cyclin H assembly factor (Xenopus laevis)	1.1	1.2	1.1	1.3	1.1	1.4
NM_005590	MRE11A	MRE11 meiotic recombination 11 homolog A (S. cerevisiae)	-1.6	-1.5	-1.3	**-2.6**	-1.1	**-3.1**
NM_002485	NBN	Nibrin	**-2.0**	-1.4	-1.5	-1.2	-1.6	-1.2
NM_182649	PCNA	Proliferating cell nuclear antigen	1.1	-1.3	-1.1	-1.7	1.0	-1.6
NM_002853	RAD1	RAD1 homolog (S. pombe)	-1.4	-1.3	-1.7	-1.9	-1.6	**-2.2**
NM_002873	RAD17	RAD17 homolog (S. pombe)	-1.5	-1.0	-1.6	-1.3	-1.6	-1.3
NM_002875	RAD51	RAD51 homolog (RecA homolog, E. coli) (S. cerevisiae)	**-2.2**	-1.1	**-2.0**	-1.2	**-2.1**	-1.2
NM_004584	RAD9A	RAD9 homolog A (S. pombe)	-1.2	1.1	1.0	1.9	1.0	1.9
NM_000321	RB1	Retinoblastoma 1	-1.4	-1.0	-1.3	-1.1	-1.2	-1.0
NM_002894	RBBP8	Retinoblastoma binding protein 8	1.1	-1.0	1.0	-1.0	-1.0	1.0
NM_002895	RBL1	Retinoblastoma-like 1 (p107)	-1.4	1.2	-1.1	1.0	-1.4	1.0
NM_005611	RBL2	Retinoblastoma-like 2 (p130)	-1.8	-1.3	-1.4	1.2	-1.3	1.1
NM_002947	RPA3	Replication protein A3, 14kDa	-1.1	-1.3	-1.1	1.1	-1.0	1.1
NM_013376	SERTAD1	SERTA domain containing 1	**4.1**	1.7	**3.5**	**2.8**	**4.1**	**2.8**
NM_005983	SKP2	S-phase kinase-associated protein 2 (p45)	-1.8	-1.3	-1.6	-1.9	-1.5	-1.9
NM_003352	SUMO1	SMT3 suppressor of mif two 3 homolog 1 (S. cerevisiae)	-1.2	-1.8	-1.3	-1.6	-1.2	-1.5
NM_007111	TFDP1	Transcription factor Dp-1	-1.2	-1.2	-1.3	**-2.1**	-1.2	**-2.2**
NM_006286	TFDP2	Transcription factor Dp-2 (E2F dimerization partner 2)	-1.4	-1.1	1.1	-1.0	1.0	-1.0
NM_000546	TP53	Tumor protein p53	**-2.0**	-1.7	-1.3	-1.6	-1.3	-1.6
NM_003334	UBA1	Ubiquitin-like modifier activating enzyme 1	-1.4	-1.3	-1.1	-1.5	-1.0	-1.5

[a]The gene descriptions are reproduced from the array product information from Qiagen.
[b]Green and red shading indicate fold-changes of ≥ 2 and ≤ 2, respectively, with $p \leq 0.05$. There were no genes that did not reach the cycle threshold value within 40 cycles.

Table 1.S3: Changes in expression of all genes related to inflammatory response and autoimmunity in jetPEI™ or polyplex-exposed HeLa S3 cells.

			Fold Change in Gene Expression[b]					
			jetPEI™		GFP (CMV) polyplexes		GFP (EF1α) polyplexes	
GeneBank	Symbol	Description[a]	4h	24h	4h	24h	4h	24h
NM_001706	BCL6	B-cell CLL/lymphoma 6	**3.9**	1.5	**4.4**	**2.1**	**4.5**	**2.3**
NM_000064	C3	Complement component 3	1.1	1.0	1.1	1.4	-1.3	-1.1
NM_004054	C3AR1	Complement component 3a receptor 1	1.6	-1.9	-1.3	**18.9**	2.3	**19.0**
NM_007293	C4A	Complement component 4A (Rodgers blood group)	-1.0	**2.2**	-1.6	**4.8**	-1.3	**2.8**
NM_006274	CCL19	Chemokine (C-C motif) ligand 19	1.2	-2.1	-1.2	-1.1	-1.2	-1.2
NM_002982	CCL2	Chemokine (C-C motif) ligand 2	1.5	1.5	2.6	-6.1	1.8	-1.1
NM_002989	CCL21	Chemokine (C-C motif) ligand 21	1.7	1.1	1.4	1.1	1.0	1.0
NM_002990	CCL22	Chemokine (C-C motif) ligand 22	3.6	6.8	5.4	**272.8**	4.3	**213.1**
NM_002991	CCL24	Chemokine (C-C motif) ligand 24	1.6	-1.0	-1.2	1.4	1.4	1.3
NM_002983	CCL3	Chemokine (C-C motif) ligand 3	-1.2	**46.5**	-1.1	**1084.1**	1.9	**989.4**
NM_002985	CCL5	Chemokine (C-C motif) ligand 5	1.1	**2.4**	**4.5**	**109.6**	**4.1**	**116.2**
NM_001295	CCR1	Chemokine (C-C motif) receptor 1	1.4	1.1	1.8	**24.2**	-2.0	**20.1**
NM_005508	CCR4	Chemokine (C-C motif) receptor 4	1.5	3.2	1.6	5.8	2.1	2.7
NM_001838	CCR7	Chemokine (C-C motif) receptor 7	1.9	-2.3	2.1	3.1	2.2	3.5
NM_005194	CEBPB	CCAAT/enhancer binding protein (C/EBP), beta	1.6	1.1	**2.5**	1.7	**2.2**	1.0
NM_000757	CSF1	Colony stimulating factor 1 (macrophage)	-1.1	**2.1**	-1.0	**8.0**	-1.2	**6.6**
NM_001511	CXCL1	Chemokine (C-X-C motif) ligand 1 (melanoma growth stimulating activity, alpha)	**2.3**	-1.0	1.0	-1.3	1.1	-1.7
NM_001565	CXCL10	Chemokine (C-X-C motif) ligand 10	-2.4	2.6	2.3	**553.0**	2.1	**652.0**
NM_002089	CXCL2	Chemokine (C-X-C motif) ligand 2	2.8	1.2	1.2	-1.3	1.3	-1.3
NM_002090	CXCL3	Chemokine (C-X-C motif) ligand 3	4.4	1.2	1.4	-1.8	1.8	-1.5
NM_002994	CXCL5	Chemokine (C-X-C motif) ligand 5	2.9	-2.8	3.2	-1.1	-1.1	1.1
NM_002993	CXCL6	Chemokine (C-X-C motif) ligand 6 (granulocyte chemotactic protein 2)	-2.8	9.0	6.0	-1.0	-1.8	1.5
NM_003467	CXCR4	Chemokine (C-X-C motif) receptor 4	**2.3**	1.3	1.6	-1.6	1.6	-1.9
NM_000639	FASLG	Fas ligand (TNF superfamily, member 6)	1.1	-1.0	1.1	1.9	1.2	-2.1
NM_001459	FLT3LG	Fms-related tyrosine kinase 3 ligand	-1.4	1.0	-1.8	**2.1**	-1.6	1.5
NM_005252	FOS	V-fos FBJ murine osteosarcoma viral oncogene homolog	**5.3**	**-2.5**	**3.8**	**-2.5**	**3.5**	**-3.4**
NM_006037	HDAC4	Histone deacetylase 4	-1.9	1.0	-1.6	-1.5	-1.7	-1.9
NM_000572	IL10	Interleukin 10	-1.5	1.1	-1.0	1.3	5.1	7.6
NM_000628	IL10RB	Interleukin 10 receptor, beta	-1.7	1.1	-1.5	2.1	-1.7	1.7
NM_001562	IL18	Interleukin 18 (interferon-gamma-inducing factor)	1.1	1.1	1.2	1.5	1.2	1.6
NM_000575	IL1A	Interleukin 1, alpha	**-2.1**	**3.3**	-1.0	**9.0**	1.1	**7.3**
NM_000576	IL1B	Interleukin 1, beta	-1.7	**2.6**	-1.2	**7.3**	-1.3	**6.3**
NM_000877	IL1R1	Interleukin 1 receptor, type I	**-6.8**	1.0	-3.4	**3.6**	**-5.8**	**3.1**
NM_002182	IL1RAP	Interleukin 1 receptor accessory protein	1.1	1.1	1.2	-1.1	1.1	-1.4
NM_000577	IL1RN	Interleukin 1 receptor antagonist	1.4	2.0	-1.1	**4.6**	1.0	**6.0**
NM_016584	IL23A	Interleukin 23, alpha subunit p19	-1.2	1.1	1.2	**7.2**	-1.6	**6.1**
NM_000600	IL6	Interleukin 6 (interferon, beta 2)	1.4	1.6	**7.5**	**11.8**	**7.1**	**12.4**
NM_000565	IL6R	Interleukin 6 receptor	1.8	**2.4**	1.2	1.2	1.1	-1.1
NM_000584	IL8	Interleukin 8	**2.8**	**2.6**	1.0	**3.4**	1.3	**2.8**
NM_000211	ITGB2	Integrin, beta 2 (complement component 3 receptor 3 and 4 subunit)	1.3	1.1	-1.1	1.6	1.0	1.6
NM_000595	LTA	Lymphotoxin alpha (TNF superfamily, member 1)	**6.2**	**4.2**	**11.4**	**53.8**	**8.1**	**60.7**
NM_002341	LTB	Lymphotoxin beta (TNF superfamily, member 3)	1.8	1.6	1.3	**2.8**	1.6	**4.1**
NM_015364	LY96	Lymphocyte antigen 96	-2.1	2.9	-2.4	2.5	-3.5	**4.3**
NM_002468	MYD88	Myeloid differentiation primary response gene (88)	-1.3	1.3	-1.3	**6.0**	-1.4	**4.3**
NM_004555	NFATC3	Nuclear factor of activated T-cells, cytoplasmic, calcineurin-dependent 3	-1.5	-1.1	-1.6	-1.0	-1.6	-1.1
NM_003998	NFKB1	Nuclear factor of kappa light polypeptide gene	1.0	1.1	-1.1	1.0	-1.2	1.1

		enhancer in B-cells 1						
NM_000625	NOS2	Nitric oxide synthase 2, inducible	**2.8**	1.1	**8.2**	**4.0**	**7.2**	**3.5**
NM_000176	NR3C1	Nuclear receptor subfamily 3, group C, member 1 (glucocorticoid receptor)	-1.2	1.1	-1.1	1.9	-1.1	1.6
NM_003821	RIPK2	Receptor-interacting serine-threonine kinase 2	-1.4	1.2	-1.1	**2.1**	-1.1	**2.2**
NM_001039661	TIRAP	Toll-interleukin 1 receptor (TIR) domain containing adaptor protein	**-3.8**	-1.0	**-2.4**	-1.1	**-3.4**	-1.5
NM_003263	TLR1	Toll-like receptor 1	**-5.8**	1.2	-1.6	**3.4**	-2.4	**2.8**
NM_003265	TLR3	Toll-like receptor 3	**-2.2**	1.1	-1.9	**11.5**	-1.7	**10.8**
NM_138554	TLR4	Toll-like receptor 4	1.1	1.6	-1.2	**3.9**	-1.3	**4.3**
NM_003268	TLR5	Toll-like receptor 5	1.2	-6.5	1.5	5.8	1.5	**9.6**
NM_006068	TLR6	Toll-like receptor 6	**-3.0**	1.1	**-2.2**	-1.1	**-2.1**	-1.3
NM_016562	TLR7	Toll-like receptor 7	5.6	-1.0	3.9	-1.0	7.4	1.3
NM_000594	TNF	Tumor necrosis factor (TNF superfamily, member 2)	**13.0**	1.2	**18.6**	**14.9**	**14.6**	**14.1**
NM_003807	TNFSF14	Tumor necrosis factor (ligand) superfamily, member 14	1.4	2.6	**4.1**	**5.2**	**3.8**	**2.8**
NM_019009	TOLLIP	Toll interacting protein	-1.4	1.2	-1.3	1.4	-1.7	1.2

[a]The gene descriptions are reproduced from the array product information from Qiagen. [b]Green and red shading indicate fold-changes of ≥ 2 and ≤ 2, respectively, with $p \leq 0.05$. Genes that were analyzed on the array but that did not reach the cycle threshold value within 40 cycles are *CCL11*, *CCL13*, *CCL16*, *CCL17*, *CCL23*, *CCL4*, *CCL7*, *CCL8*, *CCR2*, *CCR3*, *CD40*, *CD40LG*, *CRP*, *CXCL9*, *IFNG*, *IL18RAP*, *IL1F10*, *IL22*, *IL22RA2*, *IL23R*, *IL8RA*, *IL8RB*, *IL9*, *KNG1*, and *TLR2*.

Chapter 2

Cell Volume Changes During Apoptosis Monitored in Real Time Using Digital Holographic Microscopy[1]

2.1 Introduction

Digital holographic microscopy (DHM) is a recent and important high-resolution imaging technique that allows the user to obtain quantitative information about the sample being imaged. DHM has previously been used to image a number of microstructures and biological systems.[1-5] The application of DHM to live cell imaging is particularly useful for obtaining quantitative information about cell thickness and volume[6,7] which remain fairly difficult parameters to study in live cells. Additionally, cells studied by DHM can be imaged with light sources well below phototoxic levels, without staining or labeling procedures, and single cells and cell populations can be studied over time. DHM has previously been employed to image many types of cells and cellular features. Plant cells[8] and stem cells,[9] for example, have been imaged using DHM in addition to a number of types of mammalian cells.[10-12] Cellular features and processes such as cell division,[13,14] cell morphology,[15] and cell movement[16] have also been

[1]Portions of this chapter have been published: (1) Khmaladze, A.; Matz, R. L.; Zhang, C.; Wang, T.; Banaszak Holl, M. M.; Chen, Z. Dual-Wavelength Linear Regression Phase Unwrapping in Three-Dimensional Microscopic Images of Cancer Cells. *Opt. Lett.* **2011,** *36*, 912-914. (2) Khmaladze, A.; Matz, R. L.; Epstein, T.; Jasensky, J.; Banaszak Holl, M. M.; Chen, Z. Cell Volume Changes During Apoptosis Monitored in Real Time Using Digital Holographic Microscopy. *J. Struct. Biol.* **2012,** *178*, 270-278. (3) Khmaladze, A.; Matz, R. L.; Jasensky, J.; Seeley, E.; Banaszak Holl, M. M.; Chen, Z. Dual-Wavelength Digital Holographic Imaging With Phase Background Subtraction. *Opt. Eng.* **2012,** *51*, 055801. Elsevier, the Optical Society of America, and SPIE have granted permission for this content to be reprinted.

studied. DHM is a useful method for imaging cells because it yields both amplitude and quantitative phase information, making it a truly three-dimensional imaging technique.

In this chapter, the DHM technique is applied to the study of cell volume changes that occur during apoptosis. Apoptosis is the process of programmed cell death, designed to clear potentially hazardous molecules from a tissue area without negatively affecting the neighboring cells, and apoptotic volume decrease (AVD) is a morphological characteristic of apoptosis. Importantly, by employing DHM to measure AVD, we can delineate the different responses of cells upon exposure to an apoptosis-inducing agent, which bulk methods cannot detect.

This chapter is outlined as follows. First, the ideal features for a technique that measures cell volume change are defined and background information is provided on the different techniques that have previously been employed to measure cell volume. Next, the advantages of the DHM method are described and the background of AVD is more extensively discussed. The procedures for obtaining the volume measurements are provided. Finally, the results demonstrate the ability of DHM to distinguish between groups of cells with differential responses to the apoptosis-inducing agent (cells that do not change in volume, cells that exhibit apoptotic volume decrease, and cells that are removed from the substrate). The ability to differentiate between cells that do not change volume and cells that exhibit AVD represents an improvement over previous bulk methods (e.g., electronic cell sizing), which could not follow the same cell over time. The application of DHM to the study of AVD is also an advancement over previous single-cell methods such as atomic force microscopy because of the vast improvement in time resolution and number of cells that can be simultaneously imaged with DHM. The appendix details two important developments in the data analysis methods.

This research was a collaborative effort between Zhan Chen's and Mark Banaszak Holl's labs. Alex Khmaladze, then a postdoctoral research assistant in the Chen group, drove the DHM methods and techniques. Alex performed the data analyses, constructed the figures, and wrote substantial portions of the text in the publications and this thesis chapter. My work was to provide the cell culture expertise, biological design, and interpretation for the experiments, and write significant portions of

the background, experimental methods, and discussion sections for both the publications and this thesis chapter.

2.2 Background

Volume regulation is important for maintaining cell homeostasis. Cell volume changes play important roles in an extensive variety of disease states such as diabetes mellitus, renal failure, acute cerebral edemas, sickle cell anemia, hypercatabolism, fibrosing disorders, epilepsy, hyponatremia/hypernatramia, and carcinogenesis, among others.[17-23] Cell volume changes are also apparent in normal cell processes such as regulatory volume increase associated with cell proliferation and AVD associated with programmed cell death. Therefore, there is a great need for methods that can accurately measure cell volume as a function of time. An ideal method should be able to meet the following criteria: 1) accurate volume measurement, 2) sufficient time resolution to monitor the desired process, and 3) the ability to follow volume on a cell-by-cell basis as a function of time for both individual cells and a population of cells. The ability to obtain both single cell results and population data is particularly important, as population-based measurements alone suffer from the following problems: 1) convolution of individual cell responses and underestimation of the magnitude of volume change, 2) overestimation of the extent to which the entire population of cells is responding to stress, and 3) inability to connect volume changes to the detailed biological state of each cell (e.g., stage in the cell cycle). These limitations prevent a detailed understanding of the relationship of cell volume changes to biochemical signaling cascades.

Various techniques including electron microscopy,[24] electronic cell sizing,[25-27] light scattering coupled to flow cytometry[28,29] and, more recently, atomic force microscopy (AFM)[30] and combined flow cytometry/electronic cell sizing[31] have been applied to study cell volume changes. Electron microscopy provides a high spatial resolution, but requires fixing the sample, which halts biological processes. Electronic cell sizing is useful for precise measurements of cell volumes and diameters, but is a population-based technique. Flow cytometry is convenient for the study of individual live

cells by light scattering. However, it assumes a spherical shape for each cell and the signal is only proportionate to cell size, not a direct measurement of volume. Additionally, individual cells cannot be monitored over time. Elastic scattering spectroscopy is a similar technique that has been employed to measure the size of cellular components responsible for scattering light (i.e., the nucleus).[32,33] Newer instruments that combine the capabilities of electronic cell sizing and flow cytometry are powerful improvements, but single cells still cannot be examined over time. Finally, AFM allows for live-cell imaging on tissue culture plates in typical cell growth media with ~30 nm resolution, however AFM measurements are time-consuming, making it difficult to observe changes in morphology with a time resolution better than minutes. It is also challenging to image a large number of cells by AFM.

Here, we report a method for analyzing cell volume changes in real time using single-wavelength and dual-wavelength reflection DHM. DHM has been successfully applied to image a variety of microstructures of materials and biological systems.[1-4,34,35] In recent years, digital holographic transmission microscopy has been extensively used to study cellular morphology[10] as well as to measure the cellular index of refraction.[6,36,37] DHM has been also successfully used to monitor cell cycle.[38] DHM allows for direct measurement of phase changes undergone by a light wave while passing through or reflecting from objects. Such measured phases can be converted to a height profile of the sample through a variety of phase unwrapping methods including mathematical data analyses and dual-wavelength measurements. In this study, DHM was applied to image time-dependent volume changes of individual KB cells and many cells as a whole undergoing AVD in real time.

DHM allows for simultaneous measurements of volumes of both individual cells and many cells with time resolution principally limited only by the frame rate of the camera employed (in this case, 33 frames/sec); DHM, therefore provides accurate measurements of cell volume change dynamics with a much better time resolution than the techniques discussed above. Because of this excellent time resolution, initial cell volume changes at induction can be accurately detected. Here, DHM was applied to

examine AVD, an exemplary process of cell volume change, but DHM could also be used to study a variety of other processes involving cell volume changes.

AVD is a predominant and ubiquitous early-stage morphological characteristic of apoptosis, a mechanism of controlled cell death that eliminates harmful or abundant cells while minimizing inflammatory response in nearby cells and tissues,[18,30,39,40] and it has been demonstrated that AVD is a sufficient condition to induce apoptosis.[41] AVD and other morphological and biochemical features of apoptosis, such as loss of focal adhesions, the formation of cell membrane buds or blebs, and nuclear condensation[40, 42-44] suggest that apoptosis is an active, inherently programmed phenomenon, in contrast to necrosis.[40] Apoptosis can be initiated by a variety of environmental stimuli including, but not limited to, chemical insult, nutrient deprivation, radiation, and viral infection. Apoptosis plays a significant role in cancer, both in its formation and in current options for inhibition of tumor growth. The inability to initiate apoptosis enhances tumor formation, and current treatments for cancer target this pathway. Enhanced apoptosis is oftentimes a desired response to treatment because tumor volume can be controlled due to the death of a large amount of cells. Genes and proteins controlling apoptosis are also potential drug targets. Current cytotoxic drugs may already target cell death indirectly, however at the same time they may also target healthy tissue. In contrast, apoptotic inducers may potentially reduce toxicity, decrease mutagenesis, and provide fewer opportunities for acquired drug resistance. AVD was chosen for this study because it is a process in which it is important to delineate both the individual cellular volume response and the average population response as a function of time. For different individual cells, the biological response rates to AVD-inducing stimuli (e.g., exposure to staurosporine, described herein) may vary. Therefore AVD may be triggered in different cells at different times, depending on other cell characteristics such as stage in the cell cycle. In addition, AVD may not be triggered at all in some cells.

2.3 Experimental Methods

2.3.1 Digital Holographic Microscopy

DHM is a quantitative phase contrast optical technique, which converts the phase changes undergone by a light wave, while passing through or reflecting from objects, into intensity variations, which can be observed by a detector. The intensity of light passing through a nearly transparent sample changes little, but the light slows down inside the sample (proportional to its index of refraction), resulting in a phase change of the light (Figure 2.1a). Because phase change indicates a change in optical path length or optical thickness, a height profile of the sample can be deduced. It is thus especially advantageous in visualization of the height profile of mostly transparent samples ("pure phase" objects). DHM is also very useful in microscopic applications, as it permits numerical focusing from a single image frame and allows for digital correction of different aberrations of the optical system.

DHM uses a high-resolution CCD array to acquire a hologram. After the information is recorded digitally, it is encoded as the array of numbers representing the amplitude of the input optical field. This optical field can then be numerically propagated in space by using diffraction theory. A number of different methods have been previously utilized for numerical reconstruction, including Huygens convolution, Fresnel transform, and angular spectrum,[45] which is used in this work. Along with the ability for fast image acquisition and the extraction of both quantitative amplitude and phase information, DHM offers the versatility of various image-processing techniques applied to the complex field, which may not be feasible with conventional holography. DHM allows for direct measurement of phase changes, making it a true 3D imaging technique. The deduced sample height information makes the technique extremely valuable in applications of microscopy to studies of materials and biological samples. To extract the phase information from the hologram, it is necessary to numerically propagate the optical field (the intensity distribution captured by the CCD camera) along the direction perpendicular to the hologram plane until the object is in focus.

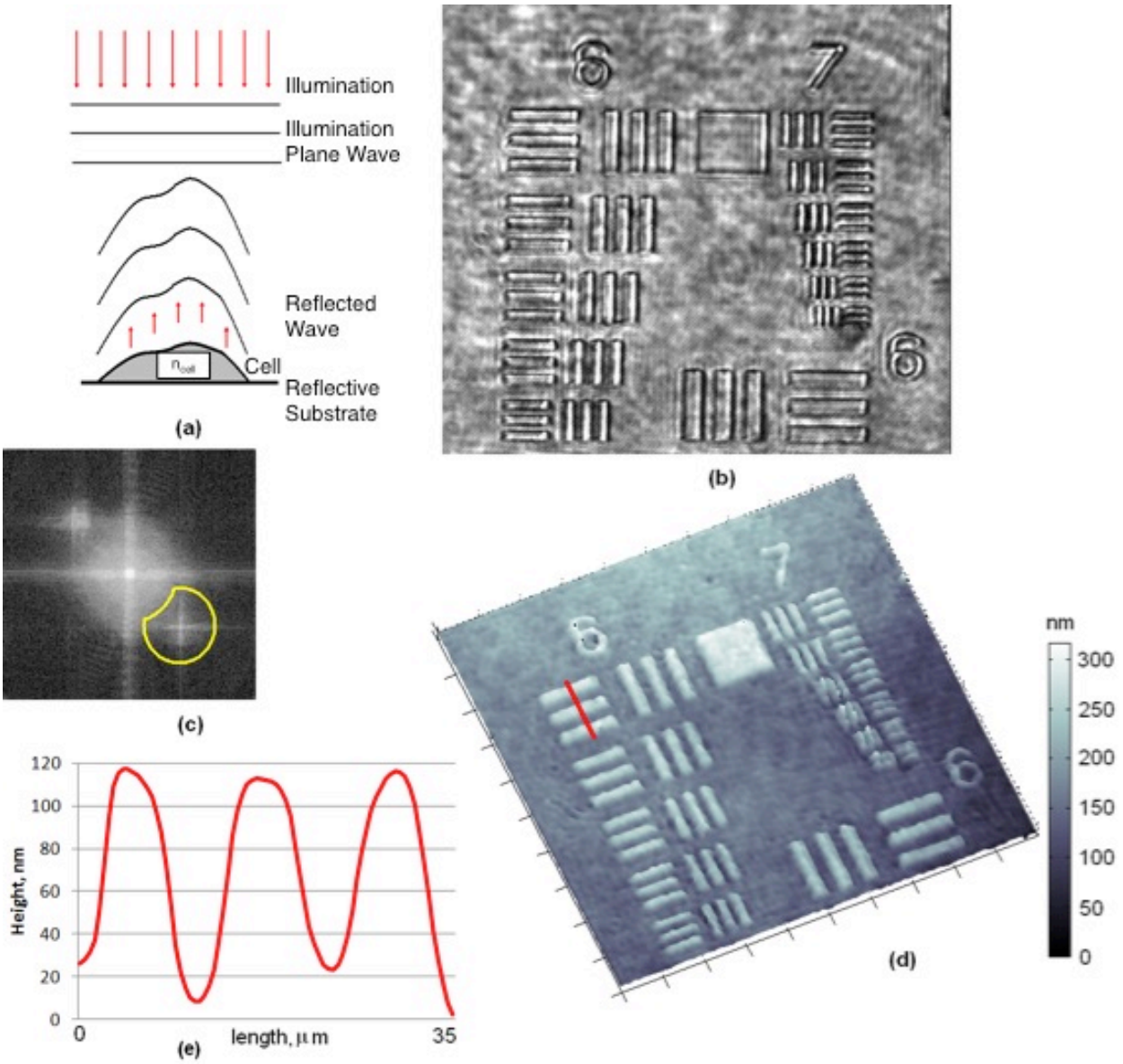

Figure 2.1: Phase imaging. (a) Light propagating through a cell, resulting in a wavefront distortion. (b) Hologram of a USAF resolution target. (c) An angular spectrum, showing the area that was selected for the reconstruction. (d) A 3D reconstruction. (e) Height profile of the line shown in (d).

Figure 2.1b shows the hologram of a standard USAF resolution target (covered with a 100 nm layer of aluminum to make it entirely reflective) recorded by our setup. Figure 2.1c shows the angular spectrum (Fourier transform), which consists of a zero-order and a pair of first-order terms. The holographic interference fringe pattern and the corresponding pair of the first order terms are clearly visible. Both first-order terms are

the angular spectrum of the object field (one is phase inverted). To numerically reconstruct the optical field, one of the first order terms is then shifted to the center of the image, filtered with a window function (shown) and propagated in space along the z-axis via multiplication by the complex transfer function exp[$ik_z z$]. The complex wave-field at an arbitrary z can be computed by simply performing the inverse Fourier transform. By calculating the final complex optical field, we can create a phase map at each point $\phi(x, y)$ which is then converted into height $h(x, y)$ via (Equation 2.1)

$$h(x,y) = \frac{\lambda}{2\pi}\varphi(x,y)$$

Here, $\lambda = \lambda_{laser}/2$ (where λ_{laser} is the laser wavelength), as the beam travels to the surface and then is reflected back. Figure 2.1d shows the 3D image of the resolution target and the height profile is shown in Figure 2.1e. The RMS noise in height is about 10 nm. If a sample is a transparent cell, Equation 2.1 becomes (Equation 2.2)

$$h(x,y) = \frac{\lambda}{2\pi}\frac{\varphi(x,y)}{(n-n_0)}$$

where $(n - n_0)$ is the refractive index difference between the cell and the buffer (or medium).

When the thickness of an object is greater than $\lambda/(n - n_0)$, the phase change exceeds 2π and the phase profile is wrapped. The consequent ambiguity in the wrapped phase values causes discontinuities in the 3D reconstructed image. One way to unwrap the discontinuities is to employ a software algorithm that searches the phase map for 2π jumps and shifts the image segments up or down. We have used a varying distance reconstruction method[46] for the software-based unwrapping, as it is fast and allows for an easy background subtraction, which is important for the volume calculations. For the larger images with many cells, a dual-wavelength optical setup was used. This method uses two laser wavelengths simultaneously to image the same object. While the two resultant phase images both contain the discontinuities, the discontinuities do not appear in the same places on the phase maps (Equation 2.2), so the phase can be unwrapped by comparing these phase images.[47] (See Section 2.8.1 for an extended discussion of this methodology.)

2.3.2 Microscope

The Chen laboratory dual-wavelength digital holographic microscope (Figure 2.2) uses a configuration based on a Michelson interferometer, as is typical for reflection DHM. We used a two pigtail diode system with wavelengths of 635 nm and 675 nm. The beams from both lasers are expanded by the microscope objectives and are combined. The beams are then collimated by lens L1 (see Figure 2.2a). A beamsplitter splits the incoming beams into the reference and object arms. Both reference (635 nm and 675 nm) beams are reflected from the mirror. Lens L2 focuses both object beams to the back focal plane of a water immersion microscope objective WOBJ, which illuminates the sample with collimated light. The intensity of both laser beams is only 2-3 mW per mm^2 (and can be even lowered if desired), so no photonic damage to the sample should occur.

The WOBJ is also used to form the image on a CCD array. The beamsplitter recombines the spherical reference wave and plane object wave to create holographic interference (see Figure 2.2b). A small angle between the reference and object waves is introduced to spatially separate the first order

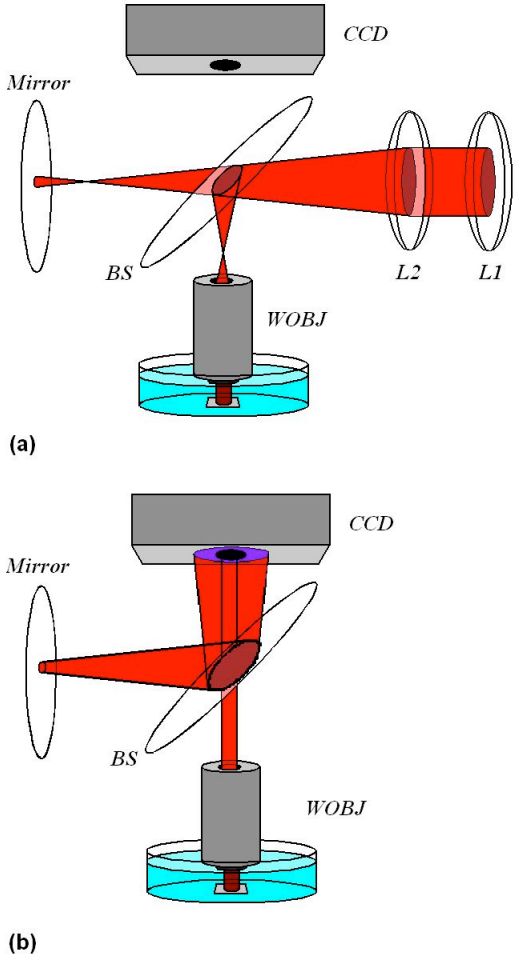

Figure 2.2: Digital holographic microscope setup: (a) lens L1 collimates both (635 nm and 675 nm) beams. The beam splits into the reference and object arms at the beamsplitter (BS), Lens L2 and water immersion microscope objectives (WOBJ) again collimate the beams; (b) WOBJ forms an image on CCD camera, which records an interference pattern between planar object and spherical reference waves (hologram). WOBJ were Olympus UMPlanFL 10x and Olympus UMPlanFL 20x for dual- and single-wavelength images, respectively.

spectral components from the zero-order term to enable effective filtering in the Fourier domain. The wave-front curvature mismatch between the reference and object waves is compensated numerically.[3]

2.3.3 Index of Refraction

Because DHM measures the optical thickness of cells, the indices of refraction (Equation 2.2) of both the cells and the surrounding medium are required in order to convert the optical thickness to physical thickness. We used $n_0 = 1.337$ as the index of refraction of the medium and $n = 1.375$ for the integral index of refraction of the cells.[36] It should be noted that while the precise value of the index of refraction of the cells is unknown, as long as it remains approximately the same during the experiment, the overall dynamics of the observed volume change is accurate. In any case, the index of refraction should not increase above that of the nucleus which is estimated to be ~2% greater than that of cytoplasm.[48]

2.3.4 Sample Preparation and Induction of Apoptosis

KB cells (human epithelial; Cat. No. CCL-17; ATCC; Manassas, VA) were seeded in 6-well plates in RPMI-1640 (Cat No. 27016-021; Invitrogen; Carlsbad, CA), supplemented with 10% fetal bovine serum, penicillin (100 units/mL) and streptomycin (100 µg/mL) at 3.5×10^5 cells/well. Each well contained one silicon slide that provided a sufficiently reflective background for holographic imaging. Prior to use, the slides were cured with sulfuric acid, resulting in a thin (several nanometers thick), hydrophilic layer of silicon dioxide to which the cells could adhere. The cells were incubated for ~5 hours at 37 °C in a humidified atmosphere containing 5% CO_2. Slides were transferred to 35 mm Petri dishes containing 4.95 mL fresh complete medium for imaging. A 50 µL volume of staurosporine (Cat No. S5921; Sigma-Aldrich; St. Louis, MO) in complete medium was added to a final concentration of 1 µM or 2 µM and mixed in order to induce apoptosis.

2.3.5 Volume Measurements

The cell volumes were calculated by adding the volumes above each pixel in the image belonging to the cells by multiplying the height (obtained from phase via Equation 2.2) and the XY size of the pixel. However, the phase obtained via the angular spectrum method only measures the relative phase at each pixel, thus the background (the phase related to the height of the slide surface on which the cells are grown) needs to be subtracted. In the case of the single-wavelength images, the background subtraction is a part of the varying reconstruction distance phase unwrapping procedure. Therefore, the volume is calculated directly after phase unwrapping. However, in the case of the smaller magnification images of many cells, the single-wavelength unwrapping sometimes failed to correctly determine the true height profile of the sample, as the cells are comparatively smaller and some are located in the areas where the phase noise is high. As a result, the height measurements obtained for the larger population of cells using a single wavelength DHM were not reliable. Thus, a dual-wavelength setup was used that allowed us to generate the volume measurement for many cells at once in real time. The resulting dual-wavelength unwrapped map was properly adjusted by subtracting the background and excluding all background pixels, so the total volume obtained only included the volume of the cells.

Here, the background phase was separated from the cells via modified polyfit method by iteratively fitting a series of polynomial surfaces to the phase map and finally subtracting the result from the original phase image.[49] The method is ideally suited for this application, as it removes the uncompensated curvature with the minimal user intervention, allowing for an automated background subtraction. (See Section 2.8.2 for an extended discussion of this methodology.)

2.3.6 Measurement Uncertainty

A number of factors affect the accuracy of the volume measurements. While DHM is sensitive to changes in the optical path length on the order of several nanometers, the XY resolution is diffraction limited to the fraction of a micron. The imperfections in the wave front, due to aberrations in the optical system, as well as

possible roughness of the surface of the slides on which the cells were grown also introduce measurement error. Also, the possibility that the index of refraction of the cells does indeed change during the experiment is a source of uncertainty. However, even if the integral index of refraction does change during the experiment, it will realistically always be within a few percent of the index of refraction of water. Moreover, the fact that the overall volume change measured by DHM is generally consistent with AVD dynamics observed by other methods indicates that the possible changes in the index of refraction of cells are not significant.

There is also a practical limit on the size of the sample that can be measured using this technique. In comparison to the light scattering experiments, where thousands of cells are routinely measured, the digital holographic microscope needs to be able to see each individual cell. Therefore, DHM is limited to the number of cells that can be observed in a single image frame. One can use a smaller magnification microscope objective to increase the field of view, but that will also make the cells appear smaller, reducing the volume resolution and thus practically limiting the total number of cells to several hundred.

2.4 Results

Figure 2.3 shows the two KB cells undergoing AVD induced by exposure to 2 μM staurosporine. For reference, Figure 2.3a shows a hologram and Figure 2.3b shows a wrapped phase image of these two cells at t = 0 min. Then, Figure 2.3c shows time-dependent 3D images of two KB cells at various time points. Although these images were acquired roughly every 15 to 45 minutes following the initial staurosporine exposure, the time resolution of acquiring images is principally limited only by the frame rate of the camera (here, 33 frames/second). The images clearly show a significant reduction of the total volume of the cells as a function of time, while the changes in the diameter of the cells are much smaller. Figure 2.4a shows the quantitative time-dependent cell volume changes deduced from the images in Figure 2.3c. The staurosporine was added at 0 min to the cell media, and the cell volume decrease

became noticeable after 25 minutes. We speculate that this time delay in AVD induction is due to both the required time for staurosporine to diffuse throughout the cell media and the natural biological response time of the cells to staurosporine. After two hours, the magnitude of cell volume change is consistent with that previously observed at the single cell level using AFM within ~10% error.[30]

As a control, two KB cells were also imaged in complete cell medium without the addition of staurosporine (Figure 2.3d). The volume of the control cells remained largely unchanged for the duration of the experiment (Figure 2.4a) with only small variations due to measurement uncertainty, and the cells showed no

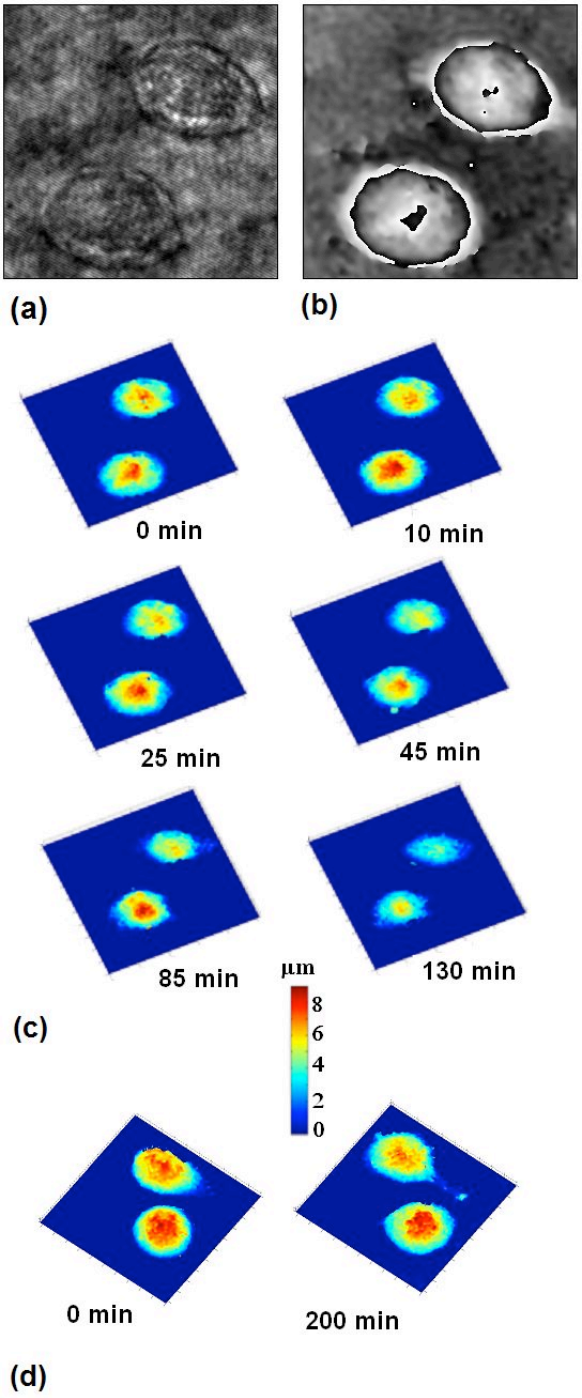

Figure 2.3: Two KB cells undergoing AVD (a-c): (a) a hologram and (b) phase image of two cells at t = 0 min; (c) Time-dependent 3D images. Two KB cells in complete medium were exposed to 2 µM of staurosporine (STS) at t = 0 min; (d) For comparison, 3D images of two control KB cells in complete medium at t = 0 and 200 min. (all images are 52 mm x 52 mm).

visible signs of distress, appearing healthy for more than 200 minutes. After 300 minutes, the cells had detached from the substrate, so volume measurements were no longer possible. Using the cell volumes measured at the first five time points (0, 20, 40, 60, and 80 min) and assuming that the real time-dependent variation in the cell volume is negligible, the standard deviation of volume measurements using DHM is 63 mm^3 or 3% of the total cell volume. We have used these standard deviation numbers as error bars in Figure 2.4. Furthermore, Figure 2.4b shows the time-dependent volume measurements of a single cell exposed to 1 μM staurosporine; the volume decrease is consistent with AVD. It should be noted that (especially at the lower concentration of staurosporine) AVD only occurred in about half of the cells after exposure to staurosporine. In the event when no cell volume change was observed over several hours, the experiment ended with cells eventually separating from the silicon slide.

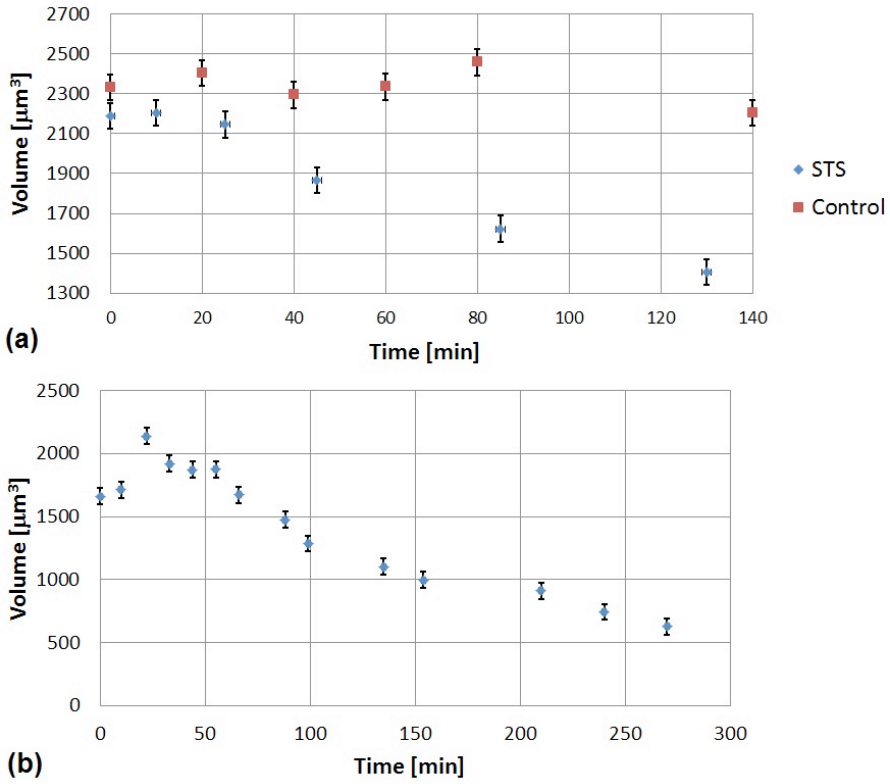

Figure 2.4: Volume change over time for (a) two apoptotic KB cells and two control KB cells (shown in Figure 2.3). The total volume for both cells is shown; (b) a single apoptotic KB cell exposed to 1 μM staurosporine (STS) at t = 0 min. Error bars are based on the volume of control cells (see text).

We also imaged a larger population of about 30 cells using DHM. To image this large quantity of cells simultaneously, a lower magnification (10x) objective lens was necessary. Because theimage of each cell was smaller in this larger population case,

the unwrapping algorithm had fewer pixels as input. Consequently, the resultant single-wavelength images were considerably more difficult to unwrap than the previous images of one or two cells. To overcome this difficulty, a dual-wavelength DHM setup was employed. Figure 2.5 shows the 3D pseudocolor rendering of the height image at various time points. Figure 2.5a shows the height map at the time of the initial exposure to staurosporine. 2.5b and Figure 2.5c are taken about one hour and three hours after the exposure. From the multiple time-dependent 3D images obtained using the dual-wavelength method, the volume of each of 30 cells was calculated to understand AVD behavior at the single-cell level. We found that the cells can be divided into three groups: (1) cells that exhibit volume decrease; (2) cells that remain essentially the same volume throughout the experiment indicating that apoptosis was not triggered in these cells; and (3) cells that detach from the substrate, rendering volume measurements no longer possible. Using the cell volumes from the group 2 (and assuming that the real time-dependent variation in the cell volume is negligible), the standard deviation of volume measurements using dual-wavelength DHM

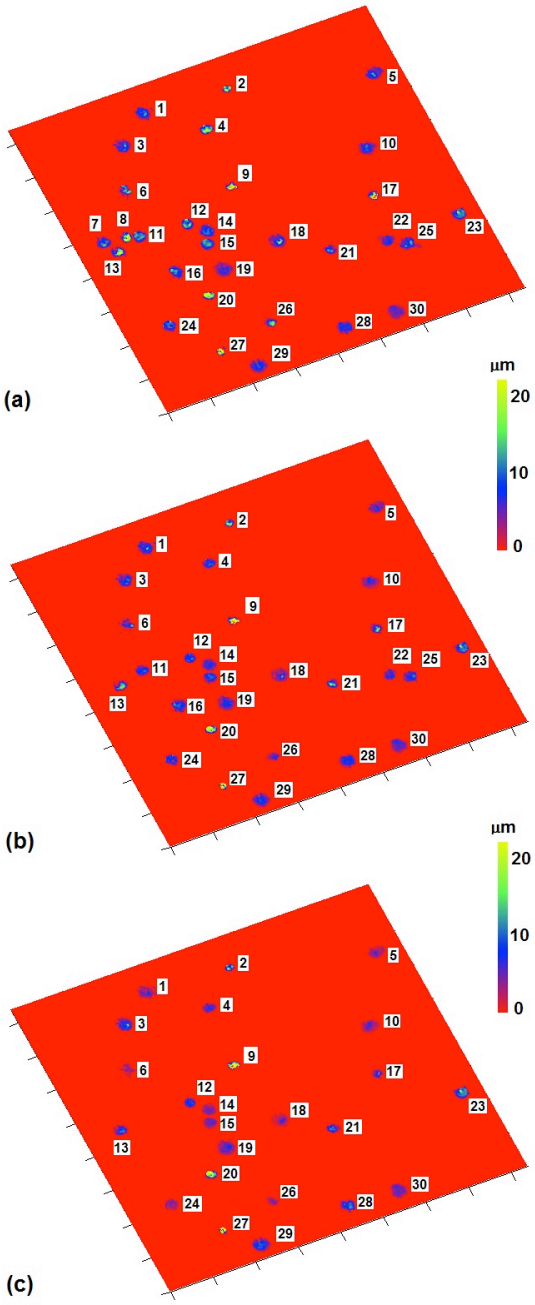

Figure 2.5: 3D rendering of many KB cells exposed to 1 µM staurosporine at t = 0 min imaged by the dual-wavelength setup (background removed): (a) at t = 0 min, (b) at t = 57 min, (c) and at t = 170 min. Examples of cells that detached from the substrate, underwent AVD, and did not change are #22, #26, and #30, respectively.

is ~5% of the total cell volume.

Figure 2.6a displays all the traces in scatter-line plot to show the distribution of the cell response in a population. The ability to identify these individual cell responses to staurosporine exposure (or to other stimuli) is a significant advantage of DHM over population-based techniques that provide only the overall average cell volume change. Figure 2.6b shows the normalized average cell volume change for all 30 cells compared to time-dependent volume change of the cells from group 1, group 2, and the sum of groups 1 and 2, the latter representing the cells that can be measured using light scattering. AVD resulted in a decrease to ~40% of the initial volume over 4 hours. Similar to the results for the single cell discussed above, the overall volume change measured for the 30 cells was comparable to that measured by AFM (within ~5% error).[30]

To further analyze the quantitative AVD results for individual cells, we also selected the cells that exhibited AVD, and compared their volume change. Figure 2.6c shows the average and standard deviation (taken from the normalized cell data) of all the AVD cells. Once again, the results are in agreement, though the larger uncertainty at the second time point (t = 18 min) is worth noting. At t = 18 min, it is likely that the difference in cell volumes is caused by the variance in initial biological response times of individual cells. Also, some of the cells seem to have actually increased in volume early in the time course. It is not clear if this is due to the measurement uncertainty and/or a change in the index of refraction in the vicinity of the cells, as an actual substantial volume increase seems unlikely.

The quick and simple way to study a large population of cells without following the volume change of each individual cell is to calculate the total volume of all cells in a frame. This volume measurement does not take into account the fact that some of the cells separated from the substrate during the experiment and so their volume was counted as zero. A simple counting of cells at each step can avoid this problem, by multiplying the average volume by the fraction of the cells left on the substrate. Figure 2.6d shows the total volume of all 30 cells, adjusted to the number of cells, showing the results that are also well correlated to the previous measurements.

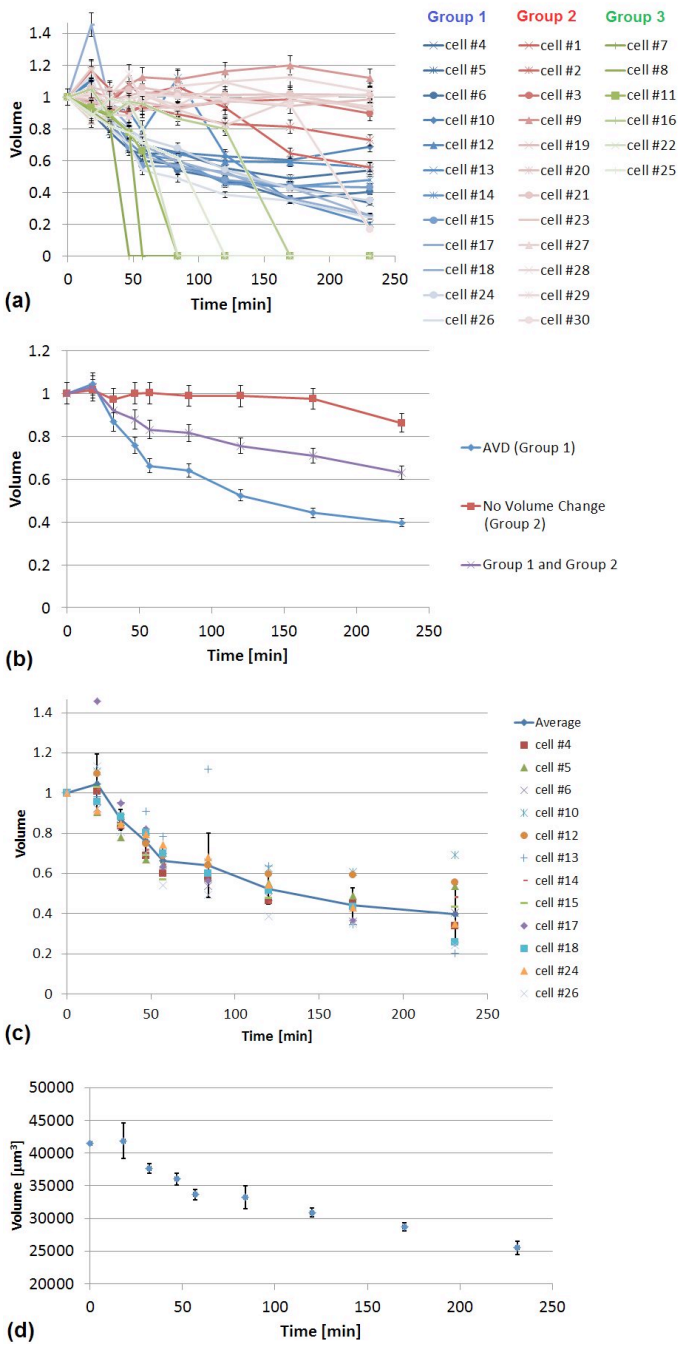

Figure 2.6: AVD Analysis: (a) cells divided into 3 groups. Group 1: AVD; Group 2: Non AVD (little/no volume change); Group 3: Cells that detached from the substrate; (b) normalized volume change for three identified groups of cells; (c) normalized volume change for all AVD cells compared to their average; (d) total volume of all cells exposed to 1 µM staurosporine as a function of time, adjusted to the number of cells. Error bars for (a) and (b) are based on the standard deviation of the normalized volume of Group 2 cells and (c) and (d) are based on standard deviation of normalized AVD cell volume measurements.

2.5 Discussion

In addition to being consistent with previously reported AFM data, the DHM results described here are qualitatively in agreement with previously reported values for cell volume changes measured by electronic cell sizing. In particular, Maeno *et al.*[50] observed by electronic cell sizing the reduction of HeLa cells to ~75-80% of the volume of control cells upon two-hour exposure to 4 μM staurosporine. Our results indicated that cell volume was reduced to ~60% of initial volume after two-hour exposure to 1 μM staurosporine. We speculate that this quantitative difference in percent volume change can be attributed to differing responses of HeLa versus KB cells to staurosporine (also considering the different staurosporine concentrations) as well as to the underestimation of the volume change magnitude that occurs when measuring AVD with a population-based technique like electronic cell sizing. We would like to emphasize that comparison of the absolute volumes obtained by DHM to those obtained previously by AFM or electronic cell sizing must be done with caution because of the approximation that we had to employ for the refractive index values. The most reliable aspect of these data is the change in volume and differential volume response of each cell.

We demonstrated that DHM is able to measure cell volume changes in real time with an excellent time and volume resolution. DHM can be applied to simultaneously measure the time-dependent cell volume for individual cells and large groups of 30 or more cells. In order to obtain a reliable height profile of the large group of cells, a low magnification objective lens was used and dual-wavelength DHM measurements were performed. The change in volume of each individual cell and the total volume of all 30 cells was measured in real time throughout the AVD process. It was found that the cells could be logically divided into three groups with markedly different time-dependent behaviors upon staurosporine exposure. The total volume change (adjusted for the number of cells) is in agreement with the average volume change for individual cells exhibiting AVD. The results of the total volume change for the entire group of cells is also well correlated to those obtained from DHM studies of a single cell using the single wavelength measurement with a higher magnification objective lens.

2.6 Conclusions and Future Work

In this chapter, we have shown that DHM is a powerful imaging technique for understanding cell volume changes that occur during apoptosis, which is important for research on the role of cell volume changes in health and disease. Most importantly, in comparison to bulk methods such as electronic cell sizing, DHM allows cells that undergo volume change and cells that do not change to be distinguished from one another. According to the numbers of cells that underwent AVD and those that did not, we would expect a bulk technique to underestimate cell volume change due to AVD by ~20% and overestimate the number of cells undergoing AVD by ~50% in this system. With DHM, many cells can be followed over time at the single-cell level with good volume resolution, and the time resolution improves over that of AFM. This study demonstrates the utility of DHM in imaging biological structures.

Future work in the application of DHM to measuring cell volume changes during apoptosis should include improvements to the physical microscope configuration, especially because the image acquisition in this study was done at ambient temperature. Adding a microscope incubator and chamber to the current setup would allow for cells to be imaged at physiological temperature (37 °C) in a humidified atmosphere containing 5% CO_2, which would be more representative of a living system. As cell survival at room temperature is limited to a few hours, this system would also allow for cells to be imaged over longer periods of time, increasing the versatility of DHM in imaging AVD and other biological processes.

Coupling DHM with fluorescence microscopy would also be a very powerful improvement over current techniques, and some studies towards this end have already been done.[51] With the combination of DHM and fluorescence microscopy, the relationship of cell volume to any biological process that can be monitored with a fluorescent dye can be studied. For example, cell volume is known to increase as cells progress through the cell cycle. By combining DHM and fluorescence microscopy, the relationship of cell cycle and expression of a fluorescent transgene could be studied. Currently, the ability to identify the same cells in a given sample with reflective digital holography (the mode used in this study) and a fluorescence microscope is limited.

However, DHM can be performed in transmission mode, which allows for easier identification of the same cells under a fluorescence microscope.

The noninvasive nature of the digital holographic microscope makes it a useful tool for the study of biomedical problems. Although many studies up until now have demonstrated that DHM can be used to successfully image biological samples, future work should exploit the benefits DHM in order to address even more biologically interesting questions. With biological problems driving the research questions, the efficacy of DHM will be demonstrated.

2.7 References

1. Cuche, E.; Bevilacqua, F.; Depeursinge, C. Digital holography for quantitative phase-contrast imaging. *Opt. Lett.* **1999,** *24*, 291-293.

2. Haddad, W. S.; Cullen, D.; Solem, J. C.; Longworth, J. W.; McPherson, A.; Boyer, K.; Rhodes, C. K. Fourier-transform holographic microscope. *Appl. Opt.* **1992,** *31*, 4973-4978.

3. Khmaladze, A.; Kim, M.; Lo, C.-M. Phase imaging of cells by simultaneous dual-wavelength reflection digital holography. *Opt. Express* **2008,** *16*, 10900-10911.

4. Xu, W.; Jericho, M. H.; Meinertzhagen, I. A.; Kreuzer, H. J. Digital in-line holography for biological applications. *Proc. Natl. Acad. Sci. U.S.A.* **2001,** *98*, 11301-11305.

5. Mann, C.; Yu, L.; Lo, C.-M.; Kim, M. High-resolution quantitative phase-contrast microscopy by digital holography. *Opt. Express* **2005,** *13*, 8693-8698.

6. Rappaz, B.; Marquet, P.; Cuche, E.; Emery, Y.; Depeursinge, C.; Magistretti, P. Measurement of the integral refractive index and dynamic cell morphometry of living cells with digital holographic microscopy. *Opt. Express* **2005,** *13*, 9361-9373.

7. Mölder, A.; Sebesta, M.; Gustafsson, M.; Gisselson, L.; Wingren, A. G.; Alm, K. Non-invasive, label-free cell counting and quantitative analysis of adherent cells using digital holography. *J. Microsc.* **2008,** *232*, 240-247.

8. Emery, Y.; Cuche, E.; Colomb, T.; Depeursinge, C.; Rappaz, B.; Marquet, P.; Magistretti, P. DHM (Digital Holography Microscope) for imaging cells. *J. Phys.: Conf. Ser.* **2007,** *61*, 1317-1321.

9. Moon, I.; Javidi, B. Three-dimensional identification of stem cells by computational holographic imaging. *J. R. Soc., Interface* **2007,** *4*, 305-313.

10. Kemper, B.; Carl, D.; Schnekenburger, J.; Bredebusch, I.; Schäfer, M.; Domschke, W.; von Bally, G. Investigation of living pancreas tumor cells by digital holographic microscopy. *J. Biomed. Opt.* **2006,** *11*, 34005.

11. Rappaz, B.; Barbul, A.; Emery, Y.; Korenstein, R.; Depeursinge, C.; Magistretti, P. J.; Marquet, P. Comparative study of human erythrocytes by digital holographic microscopy, confocal microscopy, and impedance volume analyzer. *Cytometry, Part A* **2008,** *73A*, 895-903.

12. Khmaladze, A.; Matz, R. L.; Epstein, T.; Jasensky, J.; Banaszak Holl, M. M.; Chen, Z. Cell volume changes during apoptosis monitored in real time using digital holographic microscopy. *J. Struct. Biol.* **2012,** *178*, 270-278.

13. Rappaz, B.; Barbul, A.; Hoffmann, A.; Boss, D.; Korenstein, R.; Depeursinge, C.; Magistretti, P. J.; Marquet, P. Spatial analysis of erythrocyte membrane fluctuations by digital holographic microscopy. *Blood Cells, Mol., Dis.* **2009,** *42*, 228-232.

14. Kemper, B.; Bauwens, A.; Vollmer, A.; Ketelhut, S.; Langehanenberg, P.; Muthing, J.; Karch, H.; von Bally, G. Label-free quantitative cell division monitoring of endothelial cells by digital holographic microscopy. *J. Biomed. Opt.* **2010,** *15*, 036009.

15. Yu, L.; Mohanty, S.; Zhang, J.; Genc, S.; Kim, M. K.; Berns, M. W.; Chen, Z. Digital holographic microscopy for quantitative cell dynamic evaluation during laser microsurgery. *Opt. Express* **2009,** *17*, 12031-12038.

16. Kemper, B.; Langehanenberg, P.; Vollmer, A.; Ketelhut, S.; von Bally, G. Label-free 3D migration monitoring of living cells. *Imaging and Microscopy* **2009,** *11*, 26-28.

17. De Petris, L.; Luchetti, A.; Emma, F. Cell volume regulation and transport mechanisms across the blood-brain barrier: implications for the management of hypernatraemic states. *Eur. J. Pediatr.* **2001,** *160*, 71-77.

18. Feng, Y.; Müller, V.; Friedrich, B.; Risler, T.; Lang, F. Clinical significance of cell volume regulation. *Wien. Klin. Wochenschr.* **2001,** *113*, 477-484.

19. Hoffman, E. K.; Lambert, I. H.; Pedersen, S. F. Editorial. *Acta Physiol.* **2006,** *187*, 1-3.

20. Lambert, I. H.; Hoffmann, E. K.; Pedersen, S. F. Cell volume regulation: physiology and pathophysiology. *Acta Physiol.* **2008,** *194*, 255-282.

21. Lang, F. Mechanisms and Significance of Cell Volume Regulation. *J. Am. Coll. Nutr.* **2007,** *26*, 613S-623S.

22. McIntyre, G. I. Cell hydration as the primary factor in carcinogenesis: A unifying concept. *Med. Hypotheses* **2006,** *66*, 518-526.

23. McManus, M. L.; Churchwell, K. B.; Strange, K. Regulation of Cell Volume in Health and Disease. *N. Engl. J. Med.* **1995,** *333*, 1260-1267.

24. Cornet, M.; Isobe, Y.; Lemanski, L. F. Effects of anisosmotic conditions on the cytoskeletal architecture of cultured PC12 cells. *J. Morphol.* **1994,** *222*, 269-286.

25. Beauvais, F.; Michel, L.; Dubertret, L. Human eosinophils in culture undergo a striking and rapid shrinkage during apoptosis. Role of K+ channels. *J. Leukocyte Biol.* **1995,** *57*, 851-855.

26. Klassen, N. V.; Walker, P. R.; Ross, C. K.; Cygler, J.; Lach, B. Two-stage Cell Shrinkage and the OER for Radiation-induced Apoptosis of Rat Thymocytes. *Int. J. Radiat. Biol.* **1993,** *64*, 571-581.

27. Thomas, N.; Bell, P. A. Glucocorticoid-induced cell-size changes and nuclear fragility in rat thymocytes. *Mol. Cell. Endocrinol.* **1981,** *22*, 71-84.

28. Chalut, K. J.; Ostrander, J. H.; Giacomelli, M. G.; Wax, A. Light Scattering Measurements of Subcellular Structure Provide Noninvasive Early Detection of Chemotherapy-Induced Apoptosis. *Cancer Res.* **2009,** *69*, 1199-1204.

29. Compton, M. M.; Haskill, J. S.; Cidlowski, J. A. Analysis of Glucocorticoid Actions on Rat Thymocyte Deoxyribonucleic Acid by Fluorescence-Activated Flow Cytometry. *Endocrinology* **1988,** *122*, 2158-2164.

30. Hessler, J. A.; Budor, A.; Putchakayala, K.; Mecke, A.; Rieger, D.; Banaszak Holl, M. M.; Orr, B. G.; Bielinska, A.; Beals, J.; Baker, J. Atomic Force Microscopy Study of Early Morphological Changes during Apoptosis. *Langmuir* **2005,** *21*, 9280-9286.

31. Bortner, C. D.; Sifre, M. I.; Cidlowski, J. A. New Approaches for Determining Apoptotic Volume Decrease in Cells. In *Methods in Enzymology;* Häussinger, D., Sies, H., Eds.; Academic Press: 2007; Vol. 428, pp 161-181.

32. Mourant, J. R.; Canpolat, M.; Brocker, C.; Esponda-Ramos, O.; Johnson, T. M.; Matanock, A.; Stetter, K.; Freyer, J. P. Light scattering from cells: the contribution of the nucleus and the effects of proliferative status. *J. Biomed. Opt.* **2000,** *5*, 131-137.

33. Mulvey, C. S.; Curtis, A. L.; Singh, S. K.; Bigio, I. J. Elastic Scattering Spectroscopy as a Diagnostic Tool for Apoptosis in Cell Cultures. *IEEE J. Sel. Top. Quantum Electron.* **2007,** *13*, 1663-1670.

34. Barty, A.; Nugent, K. A.; Paganin, D.; Roberts, A. Quantitative optical phase microscopy. *Opt. Lett.* **1998,** *23*, 817-819.

35. Xu, L.; Peng, X.; Miao, J.; Asundi, A. K. Studies of Digital Microscopic Holography with Applications to Microstructure Testing. *Appl. Opt.* **2001,** *40*, 5046-5051.

36. Kemper, B.; Kosmeier, S.; Langehanenberg, P.; von Bally, G.; Bredebusch, I.; Domschke, W.; Schnekenburger, J. Integral refractive index determination of living suspension cells by multifocus digital holographic phase contrast microscopy. *J. Biomed. Opt.* **2007,** *12*, 054009.

37. Rappaz, B.; Charrière, F.; Colomb, T.; Depeursinge, C.; Magistretti, P. J.; Marquet, P. Simultaneous Cell Morphometry and Refractive Index Measurement with Dual-Wavelength Digital Holographic Microscopy. In *Digital Holography and Three-Dimensional Imaging*, Proceedings of the Optical Society of America, St. Petersburg, FL, March 16-20; Optical Society of America: 2008.

38. Rappaz, B.; Cano, E.; Colomb, T.; Kühn, J.; Depeursinge, C.; Simanis, V.; Magistretti, P. J.; Marquet, P. Noninvasive characterization of the fission yeast cell cycle by monitoring dry mass with digital holographic microscopy. *J. Biomed. Opt.* **2009,** *14*, 034049.

39. Bortner, C. D.; Cidlowski, J. A. Apoptotic volume decrease and the incredible shrinking cell. *Cell Death Differ.* **2002,** *9*, 1307-1310.

40. Kerr, J. F. R.; Wyllie, A. H.; Currie, A. R. Apoptosis: A basic biological phenomenon with wide-ranging implications in tissue kinetics. *Br. J. Cancer* **1972,** *26*, 239-257.

41. Maeno, E.; Shimizu, T.; Okada, Y. Normotonic cell shrinkage induces apoptosis under extracellular low Cl– conditions in human lymphoid and epithelial cells. *Acta Physiol.* **2006,** *187*, 217-222.

42. Bowen, I. D.; Bowen, S. M.; Jones, A. H. *Mitosis and apoptosis: Matters of life and death;* Chapman and Hall: London, 1998.

43. Häcker, G. The morphology of apoptosis. *Cell Tissue Res.* **2000,** *301*, 5-17.

44. Lockshin, R. A.; Zakeri, Z.; Tilly, J. L. *When cells die: A comprehensive evaluation of apoptosis and programmed cell death;* John Wiley & Sons: New York, 1998.

45. Grilli, S.; Ferraro, P.; De Nicola, S.; Finizio, A.; Pierattini, G.; Meucci, R. Whole optical wavefields reconstruction by digital holography. *Opt. Express* **2001,** *9*, 294-302.

46. Khmaladze, A.; Epstein, T.; Chen, Z. Phase unwrapping by varying the reconstruction distance in digital holographic microscopy. *Opt. Lett.* **2010,** *35*, 1040-1042.

47. Khmaladze, A.; Matz, R. L.; Zhang, C.; Wang, T.; Banaszak Holl, M. M.; Chen, Z. Dual-wavelength linear regression phase unwrapping in three-dimensional microscopic images of cancer cells. *Opt. Lett.* **2011,** *36*, 912-914.

48. Brunsting, A.; Mullaney, P. F. Differential Light Scattering from Spherical Mammalian Cells. *Biophys. J.* **1974,** *14*, 439-453.

49. Khmaladze, A.; Matz, R. L.; Jasensky, J.; Seeley, E.; Banaszak Holl, M. M.; Chen, Z. Dual-wavelength digital holographic imaging with phase background subtraction. *Opt. Eng.* **2012,** *51*, 055801.

50. Maeno, E.; Ishizaki, Y.; Kanaseki, T.; Hazama, A.; Okada, Y. Normotonic cell shrinkage because of disordered volume regulation is an early prerequisite to apoptosis. *Proc. Natl. Acad. Sci. U.S.A.* **2000,** *97*, 9487-9492.

51. Pavillon, N.; Benke, A.; Boss, D.; Moratal, C.; Kühn, J.; Jourdain, P.; Depeursinge, C.; Magistretti, P. J.; Marquet, P. Cell morphology and intracellular ionic homeostasis explored with a multimodal approach combining epifluorescence and digital holographic microscopy. *J. Biophotonics* **2010,** *3*, 432-436.

52. Ghiglia, D. C.; Pritt, M. D. *Two-Dimensional Phase Unwrapping: Theory, Algorithms, and Software;* John Wiley & Sons: New York, 1998.

53. Khmaladze, A.; Restrepo-Martínez, A.; Kim, M.; Castañeda, R.; Blandón, A. Simultaneous dual-wavelength reflection digital holography applied to the study of the porous coal samples. *Appl. Opt.* **2008,** *47*, 3203-3210.

54. Schnars, U. *Digital Holography: Digital Hologram Recording, Numerical Reconstruction, and Related Techniques*. Springer: New York, 2005.

55. Gass, J.; Dakoff, A.; Kim, M. K. Phase imaging without 2π ambiguity by multiwavelength digital holography. *Opt. Lett.* **2003,** *28*, 1141-1143.

56. Mann, C. J.; Bingham, P. R.; Paquit, V. C.; Tobin, K. W. Quantitative phase imaging by three-wavelength digital holography. *Opt. Express* **2008,** *16*, 9753-9764.

57. Hendargo, H. C.; Zhao, M.; Shepherd, N.; Izatt, J. A. Synthetic wavelength based phase unwrapping in spectral domain optical coherence tomography. *Opt. Express* **2009,** *17*, 5039-5051.

58. Lieber, C. A.; Mahadevan-Jansen, A. Automated Method for Subtraction of Fluorescence from Biological Raman Spectra. *Appl. Spectrosc.* **2003,** *57*, 1363-1367.

2.8 Appendix

2.8.1 Dual-Wavelength Linear Regression Phase Unwrapping in Three-Dimensional Microscopic Images of Cancer Cells

2.8.1.1 Summary

Phase imaging of objects with optical height variation greater than the wavelength of light is ambiguous and causes phase wrapping. By comparing two phase images recorded at different wavelengths, the images can be accurately unwrapped. This section describes the algorithm used to unwrap the images acquired with the dual-wavelength imaging setup. This unwrapping method is an improvement over previous methods because it is computationally fast and straightforward, and can process complex topologies. Additionally, limitations on the total optical height are significantly relaxed. This methodology is widely applicable to other phase imaging techniques as well as in applications beyond optical microscopy.

2.8.1.2 Introduction

In DHM, the superposition of the object and the reference waves is recorded by a CCD array and is reconstructed by numerically propagating the optical field along the direction perpendicular to the hologram plane (z-direction) in accordance with the laws of diffraction. Once the complex field is calculated, the phase $\phi(x,y)$ can be calculated. If the light wave reflects from an object, then its surface is described by a height map $h(x,y)$ which is determined from the phase map $\phi(x,y)$ of the holographic reconstruction at a given wavelength (Equation 2.1). If the object is a mostly transparent cell on a reflective substrate, such that the light propagates through it, reflects from the substrate, and propagates back, then the physical height is given by Equation 2.2. The phase images of objects with the optical thickness variation greater than λ are ambiguous and contain 2π-discontinuities. Such phase images need to be unwrapped. A great number of software algorithmic approaches to unwrap phase have been developed.[52] However, all of them are computationally intricate and often slow. Moreover, they cannot handle certain complex phase topologies, such as those generated from porous materials.[53] Even a relatively sophisticated software phase unwrapping algorithm can mistakenly

identify low intensity areas as multiple phase steps, producing artifacts in height features.

Previously, multiple-wavelength techniques that remove the 2π-discontinuities were introduced.[54-57] These methods are based on the comparison of the phase maps $\phi(x,y)$ obtained with different wavelengths, as the discontinuities in those phase images do not occur at the same places. Suppose the object under study is a reflective surface that is being imaged by using two beams with different wavelengths, and each wavelength is smaller than the overall object height. Then, the height map is (Equation 2.3)

$$h(x,y) = \frac{\lambda_1}{2\pi}\varphi_1(x,y) + \lambda_1 m_1(x,y)$$
$$= \frac{\lambda_2}{2\pi}\varphi_2(x,y) + \lambda_2 m_2(x,y)$$

where m_1 and m_2 are the unknown non-negative integer numbers at a point *(x,y)*. From these equations, we have (Equation 2.4)

$$\frac{\varphi_1(x,y)}{2\pi} + m_1(x,y) = \frac{h(x,y)}{\lambda_1}$$
$$\frac{\varphi_2(x,y)}{2\pi} + m_2(x,y) = \frac{h(x,y)}{\lambda_2}.$$

Subtracting the second equation from the first in Equation 2.4 gives (Equation 2.5)

$$h(x,y) = \frac{\lambda_2\lambda_1}{\lambda_2 - \lambda_1}\cdot$$
$$\left[\frac{\varphi_1(x,y) - \varphi_2(x,y)}{2\pi} + m_1(x,y) - m_2(x,y)\right].$$

The term $\Lambda_{12} = (\lambda_2\lambda_1)/(\lambda_2 - \lambda_1)$ is known as the synthetic or beat wavelength. Assuming that λ_2 is bigger than λ_1, then m_1 cannot be smaller than m_2. If we also assume that the total height of the object is less than the synthetic wavelength, then the term $\frac{\phi_1(x,y) - \phi_2(x,y)}{2\pi} + m_1(x,y) - m_2(x,y)$ must be nonnegative and less than 1. Because $0 \le \phi_{1,2}(x,y) \le 2\pi$, the first term in brackets is between -1 and +1. Therefore, depending

on whether this term is positive or negative, the term $m_1(x,y) - m_2(x,y)$ *must* be equal to either 0 or 1.

Thus, subtracting the two phase maps obtained from the same object using two wavelengths of the input light beams and adding 2π whenever the phase difference is negative yields a new phase map which corresponds to the beat wavelength Λ_{12}. The height image of the object can then be obtained. In practice, however, this method, while extending the range of unambiguous phase measurement, also increases error.[55] For example, if the laser wavelengths of 633 nm and 532 nm are used to generated two phase maps, we then have $\Lambda_{12} = 3.3$ μm. If we assume that each phase measurement has uncertainty of 0.1 rad, an optical thickness profile map obtained from a single wavelength will have the error of only about 10 nm. However, the error of the extended range optical thickness profile will be approximately 70 nm, which is unacceptably high. This severely limits the applicability of this method for any measurements obtained by the dual-wavelength method. It is possible to use the dual-wavelength profile as a rough guide to correct one of the original single wavelength maps. However, this method fails if the noise in the phase map, obtained by each of the single wavelengths, exceeds a certain limit.[55] It also requires the two wavelengths to be sufficiently far apart, reducing the total measurable range because of the decrease of Λ_{12}.

2.8.1.3 Phase Unwrapping Algorithm

Here, we present a method for phase unwrapping that bypasses the generation of the synthetic wavelength profile. This method also allows for increase of the measurable height range. Rearranging Equation 2.3, we have (Equation 2.6)

$$m_1(x,y) = \frac{\lambda_2}{\lambda_1} m_2(x,y) + \frac{1}{2\pi}\left(\frac{\lambda_2}{\lambda_1}\varphi_2(x,y) - \varphi_1(x,y)\right).$$

Theoretically, in the absence of any uncertainty in phase and wavelength measurements, this linear equation of m_1 in terms of m_2 can be solved exactly for integer values m_1 and m_2. Moreover, unless the two wavelengths have a common divisor (e.g., the wavelengths are *exactly* 500 nm and 600 nm), the range for

unambiguous height measurements extends to infinity, as there is only one set of integers m_1 and m_2 where Equation 2.6 holds exactly true. When the real phase measurements are involved, this linear equation of m_1 in terms of m_2 can be used to determine the most likely integers m_1 and m_2 by rounding (Equation 2.7)

$$m_1(x,y) = round\left(\frac{\lambda_2}{\lambda_1} m_2(x,y) + \frac{1}{2\pi}\left(\frac{\lambda_2}{\lambda_1}\varphi_2(x,y) - \varphi_1(x,y)\right)\right)$$

where m_2 is such that the difference between Equations 2.6 and 2.7 is at the minimum (i.e., the left side of Equation 2.6 is closest to an integer). Equation 2.5 is a special case of Equation 2.7, where the difference between m_1 and m_2 is allowed to be either 0 or 1, that is, m_1 = int[m_2 λ_2/λ_1]. However, in a general case, the object's overall height is different from Λ_{12}, and there is no need to set this limit for the value of m_2. The range of allowed m_2 values can be selected based on the overall height of the sample, which can be estimated by observing the wrapped phase image and counting the number of observable phase jumps.

Because the wavelengths of the input laser light beams can be measured very accurately, the slope of the line $m_1(m_2)$ (Figure 2.S1) has much smaller uncertainty than the *y*-intercept, which is dependent on the measured phases for each point of the image. By finding the value of m_2 at which m_1 is closest to the nearest integer, we can determine the correct number of integer wavelengths and recreate the optical thickness profile of the original object. In practice, there may be areas in one or both of the single wavelength images that are corrupted by excessive noise, such that the algorithm will not pick the right m_2 but may select the neighboring value instead. The likelihood of this increases if the two

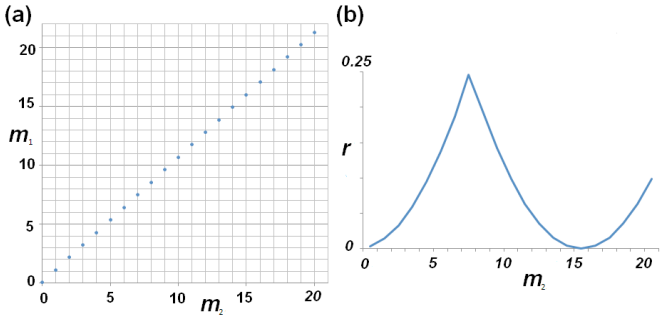

Figure 2.S1: Linear regression phase unwrapping: (a) $m_1(m_2)$ via Equation 2.8 and (b) $r(m_2)$ – the square of difference between m_1 and the nearest integer. In this example, the wavelengths are 675 nm and 635 nm, and $r(m_2)$ is minimal at m_2 = 16.

wavelengths are closer to each other, as then the slope in Figure 2.S1 is closer to 1, and different values of m_2 are more difficult to distinguish. Therefore, once the phase unwrapping is complete, if some of the areas in the image are noisy, the pixels in these areas need to be shifted back to their proper places by using a software algorithm which looks for λ_2 jumps in the final image and corrects them by shifting the pixels up or down.

2.8.1.4 Live Cell Imaging

Figure 2.S2 shows the phase image of two KB cells, obtained by our dual-wavelength digital holographic microscope. The light from two pigtail laser diode systems (675 nm and 635 nm) is combined using a beamsplitter and is then split again into object and reference arms. The two beams are recombined and the interference pattern is imaged on a CCD array using a water immersion objective. The curvature mismatch between the reference and object waves is compensated numerically.[3] It is clear from the single wavelength images (Figures 2.S2a and b) that the object is about two wavelengths high and, therefore, there is no need to extend the range beyond that. Figures 2.S2c and d, obtained by our linear regression dual-wavelength method, present the final unwrapped image, free of discontinuities.

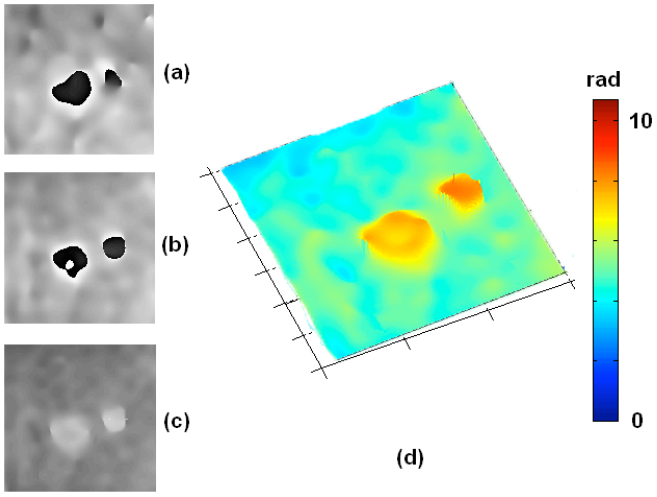

Figure 2.S2: Digital holographic images of KB cells. (a) Phase image at 675 nm. (b) Phase image at 635 nm. (c) Dual-wavelength unwrapped phase image. (d) 3D pseudo-color rendering of (c). Images are 150 x 150 pixels, 60 x 60 µm.

If the object is many wavelengths high, this method is still capable of unwrapping the phase and producing the final height map free of discontinuities. Figure 2.S3 shows two SKOV-3 ovarian cancer cells on a substrate, which was tilted with respect to the optical axes in order to increase its overall height range to demonstrate this method.

While the object in Figure 2.S3 is twice the height of the synthetic wavelength Λ_{12}, it is still unwrapped correctly, which would have been impossible previously using only two wavelengths.[55] The height range at which the unambiguous phase-imaging can be performed is still somewhat limited by noise, because if the object is very thick (the maximum m_2 is allowed to be large and so the graph in Figure 2.S1 includes many minima), there is more room for error; in that case, determining the right value of m_2 can be problematic. However, a flexible tradeoff is achieved between the higher height range and higher accuracy.

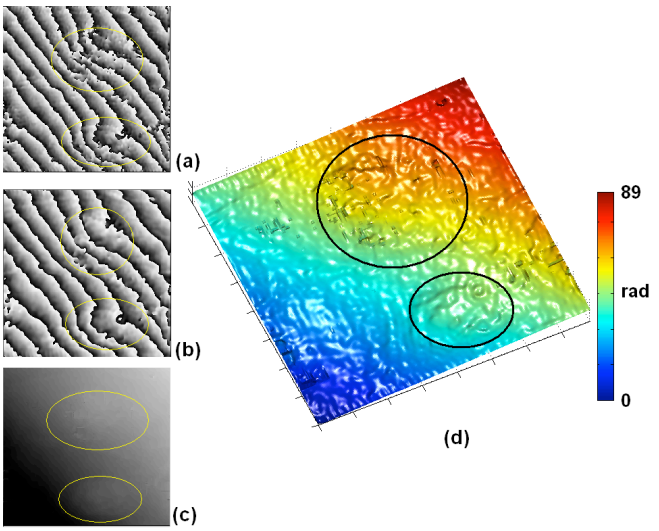

Figure 2.S3: Digital holographic images of two ovarian cancer cells (marked with circles) with the substrate at an angle. (a) Phase image at 532 nm. (b) Phase image at 633 nm. (c) Dual-wavelength unwrapped phase image. (d) 3D pseudo-color rendering of (c). The images are 256 x 256 pixels, 78 x 78 μm , and m_2 was set to 12.

2.8.1.5 Conclusion

In conclusion, our dual-wavelength unwrapping is well equipped to deal with complicated phase topologies, and is computationally fast (only limited by the speed at which the angular spectra for both wavelengths are calculated). The method's application is not limited to DHM, but also can be applied to other phase-imaging techniques, such as phase shifting interferometry. By extending unambiguous optical phase-imaging methods to objects of different heights, linear regression dual-wavelength unwrapping method makes phase-imaging much more practical, allowing three-dimensional measurements of a wide variety of biological systems and microstructures.

2.8.2 Dual-Wavelength Digital Holographic Imaging with Phase Background Subtraction

2.8.2.1 Summary

Three-dimensional measurements by DHM often require removing the background from the phase image. DHM measures the phase difference between plane object and reference waves, which, along with the phase difference due to the actual optical thickness variation of a sample, includes phase difference due to the path length difference between the object and reference arms. If this path length difference is not the same for each pixel in the phase image, background curvature will be present. Some of this background curvature can be compensated numerically by multiplying the propagating wavefront by a phase factor.[3] However, that may still leave a small amount of uncompensated background curvature, which can be problematic, as even a small variation in the background due to incompletely compensated curvature can drastically affect total volume measurements. Here, we present an automated iterative algorithm based on slowly varying polynomial fitting of the phase map, with subsequent removal of the background curvature. The efficacy of the method is demonstrated by removing background both from a simulated surface and from an image containing ~30 KB cells. This method is an extension of the dual-wavelength phase unwrapping algorithm described in Section 2.8.1, and allows for accurate volume measurements of several small objects within the same image frame.

2.8.2.2 Phase Background Removal From a Simulated Surface

Figure 2.S4 shows several simulated cells on a flat substrate. A small amount of uncompensated curvature in each of the single-wavelength images (Figures 2.S4b and c), is present in the final unwrapped image (see Figure 2.S4d). To properly calculate the total volume of all cells, this curvature needs to be removed. The ideal method for background subtraction will remove the uncompensated curvature with the minimal user intervention, while still retaining the shapes of the cells. In order to separate the background from the cells, we implemented an algorithm, based on modified polynomial fitting.[58] The method is as follows:

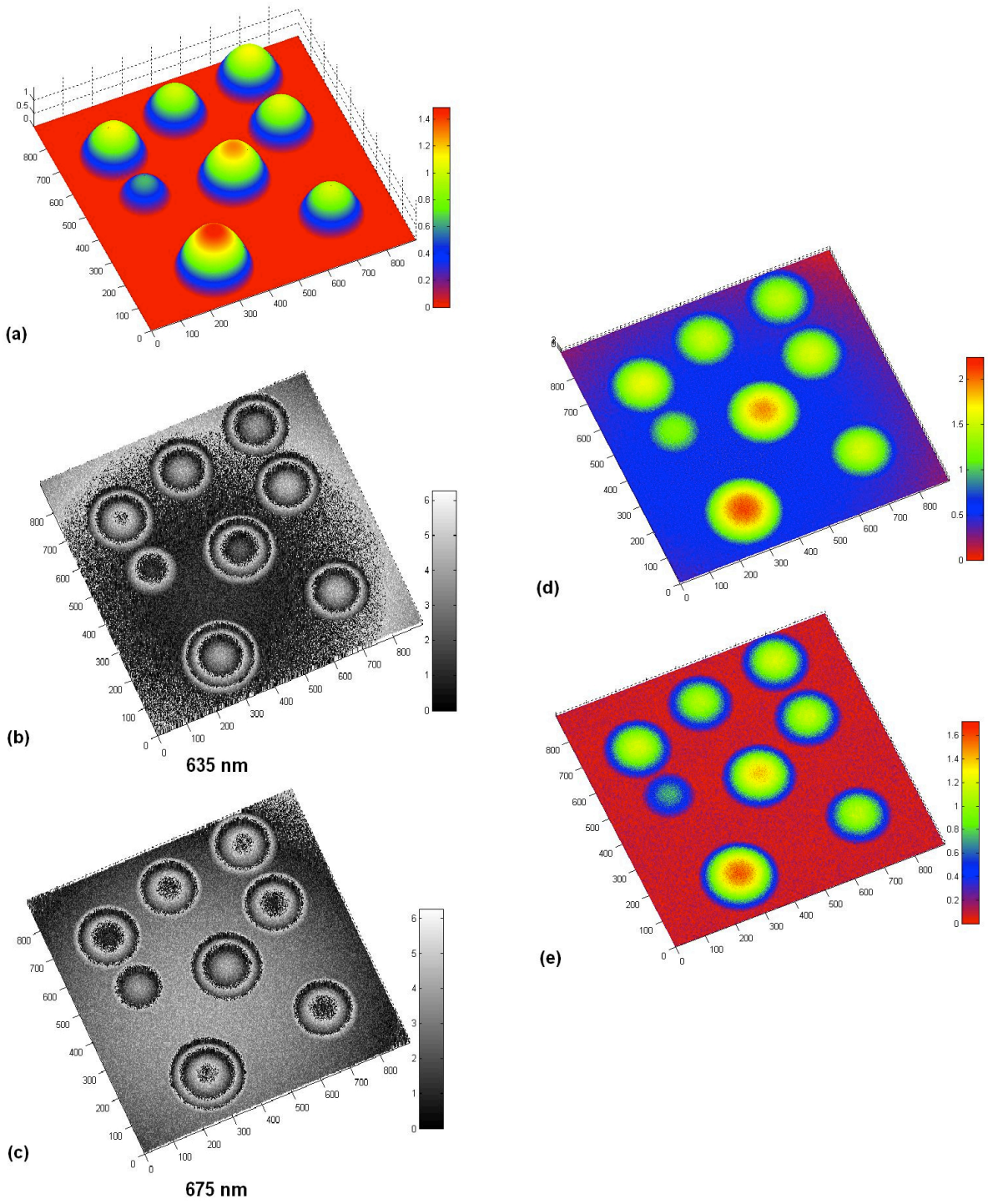

Figure 2.S4: Unwrapping and background removal. (a) Simulated cells on the flat substrate. (b) Phase image at 635 nm with up to 20% phase noise. (c) Phase image at 675 nm with up to 20% phase noise. (d) Dual-wavelength unwrapped phase image. (e) Dual-wavelength unwrapped phase image with background removed (vertical scale is in radians).

1. Fit a polynomial (order 2) surface to the unwrapped phase image.
2. Compare the polynomial surface with the original image pixel by pixel and retain the lower of two values. Generate a new profile.
3. Substitute the unwrapped phase image with the new profile obtained in Step 2.
4. Repeat Steps 1, 2 and 3 several times until the profile converges.

Finally, the processed background is subtracted from the original unwrapped phase image, yielding a phase profile with a near-null background.

We have found that this method,[58] while substantially reducing the background, tends to "overcompensate" any curvature that it finds in the original unwrapped phase image. To illustrate this point, consider a curved profile (Figure 2.S5). The first iteration (dotted line), while removing the original peaks, also goes under the original curved profile near the ends of the frame, resulting in the curvature being overcompensated (dashed line). We have found that this overcompensation can be fixed by modifying Step 2 of the algorithm as follows:

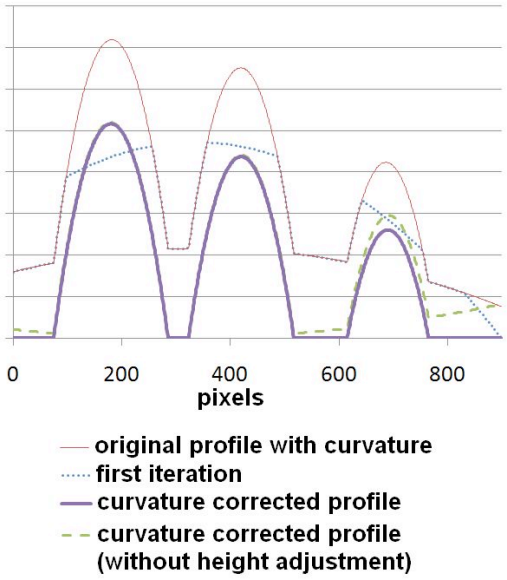

Figure 2.S5: Background subtraction by polyfit method, showing original profile with curvature, first iteration of the polyfit method, as well as the results of the algorithm with/without height adjustment (steps 2a-2c) applied.

2a. Compare the polynomial surface with the original image.
2b. Find the maximum difference between the fit and the original profile.
2c. Add a fraction of that maximum difference to the polynomial surface.

This modification, although making the convergence much slower, does result in a much flatter final image (Figure 2.S5, solid line). The fraction, used in Step 2c, can be as high as 95 percent and is limited only by computational rounding errors. Generally, the higher the number, the longer it takes for the method to converge. The result of this modified algorithm applied to the simulated cells in Figure 2.S4a is presented in Figure 2.S4e.

2.8.2.3 Phase Background Removal From a Live Cell Image

Figure 2.S6 shows the results of both linear regression unwrapping and modified polyfit background subtraction for a sample of about 25 KB human epithelial cells. As evidenced from Figure 2.S6c, the application of both methods is highly successful in removing phase discontinuities and background curvature, which allows for accurate measurement of the total volume of all the cells in the sample.

It is worth noting that one of the sources of phase noise is a result of misalignment between the two wavelengths (i.e., the phase images produced by each wavelength are not entirely consistent with each other. Thus, using three or more wavelengths to further extend the range of unambiguous phase measurements[54] can actually lead to higher noise and therefore may not be desirable. Additionally, while the method generally performs well,

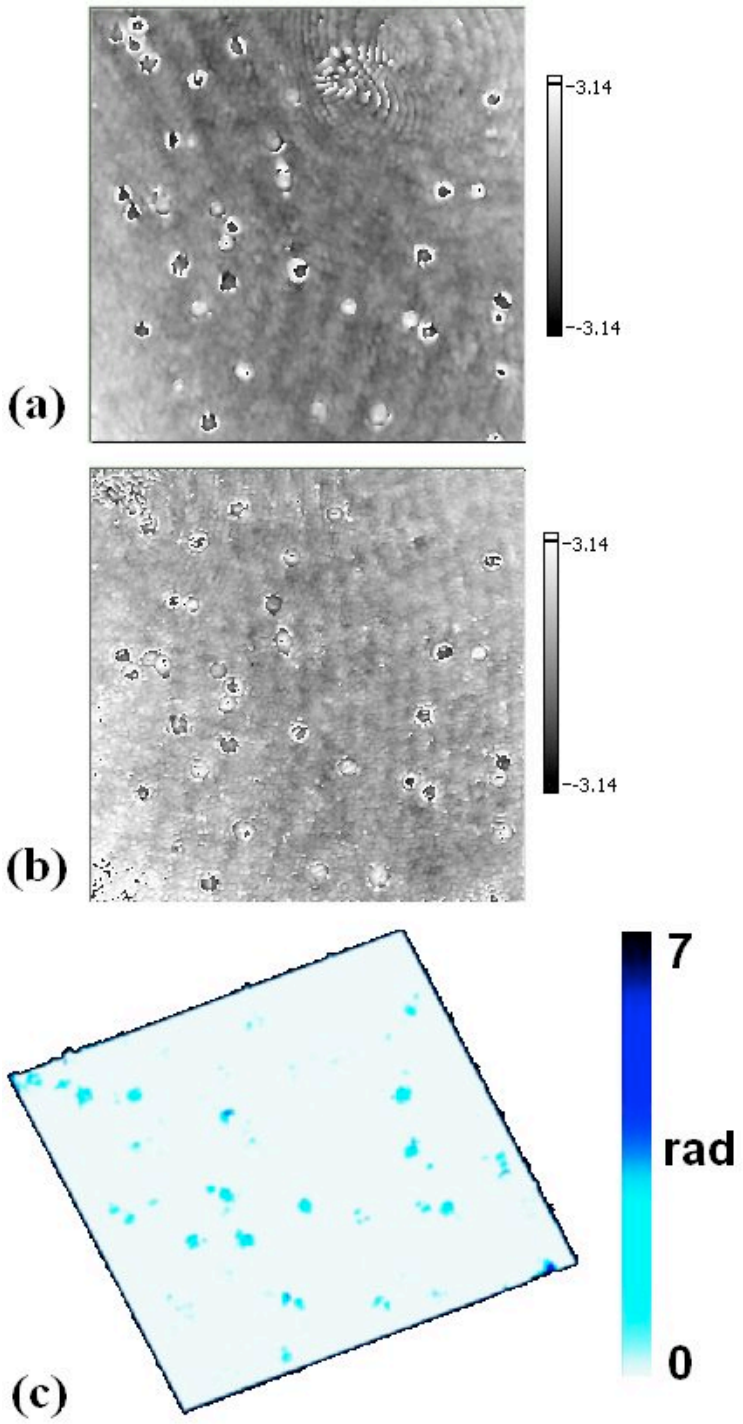

Figure 2.S6: Imaging KB cells. (a) Phase image at 635 nm. (b) Phase image at 675 nm. (c) Dual-wavelength unwrapped phase image with background subtracted by polyfit method. All images are 140 x 140 µm (700 x 700 pixels).

in some of the images there may be areas where one of the single-wavelength images is corrupted by excessive noise. This results in the algorithm selecting a neighboring value of m_2, producing occasional “spikes”. Therefore, once the unwrapping is complete, these areas still need to be shifted back to their proper places using a software algorithm that looks for λ_2 jumps in the final image and corrects them by shifting the segments up or down.

Chapter 3

Concurrent Enrollment in Lecture and Laboratory Enhances Student Performance and Retention[1]

3.1 Introduction

Science, technology, engineering, and mathematics (STEM) education in the United States (US) has received increased attention in the past two decades (Committee on Prospering in the Global Economy of the 21st Century, 2007, 2010). This is largely because the evolving global economy, especially the recession that began in 2008, has revealed the imperative need for quality STEM education at all levels in order to remain financially competitive. In an address to Forsyth Technical Community College in Winston-Salem, North Carolina in 2010, President Obama declared that rising to the challenge of creating an innovation-based economy is this generation's "Sputnik moment". Currently, a major public agenda is maintaining and increasing national support for STEM education from kindergarten through graduate school. For example, the American Competitiveness Initiative (ACI), announced by President George W. Bush in the 2006 State of the Union Address, aimed to increase federal funding for STEM education with the goals of, among others, administering math and science curriculum development grants, increasing the number of highly qualified math and science teachers, and increasing the number of post-secondary students and postdoctoral fellows in STEM fields. Replacing the ACI, the America

[1]Portions of this chapter have been published: Matz, R. L., Rothman, E. D., Krajcik, J. S., & Banaszak Holl, M. M. (2012). Concurrent Enrollment in Lecture and Laboratory Enhances Student Performance and Retention. *Journal of Research in Science Teaching*, *49*(5), 659-682. John Wiley & Sons has granted permission for this content to be reprinted.

COMPETES Act was signed into law in 2007 (and reauthorized in 2010), providing assistance for educating STEM professionals and improving undergraduate research experiences, and calling on federal agencies to provide curriculum support and materials to educational institutions. Additionally, the President's Council of Advisors on Science and Technology (PCAST) released a report earlier this year describing the need for one million more university graduates with STEM degrees in the next decade over the amount the US would already be expected to produce (President's Council of Advisors on Science and Technology, 2012).

Amidst this national discourse, universities are responsible for teaching according to best practices established in the educational literature. Many initiatives are already underway to bolster STEM education specifically at universities. The Association of American Universities (AAU), for example, announced a five-year plan in 2011 that would improve the quality of teaching and learning in STEM fields at its member institutions (Association of American Universities, 2011). Alongside these "top down" initiatives, many faculty and students are working hard to implement and evaluate educational improvements that they have made in the classroom, with thousands of articles being published in STEM education disciplines every year. The research presented here describes one such "bottom up" approach. As the achievement gap between the US and other countries has been narrowing for many years, we find that such improvements in STEM education are still needed, being especially mindful of the context of constricted university budgets.

Towards the national goal of improving STEM education at the undergraduate level, in this chapter, we report a study of enrollment practices in an introductory science sequence at the University of Michigan. The study describes the impact of concurrently enrolling in general chemistry lecture and laboratory courses, as opposed to enrolling in the lecture first and the laboratory later or not at all. We find that concurrent enrollment both positively impacts student's final grades in the lecture and decreases their withdrawal rate. Based on the number of students who enroll in the course, the study predicts that more than 400 students annually would be positively impacted by a departmental policy that required concurrent enrollment. This research can be used as a

model for studying similar questions in other contexts, such as at other universities and/or in different academic disciplines.

The chapter begins with background in laboratory learning goals and an assessment of the prevalence of concurrent enrollment at similar universities. Next, details regarding the different formats of the lecture and laboratory courses are provided, and the methods for data collection and analysis are given. Regression results showing the relationship between concurrent enrollment and the two outcome variables are then presented. The chapter concludes with proposed reasons for the observed results, including an extensive discussion on the collaborative nature of the laboratory course, and implications for the University of Michigan and science educators more broadly. Finally, future work is proposed.

I was the lead researcher on this project. My work was to obtain, clean, and analyze the data set, interpret the analyses, present the findings to the other coauthors on the manuscript, and write the entirety of the manuscript for publication. Ed Rothman provided statistical expertise and guidance, Joe Krajcik provided perspective on situating our work in the science education field, and Mark Banaszak Holl provided expertise in teaching general chemistry as well as overall guidance for the project.

3.2 Background

Laboratories have historically been important tools for teaching and learning in the natural sciences; for more than 100 years, laboratories have been employed to help students interact with scientific phenomena (Hofstein & Lunetta, 1982, 2004). In multiple disciplines as well as across educational levels, laboratories have been shown to improve creative thinking and problem-solving abilities (Hill, 1976), scientific thinking (Raghubir, 1979; Wheatley, 1975), intellectual development (Renner & Fix, 1979), and practical skills, and increase favorable attitudes towards science (Ben-Zvi, Hofstein, Samuel, & Kempa, 1976; Bybee, 1970). Because laboratory experiences have been found to promote learning in so many disciplinary contexts, the laboratory has truly become a cornerstone of science education.

Recently, the National Research Council defined a core set of seven science learning goals for students that laboratories should advance in *America's Lab Report* (2006): "enhancing mastery of subject matter, developing scientific reasoning, understanding the complexity and ambiguity of empirical work, developing practical skills, understanding the nature of science, cultivating interest in science and interest in learning science, and developing teamwork abilities" (p. 76-77). The general goals for science education are similar, but laboratories are especially and uniquely suited for helping students develop practical skills and understand the complexity and ambiguity of empirical work (Millar, 2004). The extent to which these goals are attained in laboratories at any educational level differs according to instructor competence, available resources, integration with other instructional activities, and students' prior knowledge and experiences. The specific rationale for each goal in learning science necessarily varies. For example, scientific reasoning skills, such as developing scientific arguments and models, are indispensible for examination of the material world and are not easily learned without structured education (Zimmerman, 2000). Decades of studies have shown that both students' and the general public's understanding of the nature of science is oftentimes naïve and inaccurate (Driver, Leach, Millar, & Scott, 1996; Lederman, 1992), therefore another goal of laboratories is to improve understanding of the nature of science. Student achievement of these seven goals in concert is vital for fostering general scientific literacy and training future scientists, engineers, and citizens at large.

For as many years as laboratories have been lauded for achieving science learning gains, however, they have also come under fire for being expensive in terms of materials and personnel as well as time-consuming (Baker & Verran, 2004). Budget restrictions, safety concerns, increased attention to test scores on state- and nation-wide standardized exams, and lack of adequate instructor preparation for teaching laboratories have all contributed to the reduction in time students are able to spend doing laboratory experiments, and, in some cases, these factors have been instrumental in the elimination of laboratories altogether at the high school level (Council, 2005; Washam, 2007). Indeed, one of the key conclusions of *America's Lab Report* is "the

quality of current laboratory experiences is poor for most students" (p. 6). Students at schools with low socioeconomic status and/or high proportions of non-Asian underrepresented ethnic groups are especially likely to experience a lack of adequate laboratory space, equipment, and materials, and these circumstances play a role in these students spending less time doing laboratory activities than others (Banilower, Green, & Smith, 2004). This is problematic because the balance of remaining laboratory instructional time may not reflect established educational design principles. Laboratories may lack explicit learning goals or adequate connection to other instructional activities, for example, and this can reduce laboratory experiences to "cookbook" procedures where coverage of long lists of science topics takes precedence. In these weak (or nonexistent) laboratory environments, students may pick up some subject matter, but are unlikely to attain other important science learning goals for laboratories, namely developing scientific reasoning, understanding the nature of science, and cultivating interest in science (Council, 2005).

The high financial, time, and personnel commitments required for running laboratories has for decades motivated research studies comparing laboratory instruction with other modes of teaching with the goal of identifying equally beneficial but more cost-effective methods, and some have fought for the removal of wet laboratories altogether (see (Hofstein & Lunetta, 1982, 2004) and references therein). Some of these studies concluded that laboratory experiences are no more beneficial to students than other types of instruction such as viewing a movie, doing group work, or having a class discussion, with the exception that students in traditional laboratory settings have better abilities to perform practical manipulations in the laboratory. However, the usual method of student evaluation in these studies was paper-and-pencil tests that did not measure many of the important science learning goals described above. Given, then, that the laboratory is uniquely suited for helping students achieve some specific learning goals, but also that it is expensive and time-consuming, current studies are needed to assess the value of laboratories in terms of encouraging science learning. Here, we demonstrate that enrolling in an introductory college-level laboratory concurrently with

the corresponding lecture course promotes learning gains and retention in comparison to students who enroll in the lecture alone.

3.3 Rationale and Research Question

Most scientists and educators agree that laboratory experience is imperative for learning science (Carnduff & Reid, 2003); teaching general chemistry apart from the laboratory has even been considered "pedagogically and philosophically unsound" (Wojcik, 1990). Even so, a survey of the most recent available course guides at 40 public, U.S. universities with high undergraduate enrollment revealed that 38%, 43%, and 33% offer general biology, chemistry, and physics lectures and laboratories, respectively, as separate courses without requiring concurrent enrollment (Table 3.1). This separation does provide some perceived benefits. Practically, it can act to ease students' scheduling conflicts. Oftentimes these general science courses act as service courses for other disciplines, so offering the lecture and laboratory separately can also "benefit" students who are required to take only one of them for a particular course of study (Long, McLaughlin, & Bloom, 1986) and may ease the financial burden of the laboratory on the department (Dubravcic, 1979). Additionally, universities may not have sufficient physical laboratory space for all of the lecture students in a given term to enroll in the laboratory. The separation of lecture and laboratory courses may also help deconvolute a student's grades; in other words, a student who performs well in the laboratory but has trouble in the lecture earns separate lecture and laboratory grades that more accurately reflect the student's abilities than a single, all-inclusive grade (Cawley, 1992). Similarly, as a department chair at the university studied aptly stated, it allows students to fail one course while still receiving credit for the other; that is, it reduces the risk of taking a four- or five-credit course by dividing the class into three- and one- or two-credit segments.

Offering collegiate-level lectures and laboratories in the sciences as separate courses is typical and may have some benefits for the practical issues of scheduling and finances. There are, however, advantages to offering the lecture and laboratory as

Table 3.1: Introductory Science Lecture and Laboratory Enrollment Requirements at 40 NCAA, Public Universities

NCAA Conference	University	Biology		Chemistry		Physics	
		C[a]	NC[b]	C[a]	NC[b]	C[a]	NC[b]
Atlantic Coast	Clemson University	✓		✓			✓
	Florida State University	✓			✓	✓	
	Georgia Institute of Technology	✓		✓		✓	
	North Carolina State University	✓		✓		✓	
	University of Maryland	✓		✓			✓
	University of North Carolina		✓		✓	✓	
	University of Virginia		✓	✓			✓
	Virginia Polytechnic Institute	✓			✓	✓	
Big Ten	Indiana University		✓		✓	✓	
	Michigan State University		✓		✓		✓
	Ohio State University	✓		✓		✓	
	Pennsylvania State University	✓			✓	✓	
	Purdue University		✓	✓		✓	
	University of Illinois		✓		✓	✓	
	University of Iowa	✓		✓		✓	
	University of Michigan		✓		✓		✓
	University of Minnesota	✓		✓		✓	
	University of Nebraska		✓	✓			✓
	University of Wisconsin	✓		✓		✓	
Pacific-10	Arizona State University	✓			✓		✓
	Oregon State University	✓			✓	✓	
	University of Arizona		✓	✓		✓	
	University of California (Los Angeles)	✓		✓			✓
	University of California (Berkeley)	✓			✓	✓	
	University of Colorado		✓	✓			✓
	University of Oregon	✓			✓	✓	
	University of Utah		✓	✓			✓
	University of Washington	✓		✓		✓	
	Washington State University	✓		✓		✓	
Southeastern	Auburn University	✓			✓	✓	
	Louisiana State University		✓		✓		✓
	Mississippi State University	✓			✓	✓	
	University of Alabama		✓	✓		✓	
	University of Arkansas	✓		✓		✓	
	University of Florida	✓		✓			✓
	University of Georgia	✓		✓		✓	
	University of Kentucky		✓		✓		✓
	University of Mississippi	✓			✓	✓	
	University of South Carolina		✓	✓		✓	
	University of Tennessee	✓		✓		✓	
Total		25	15	23	17	27	13

Note. The most recent available course guides (either 2010-2011 or 2011-2012) from flagship campuses were surveyed. [a]Concurrent enrollment is required. [b]Concurrent enrollment is not required. We considered an institution to offer nonconcurrent enrollment if the lecture was listed as a corequisite for the laboratory but the laboratory was not listed as a corequisite for the lecture, or if multiple introductory tracks were offered and any allowed for nonconcurrent enrollment.

a single course or, at least, requiring concurrent enrollment. In particular, encountering the same scientific concept in multiple contexts has been shown to promote deeper conceptual understanding and facilitate transfer (Bransford & Schwartz, 1999). Also, isolated laboratory experiences have not been compelling in effecting mastery of specific scientific subject matter, whereas laboratory experiences combined with other instructional activities have promoted science learning (Hofstein & Lunetta, 2004). When laboratories are paired with other types of instruction such as lectures and group discussion, students are more apt to demonstrate interest in and positive attitudes towards science, and integrated instruction has been shown to specifically benefit lower ability students' scientific reasoning skills (White & Frederiksen, 1998). These and other positive outcomes of integrated instructional methods support a concurrent approach to teaching science lectures and laboratories.

Although literature support exists for the role of laboratories in learning science at the collegiate level, comparatively little has been published on the impact of the timing of laboratory enrollment in comparison to the lecture, that is, concurrent versus nonconcurrent enrollment; only a few studies that support concurrent enrollment have been reported. In the community college context, concurrently enrolled general biology students achieved higher learning gains on exams and reported more positive attitudes on attitude inventories than nonconcurrent students (Saunders & Dickinson, 1979). Concurrent enrollment in general physics lecture and laboratory courses was found to increase the lecture grades of students with intermediate grade point averages (GPAs) by approximately one third of a letter grade, though no significant effect was found for students with the highest and lowest GPAs (Long, et al., 1986). Here, we sought to understand the impact of concurrent enrollment in general chemistry lecture and laboratory on the withdrawal rates and final grades of students in the lecture at University of Michigan, a large, public university with high undergraduate enrollment. We hypothesized that concurrent enrollment would positively impact students in terms of both withdrawal rates and final grades because of the aforementioned goals of laboratories, particularly enhancing mastery of subject matter.

General chemistry at University of Michigan is an interesting context in which to investigate this issue of enrollment because of the strong emphasis on collaborative learning and teamwork in the laboratory studied; we suspected that concurrent enrollment would benefit students in part for this reason. Across many years and disciplines, collaborative work has been shown to enhance student achievement, retention, and attitudes, among other outcomes (Bowen, 2000; Council, 2006; Springer, Stanne, & Donovan, 1999). Proposed causal mechanisms for this relationship include that students working in groups perform metacognitive processes when they explain their reasoning to other group members (Hogan, 1999; White & Frederiksen, 1998), and ensuing peer interaction and argumentation enhances students' cognitive development by requiring students to validate their ideas (Chin & Osborne, 2010; Driver, Newton, & Osborne, 2000; Lumpe & Staver, 1995; Richmond & Striley, 1996). More broadly speaking, productive argumentation can promote science literacy (Cavagnetto, 2010). In the specific context of college-level chemistry courses, collaborative work has been shown to positively affect students' attitudes and perceptions (Cooper & Kerns, 2006; Tien, Roth, & Kampmeier, 2002), problem-solving strategies and abilities (Cooper, Cox, Nammouz, Case, & Stevens, 2008), overall achievement level (Bowen, 2000; Tien, et al., 2002), and has even been implicated in increasing retention among females in general chemistry laboratories (Cooper, 1994).

As compared to what is currently available in the literature, our data set is unique, covering six years and nearly 10,000 students. Of the studies we found specifically pertaining to concurrent versus nonconcurrent enrollment in science lecture and laboratory settings, one observed ~2,500 students over five years, but the other studied only 500 students over a single year, and both studies are dated (Long, et al., 1986; Saunders & Dickinson, 1979). Also, much time and attention has recently been paid to reforming "traditional" learning settings into "studio-style" settings. In this closely related set of literature, the majority of studies are current, yet report on usually less than 1000 students over one or two years (DiBiase & Wagner, 2002; Hoellwarth, Moelter, & Knight, 2005; Oliver-Hoyo, Allen, Hunt, Hutson, & Pitts, 2004). Our study is additionally based on relatively current student demographics; as the proportions of female, Hispanic,

Asian/Pacific Islander, and Black students in post-secondary classrooms have steadily increased since the 1970s (Education, 2011), this research probes a fundamentally different population of students than those in studies from the 1970s, 1980s, and 1990s.

Withdrawal rates were specifically examined in light of the national need to encourage retention of post-secondary students in the natural and physical sciences (Committee on Prospering in the Global Economy of the 21st Century, 2007; Maltese & Tai, 2011). As general chemistry is a "gateway course" to many scientific disciplines, withdrawal at this introductory level not only increases time-to-degree but is also a serious barrier to progression in the sciences and engineering (Seymour & Hewitt, 1997; Strenta, Elliott, Adair, Matier, & Scott, 1994). In the data described herein, for example, there were 260 students who withdrew from general chemistry lecture. Of these students, only 109 (42%) returned to take the course a second time. The retention of nonscience majors in science courses is also an important issue due to the need for a scientifically literate and critical public (Council, 1996, 2005; Glynn, Taasoobshirazi, & Brickman, 2007; Martens, 2007). Considering only the 3,359 general chemistry students in this study who had graduated by the time the data were obtained, we found that 35% (1,172) did not major in a science or engineering field (Table 3.2).

We also specifically examined final grades because exam and overall course grades are routinely used as measures of cognitive outcomes, that is, student performance, achievement, and/or learning (Dubravcic, 1979; Long, et al., 1986; Marshall & Dorward, 2000; Saunders & Dickinson, 1979). A student's college grades are also useful as a gauge of how well they have adapted to the college environment, and are a strong predictor of earning a bachelor's degree (Pascarella & Terenzini, 2005). We recognize that there are significant pitfalls in blindly assuming that grades reflect real learning (Pascarella & Terenzini, 2005; Walvoord, 2004), however, grades are generally useful as tools for approximating cognitive results.

Table 3.2: Summary of Student Characteristics

Characteristic	Lecture format[c]			Total
	Traditional	Extra time	Studio	
Total	8624	466	348	9438
Laboratory enrollment				
Concurrent	5390	232	348	5970
Nonconcurrent	3234	234	0	3468
Gender				
Female	3930	324	192	4446
Male	4694	142	156	4992
Ethnicity				
Asian	1276	29	63	1368
Black	525	165	24	714
Hispanic	394	50	14	458
Native American	69	12	1	82
White	5609	192	222	6023
None	615	13	21	649
Missing	136	5	3	144
Age[a]				
Freshman (≤ 2)	7519	395	339	8253
Sophomore (2 < x ≤ 4)	820	54	6	880
Junior (4 < x ≤ 6)	158	10	1	169
Senior (> 6)	115	7	2	124
Missing	12	0	0	12
Degrees earned[b]				
Science or engineering	2077	55	55	2187
Concurrent	1228	26	55	
Nonconcurrent	849	29	0	
Nonscience or –engineering	1047	81	44	1172
Concurrent	551	34	44	
Nonconcurrent	496	47	0	
Missing	5500	330	249	6079

[a]Student's ages are reported according to the cumulative number of terms they had been enrolled at the university prior to and including the term in which they first enrolled in the lecture. [b]Describes students who had completed a major (minors not included) in a science or engineering field by the time that these data were collected in 2008. [c]Lecture formats are fully described in the Study Context section.

3.4 Methods

3.4.1 Study Context: General Chemistry at University of Michigan

This study was performed at a large, public, midwestern university where general chemistry consists of separate lecture and laboratory courses, each one semester in

length. Students have the option to enroll in the lecture and laboratory either concurrently or nonconcurrently, and some students enroll in the lecture without ever enrolling in the laboratory. In this data set, 63% of students were concurrent, 22% were nonconcurrent (though neither course is a prerequisite for the other, the vast majority of these students—97%—enroll in the lecture first), and 15% enrolled in the lecture only. Because the majority of nonconcurrent students enroll in the lecture first, the students who enrolled in the lecture only were considered nonconcurrent students in this research. Students have the option of taking the lecture in one of three different formats, and in any given year, approximately 91% of students enroll in the traditional lecture format with the remaining 9% roughly evenly split between the other two formats. For all courses, the content was generally stable from year to year, and technological advances mainly influenced changes in structure. Based on the students for whom we have degree information, 66% of students in the traditional lecture format eventually completed science and/or engineering majors, the highest percentage of all three lecture formats (Table 3.2). Additionally, in the traditional format, the majority of students were concurrently enrolled regardless of whether they completed a science/engineering or nonscience/nonengineering degree (59% and 53% concurrently enrolled, respectively) (Table 3.2). A quasi-experimental design was employed in which the assignment of students to (1) the concurrent or nonconcurrent group or (2) a particular lecture format was uncontrolled because of the disruption to the students' education that using random assignment in a true experiment would have caused, and we have attempted to control for resultant confounding variables. For all courses described here, students were graded on an absolute scale as opposed to on a curve.

The first lecture format is a traditional course that meets three times weekly for 50 minutes; 63% of students who take the lecture in the first format are concurrently enrolled. This course is a general introduction to chemistry, considering the following major topics: measurement, atomic theory and structure, stoichiometry, types of chemical reactions, gas laws, thermochemistry, quantum theory, electron configurations and periodicity, bonding, molecular orbital theory, states of matter, equilibrium, and acid-base chemistry. In addition to lecture time, students have a 50-minute discussion once

per week with a graduate student teaching assistant. Discussion attendance is not explicitly required, but most students attend most discussions because weekly quizzes are administered there, and these eventually count for 20% of the final grade. The grading scheme places a large emphasis on exams with 70% of the final grade derived from the two midterms plus the final exam. All exams are multiple-choice, whereas quizzes require work to be shown, and the online homework is a hybrid that requires student-generated responses. Of all the courses described here, this version has the most variance in terms of the number of instructors involved, with 12 unique instructors having taught one or more sections (each section is ~400 students) over the years of this study. A single instructor has served as the course coordinator throughout this time, providing continuity in course structure and content. The average total class size during this period was ~1,400 students. This format serves the largest number of students by far, so the results presented here should be interpreted as mainly reflective of the effect of enrollment for students' final grades in and withdrawal rates from this lecture format.

The second lecture format is designed for students who were expected to benefit from extra in-class time and office hours, generally underrepresented ethnic groups, first-generation college students, and students from low socioeconomic status backgrounds and/or very small high schools. In this format, students meet with an experienced instructor four times weekly for 50 minutes each, and 50% of these students are concurrently enrolled. As in the first lecture format, students attend one 50-minute discussion per week with a graduate student teaching assistant and have the same structure for quizzes, though the number of students per discussion is smaller compared to the traditional format. The extra class period as well as extra faculty and teaching assistant office hours are provided for in-depth analysis of central concepts and extra practice time for students. The content of this lecture format is the same as that of the traditional format, and the syllabi, grading schemes, homework, quizzes, and exams are uniform across the two formats. The primary difference between this format and the traditional format is pacing, having 200 and 150 minutes per week of contact time, respectively, to teach the same material. The instructor for this lecture format was the same across all years of this study, and average class size was ~80 students.

Students can gain access to this lecture format in one of a few different ways. Firstly, based on the factors described above, the Office of Undergraduate Admissions (OUA) identifies incoming students as eligible for participation in a comprehensive academic support program, which includes access to extended forms of introductory courses such as this general chemistry lecture format. Students in the comprehensive program are encouraged to enroll in this lecture format but may elect not to do so. Secondly, students who are not identified by OUA as eligible for the comprehensive program may apply to become an affiliate of the program and thus gain access to the resources that the program offers, including this lecture format of general chemistry. Thirdly, students who are not at all affiliated with the comprehensive program may be able to register for this format if they demonstrate a scheduling conflict with all sections of the traditional format of the course. In these data, the percent of students who are affiliated with the comprehensive academic support program in this lecture format and the traditional format is 52% and 7%, respectively.

The general chemistry laboratory course is offered in a single format; students who enroll in either of the lecture formats described above may take this laboratory course. Students attend one three-hour laboratory/discussion session and one 50-minute lecture per week. The topics of experiments in this course include solubility, solution analysis, redox reactions, acid-base chemistry, metal complexes, and analysis of reactions, and though the topics are obviously similar to those taught in the lecture, the laboratory content is not explicitly linked to or aligned with the lecture content in any way. The pacing of the two courses is uncorrelated, and lecture exams do not intentionally test understanding of phenomena encountered in the laboratory. The laboratory course is inquiry-based and the experiments have evolved from requiring mostly individual work to teamwork in the last decade. Heterogeneous groups of generally four students are formed by the instructor based on factors such as prior chemistry knowledge, familiarity with computers, gender, age, and location on campus, and all group members receive the same grade for team assignments which discourages competition among students, with team points accounting for ~50% of the final grade. Students receive instruction regarding how to productively work in teams,

such as strategies for conflict resolution, and rotate amongst well-defined roles for each experiment: team manager (keeps group on task, presents the team answers to oral discussion questions), recorder (documents team data, records abstract and outline for answers to oral discussion questions), chemist/safety officer (measures reagents, responsible for proper disposal and monitoring safety of all group members), and technologist (operates instruments, records group data into class data banks). Other major features of this course are that students produce group laboratory reports, give team oral presentations, and the experiments are designed such that students evolve concepts from their observed data. The exams include both multiple-choice questions and computational and conceptual problems that require students to show their work. A single instructor taught the laboratory course over the years of this study, and average class size was ~1,300 students with lecture sections averaging ~400 students and laboratory sections averaging ~20 students.

The third format integrates the lecture and laboratory into one five-credit “studio” course that explicitly aligns all “lecture” and “laboratory” topics. Therefore, unlike the first and second formats, the third format requires concurrent enrollment. With enrollment capped at 96 students per term, this format is also characterized by a small class size yielding more personal attention in comparison to the traditional lecture format. Students attend three 50-minute lectures and five hours of laboratory/discussion time per week. These five hours were fluidly allocated to laboratory or discussion time, so though points were not given for attendance, students were essentially required to attend all five hours each week due to the course design. The studio course is an intimate and creative version of general chemistry that is completely isolated from the lectures and laboratory described above, and enrollment in this format is completely determined by self-selection. The same subject matter is covered in approximately the same order, but both the lecture and laboratory/discussion incorporate more hands-on activities and small group discussions. This course is also project-based, with the major group project (27% of the final grade) culminating in a group paper and poster presentation. The overall grading scheme deemphasizes exam grades (35% of the final grade) in comparison to the first and second lecture formats, and the exams are different from

those administered in the other formats. Points from online homework, class participation, and individual laboratory reports make up the balance of the grades. For the fall terms in 2006 and 2007, this course was taught in a (then) new undergraduate science building with innovative laboratory and "dinner theater" classroom space, whereas all other courses described here have always been held in the chemistry building. Designed to facilitate both small-group collaboration and large-group interaction, the "dinner theater" classroom is tiered with each level containing four to five small tables, each accommodating up to four students. There were two unique instructors for this course over the years of this study, and the average class size was ~60 students.

3.4.2 Data Collection

Data were collected from the Office of the Registrar for the 9,438 students who enrolled in the general chemistry lecture during the fall terms between 2002 and 2007, inclusive. The data consist of various demographics (e.g., gender, ethnicity, age), high school GPA, SAT and ACT scores, mathematics and chemistry placement exam scores, participation in honors programs, degrees earned, and other factors (see Table 3.2 for a breakdown of some student characteristics according to lecture format). We also collected information about any general chemistry laboratory and organic chemistry laboratory and lecture courses in which students had enrolled between Fall 2002 and Spring 2008, including term enrolled, section number, final grade (measured on a 4.0 scale), and the drop date if the student withdrew from the course. Students who withdrew before the "normal" drop/add deadline, which is the end of the third week of class, were not considered in this study as withdrawals occur for a broad range of reasons early on each term. Students' names were not used; rather, they were identified by eight-digit numbers.

3.4.3 Data Analyses

The data were imported into the statistical software package PASW Statistics (version 18.0). Students were partitioned into four clusters according to their

standardized (Z) scores on the university's mathematics and chemistry placement exams by pairwise K-means cluster analysis, a method that attempts to identify the centers of natural, homogeneous clusters in the data; Table 3.3 describes the clusters. There was a significant effect of cluster number on final lecture grade, $F(3, 3815) = 665.63$, $p < 0.05$, $\omega = 0.44$, and the *post hoc* Games-Howell procedure revealed that all clusters are significantly different from one another (Welch's F was used because the homogeneity of variance assumption was broken). Doing the cluster analysis pairwise means that students are assigned a cluster number if they have a mathematics placement exam score, a chemistry placement exam score, or both. Only students who are missing scores for both the placement exams (5.4%) will not be assigned a cluster number. Most students (91%) have valid data for both their mathematics and chemistry placement exam scores. This clustering technique was used because these two variables are positively correlated with each other ($r = 0.34$ [8538], p [two-tailed] < 0.01, representing a medium-sized effect). Using the variables separately in multiple regressions can lead to multicollinearity where the accuracy of individual predictors may be compromised, though the predictive power of the whole model is usually unaffected (Field, 2009; Hutcheson & Sofroniou, 1999). Therefore, the regressions were also performed using the placement exam scores as separate, continuous variables, and we found results similar to those reported here (see Tables 3.S1 – 3.S4 in the appendix). Differences in final lecture grades according to enrollment status (i.e., concurrent vs

Table 3.3: Summary of Student Clusters Based on K-Means Cluster Analysis

Cluster no.	No. of students		Avg. mathematics placement exam score[b]	Avg. chemistry placement exam score[b]	Final grade[c]	
	Total	Retained			*M*	*SD*
0	1681	1551	10.9	13.6	2.29	0.81
1	1743	1712	14.0	20.8	2.77	0.68
2	3848	3811	21.2	17.8	2.99	0.66
3	1657	1650	22.3	27.5	3.36	0.58
-[a]	509	454	-	-	-	-

[a]Students who were missing both placement exam scores were not assigned a cluster number. [b]The mathematics and chemistry placement exams were scored out of 25 and 40, respectively. [c]These statistics do not include withdrawn students.

nonconcurrent) by cluster number are also reported (Table 3.4); these data are consistent with previous work in physics education research that has shown strong, positive correlations between preinstructional measures and normalized learning gains (Coletta, Phillips, & Steinert, 2007; Meltzer, 2002).

It is noted that without having access to placement exam scores from other universities, it is difficult to quantitatively comment as to whether other students would cluster in a similar fashion as students at University of Michigan. The nature of these particular placement exams also complicates comparison to other universities' exams. Here, the chemistry placement exam is designed to generate a normal bell-shaped distribution centered on a mean score of 50% whereas the mathematics placement exam is designed to generate a negatively skewed distribution with a mean score of 70% and, of course, placement exams at other universities may not be designed with such intended outcome distributions. One of the reasons we employed the clustering technique was to generate a handle for thinking about different types of students, broadly speaking. We wanted to have a method for assessing how concurrent enrollment affected the highest-performing versus the lowest-performing students, and suspected that placement exam scores would generally reflect the students' abilities and background well. That being the case, we reasonably expect that students at any university would exhibit a similar distribution as the students in this study, with overall low-, medium-, and high-performers.

Table 3.4: Differences in Final Lecture Grades According to Enrollment Status By Cluster

Cluster	Concurrent			Nonconcurrent			Difference		
no.	*M*	*SD*	*N*	*M*	*SD*	*N*	*M*	*t*	*p*[a]
0	2.42	0.73	888	2.11	0.87	663	0.31	-7.48	< 0.01
1	2.83	0.67	1107	2.66	0.70	605	0.17	-4.83	< 0.01
2	3.05	0.62	2597	2.86	0.71	1214	0.19	-8.03	< 0.01
3	3.37	0.58	1065	3.34	0.57	585	0.03	-0.99	0.32

Note. These statistics do not include withdrawn students. [a]The significance of differences in final grades between concurrent and nonconcurrent students was determined by independent-samples *t*-tests.

Binary logistic and linear regressions were used to evaluate the impact of concurrent enrollment on withdrawal rates and final course grades in the lecture, respectively, at a significance level of 0.05. Because of the major differences in assessments and grading systems between the studio and other lecture formats, we have excluded the studio students from the main analyses and instead report results for these students in a separate section. Although it is nonideal to use *post hoc*, observational data to identify outcomes of an educational experience (due to hindsight bias, e.g.), we also find support for these descriptive and inferential statistical procedures as common and accepted for empirical studies in this discipline (Creswell, 2008; Fayowski & MacMillan, 2008; Goldstein & Perin, 2008; Long, et al., 1986; Shavelson, 1996). Both binary logistic and linear regressions use covariates (independent variables) to predict the value of an outcome variable (dependent variable). Binary logistic regression is used when the outcome variable is dichotomous (e.g., withdrawn or not withdrawn) and linear regression is used when the outcome variable is a scale variable (e.g., final course grades).

Five covariates were used in the regressions: (a) the student's high school GPA, (b) the student's comprehensive SAT score (scores for students who had taken the ACT but not the SAT were converted using a concordance table published by The College Board (Board, 2006)), (c) the student's cluster number, (d) whether or not the student concurrently enrolled in the general chemistry lecture and laboratory, and (e) the product of (c) and (d) which was included in order to elucidate any interaction between them. High school GPA and comprehensive SAT scores were used as covariates because they have been found to be good predictors of freshman college achievement in multiple contexts (Daugherty & Lane, 1999; Fincher, 1974; Wolfe & Johnson, 1995), though they do not have equal predictive power across racial groupings (Sue & Abe, 1988; Ting & Robinson, 1998) and, thus, we treated them independently. The correlations between covariates do not represent large effect sizes, with the exception that the product term (e) is, as expected, highly correlated with (c) cluster number and (d) enrollment status (Table 3.5). Additionally, variance inflation factors for all covariates

Table 3.5: Correlation Coefficients for Covariates Used in Regression Models

	(a) HS GPA	(b) SAT	(c) Cluster	(d) Enrollment	(e) (c)*(d)
(a) HS GPA	1	0.13	0.11	0.10	0.12
(b) SAT	8932	1	0.43	0.08	0.27
(c) Cluster	8666	8919	1	0.07	0.56
(d) Enrollment	8938	9346	8929	1	0.75
(e) (c)*(d)	8666	8919	8929	8929	1

Note. All correlations are significant at the 0.01 level (two-tailed).

are less than 10, implying that multicollinearity due to covariate correlations does not substantially bias the regressions (Field, 2009).

Both types of regressions were performed listwise, which means that in order for students to be included in the analysis, they were required to have valid data for all of the covariates used. Because of this stipulation, 91.6% of all nonstudio students (N = 9,090) were included in the binary logistic regression where withdrawal rate was the outcome variable, and 92.1% of retained nonstudio students (N = 8,834) were included in the linear regression where final grades was the outcome variable. There was no way to determine whether the missing data are completely random with respect to the outcome variables (Little & Rubin, 2002). If a student took the lecture or laboratory more than once, only the first time that they enrolled in the course(s) was analyzed.

Finally, these analyses were based on an observational study and we attempted to design predictive models that would adjust for differences in students, and, in particular, the analytic form of the equations were selected specifically to work for these data. In other words, we sought to disentangle the effect of concurrent enrollment from a student's GPA, SAT, and mathematics and chemistry placement exam scores by using these variables as covariates in our models. Of course, subsequent analyses may reveal other functional forms and other functional variables that may be more effective at describing the already substantial variation in student scores.

3.5 Results

3.5.1 Final Course Grades

The linear regression model revealed a systematic relationship between concurrent enrollment and final course grades. Specifically, concurrent enrollment positively affected students' final grades in the lecture by up to 0.19 grade points (Table 3.6). This linear model predicts that a student who enrolls concurrently in the lecture and laboratory can earn almost one third of a letter grade higher (e.g., B to B+) than a student who takes the lecture first and the laboratory in a later semester or not at all. A simple point-biserial correlation between enrollment status and final grade points reveals $r_{pb} = 0.14$ [8822], p [two-tailed] < 0.01, representing a small-sized effect.

Importantly, the interaction covariate (e) term in this model reveals a differential impact of concurrent enrollment on final grades that is dependent on cluster number. For example, students in cluster three, those with the highest average mathematics and chemistry placement exam scores, benefitted from concurrent enrollment on average by 0.07 grade points. This difference is due to the interaction covariate (e) term in the linear equation (since, in the linear equation, the coefficient B is multiplied by the interaction term for concurrent students in cluster three: 0.07 = 0.19 + (-0.04 * 3)). However, students in cluster zero, those with the lowest average mathematics and chemistry placement exam scores, benefitted from concurrent enrollment on average by 0.19 grade points in their lecture grade (here, in the linear equation, the coefficient B is multiplied by the interaction term for concurrent students in cluster zero: 0.19 = 0.19 + (-0.04 * 0)). In summary, the average increase in final lecture grades for concurrently enrolled students according to cluster number was 0.19 for cluster zero, 0.15 for cluster one, 0.11 for cluster two, and 0.07 for cluster three. This shows that in terms of final grades in the lecture, the lowest-scoring students according to mathematics and chemistry placement exams receive the most benefit from concurrent enrollment.

Although we have controlled for differences in high school GPA, comprehensive SAT scores, and mathematics and chemistry placement exam scores, we may not have accounted for other important measures of student quality. Motivation, for example, has

Table 3.6: Impact of Concurrent Enrollment on Final Grades in the Lecture

Covariates	*B*	*SE B*	*t*	*p*
Constant	-2.43	0.128	-19.0	< 0.01
(a) High school GPA	0.86	0.029	29.4	< 0.01
(b) Comprehensive SAT score	0.00[a]	0.000	18.4	< 0.01
(c) Cluster number	0.27	0.012	22.0	< 0.01
(d) Concurrent or nonconcurrent enrollment	0.19	0.027	6.9	< 0.01
(e) Interaction of (c) and (d)	-0.04	0.015	-2.5	0.01

Note. The proportion of variance (R^2) in final grades accounted for by this linear regression model is 0.32. [a]The coefficient B is positive for this covariate but rounds to zero.

been found to foster science achievement in large, introductory biology courses (Glynn, et al., 2007), and logical thinking skills have positively predicted student performance in physical chemistry courses (Nicoll & Francisco, 2001). These and/or other measures could contribute to the result that concurrent students earn higher final grades in the lecture than nonconcurrent students. Though the analysis works well for these practical measures that are routinely employed, it is important to ascertain the extent to which these results are confounded.

Determining the regression equation for one group of students and applying it to a second group can address this issue of prediction bias (Sue & Abe, 1988). The modeling described here deals with the issue of stronger students potentially self-selecting into concurrent enrollment by isolating the effect that concurrent enrollment has on increasing final lecture grades. First, we selected only concurrently enrolled students and, based on their data, calculated a linear regression model that shows the progression of performance (final lecture grade) as a function of covariates. The covariates used in this model were the student's high school GPA, cumulative SAT score, and cluster number. Then, this model was applied to the nonconcurrent students. This process essentially applies the "treatment" of concurrent enrollment to the nonconcurrent students. After applying the concurrent enrollment "treatment" to the nonconcurrent students, we observed the difference in mean final grades for each of the two groups to be 0.10 units on average (Table 3.7). This implies that the concurrent

Table 3.7: Descriptive Statistics of Linear Regression Models Addressing Uncontrolled Variables

		N	*Min*	*Max*	*Mean*	*SD*
Concurrent	Average final lecture grade	5538	0.00	4.00	2.95[a]	0.72
	Predicted average final lecture grade with nonconcurrent treatment applied	5253	1.11	3.77	2.83[a]	0.40
Nonconcurrent	Average final lecture grade	3284	0.00	4.00	2.73[b]	0.84
	Predicted average final lecture grade with concurrent treatment applied	2887	1.15	3.83	2.85[b]	0.44

[a]The difference between the concurrent students' average final lecture grade and the average grade that the concurrent model predicts for nonconcurrent students is 0.10 (0.10 = 2.95 – 2.85). [b]The difference between the nonconcurrent students' average final lecture grade and the average grade that the nonconcurrent model predicts for concurrent students is 0.10 (0.10 = 2.83 – 2.73).

treatment may not be entirely responsible for the increase in final lecture grades that concurrently enrolled students have. To check the quality of this linear model, we calculated the linear regression model based on nonconcurrent students only and applied it to the concurrent students. Again, this process essentially applies the "treatment" of being nonconcurrently enrolled to the concurrent students. Here, the observed difference in mean scores for each of the two groups is again 0.10 final grade units on average (Table 3.6). That the difference found in this model is similar to the average difference found in the first model is confirmation that the models themselves are reasonable and accurate.

This modeling exercise affirms that the highest-performing students, according to the preinstructional measures used as covariates in the regressions, are not randomly distributed between concurrent and nonconcurrent enrollment. Rather, these students are more often concurrently than nonconcurrently enrolled, perhaps due to self-selection, advising, and/or other reasons. In fact, for an average of 0.10 final grade units out of the 0.19 potential increase in final grade, we cannot deconvolve the contribution of concurrent enrollment and other factors that we have not measured about the students in this data set. Because the magnitude of the mean final grade difference

(0.10) is greater than or very similar to the effect of concurrent enrollment determined for clusters two (0.11) and three (0.07), it is untenable to claim that concurrent enrollment is exclusively responsible for the increase in final grades in these clusters. However, this does not necessarily imply that concurrent enrollment has no positive effect for the two highest clusters. In reality, concurrent enrollment may benefit students in the two highest clusters, but we cannot know this with statistical certainty. Regardless, the significant positive effect of concurrent enrollment for the students in clusters zero and one remains. Furthermore, considering the number of students with "borderline" final grades in clusters zero and one for a representative term of data and that enrollment in general chemistry exceeds 2,000 students annually, we find that the final grades of approximately 400 students (20%) would be positively impacted on an annual basis by concurrent enrollment.

3.5.2 Withdrawal Rates

Concurrent enrollment in general chemistry lecture and laboratory was found to systematically decrease the withdrawal rate from the lecture according to the binary logistic regression model, with concurrent and nonconcurrent students' retention rates being 99% and 95%, respectively (χ^2 (1) = 101.87, $p < 0.001$). Overall, the odds of a concurrent student being retained in the lecture were 2.2 times higher than students who took the lecture and laboratory separately, or those who never took the laboratory at all (Table 3.8). In this regression, the interaction covariate (e) term of cluster and enrollment status was nonsignificant ($p > 0.05$), therefore, there is no significant differential effect of enrollment status according to cluster number. The odds of concurrent students from any cluster being retained in the lecture are 2.2 times higher than nonconcurrent students, according to this model. Practically speaking, increasing the retention rate of nonconcurrent students to 99% translates into approximately 125 more students being retained in the lecture course over the years of this study. It is noted that other features of students reflecting their overall quality were unavailable; therefore, self-selection may bias our estimate of the impact of concurrent enrollment on withdrawal rates.

Table 3.8: Impact of Concurrent Enrollment on Withdrawal Rate from the Lecture

Covariates	*B*	*SE B*	*Exp(B)*	*p*
Constant	-5.41	0.98	0.00	< 0.01
(a) High school GPA	0.94	0.23	2.56	< 0.01
(b) Comprehensive SAT score	0.00[a]	0.00	1.00	< 0.01
(c) Cluster number	0.70	0.12	2.02	< 0.01
(d) Concurrent or nonconcurrent enrollment	0.79	0.21	2.19	< 0.01
(e) Interaction of (c) and (d)	0.19	0.19	1.20	0.32

Note. The proportion of variance (R^2) in withdrawal rate accounted for by this binary logistic regression model is 0.19. [a]The coefficient B is positive for this covariate but rounds to zero.

3.5.3 Lecture Format Designed for Additional Academic Support

Students have the option of enrolling in general chemistry lecture in one of three different formats (delineated in the Study Context section), and one format is designed for students who may benefit from extra academic support. Even though 75% of the students who enrolled in this lecture format are in cluster zero (they have the lowest average placement exam scores), and the difference in average final grade between the students, taking into account all clusters, in the academic support section (M = 2.36, SD = 0.84, SE = 0.04, N = 418) and those not enrolled in this format (M = 2.89, SD = 0.76, SE = 0.01, N = 8404) is significant $t(452) = 12.94$, $p < 0.05$, our analyses indicate that there is no significant difference between the two groups in the amount that concurrent enrollment helps students' final lecture grades. Statistically, students in the lecture format designed for additional academic support are no more likely to be helped by concurrent enrollment than students in the traditional format. The same conclusion holds true when withdrawal rates are the outcome variable.

Also, in performing regression analyses to explore whether enrollment in this lecture format influenced final grades or retention, regardless of concurrent versus nonconcurrent enrollment, we found no significant effect for either metric, indicating that comparable students who enroll in this format and the traditional format would not be predicted to have different final grades or retention outcomes. Together, these results suggest that the traditional lecture and laboratory provides students with a strong

enough academic experience such that the extra resources provided in the academic support section are nonessential.

3.5.4 Studio-Style Course Format

The students who enrolled in the studio-style format of general chemistry were required to register for a single five-credit course, meaning nonconcurrent enrollment was not an option for these students. Enrollment in the studio format was found to have no significant effect on withdrawal rates from the lecture when compared to nonstudio students, whether nonconcurrent students were included in the analyses (χ^2 (1) = 3.48, $p > 0.05$) or not (χ^2 (1) = 0.19, $p > 0.05$).

The studio instructors sought to generate similar final grade distributions as in the traditional and extra support formats, however the studio assessment techniques do differ from the other formats, and the following direct comparisons of final grades across the different formats should, accordingly, be cautiously interpreted. Considering both concurrent and nonconcurrent students, studio students had significantly higher final grades (M = 3.10, SD = 0.65, SE = 0.04, N = 344) than those in the nonstudio lecture courses (M = 2.87, SD = 0.78, SE = 0.01, N = 8,822) t(382) = -6.45, $p < 0.05$. Comparison of the studio students to the group that most closely mimics their experience, the concurrent students in the traditional lecture format (M = 2.97, SD = 0.72, SE = 0.01, N = 5,322), reveals a mean difference of 0.13 grade point units t(5,663) = -3.35, $p < 0.05$. Though this represents a statistically significant positive effect of the studio course on final grade, the uncertainty about how the differing assessments across the formats could impact the statistics as well as the results regarding withdrawals implies that, overall, there is no benefit to enrollment in the studio course over concurrent enrollment in a nonstudio format based on these metrics.

3.5.5 Limitations

Our objective was to analyze the first experience of each student in the lecture and laboratory courses. However, because data were collected between Fall 2002 and Spring 2008, we cannot exclude cases where students enrolled prior to Fall 2002. The

overall number of students in this data set who enrolled more than once in the lecture (65 students or 0.7% overall) or laboratory (38 students or 0.4% overall) is small. Therefore, we reasonably expect that the number of students who are affected by this limitation is minimal, and we do not think the bias is substantial. Similarly, general chemistry lecture data were collected for the fall terms between 2002 and 2007, inclusive, however, any student who enrolled in the lecture more than once could have enrolled during a winter or spring term. In this case, we could have compared outcomes of a student's second enrollment in the lecture with that of other students' first enrollment. One guard against this potential error is that the bulk of general chemistry students regularly enroll in the lecture in the fall term. Average enrollment in the lecture during the fall, winter, and spring terms between Fall 2002 and Spring 2008 was 1,589, 518, and 50 students, respectively; in a given academic year, then, approximately 74% of general chemistry lecture students enroll in the course in the fall. Additionally, this study does not attempt to make comparisons between students who enrolled in the laboratory only and any other group, primarily because the number of students who enroll in the laboratory without ever enrolling in the lecture is very small. Finally, the instructors of the lecture courses were uncontrolled.

3.6 Discussion and Implications

The key findings of this study are that concurrent enrollment in general chemistry lecture and laboratory positively impacts (1) retention in the lecture for all students, and (2) final lecture grades for the students who score lowest on mathematics and chemistry placement exams. Considering that increasing retention of students, especially in science courses, is a consistent challenge in post-secondary education (Committee on Prospering in the Global Economy of the 21st Century, 2007; Peterfreund, Rath, Xenos, & Bayliss, 2007) and that educators fear driving students permanently away from the sciences, these findings provide an important guide to practice at universities that do not require concurrent enrollment in introductory science lectures and laboratories. These findings could, for example, impact students by means of curriculum advisors. Personal communication with a prehealth advisor (P. K. Zitek, September 13, 2009) at University

of Michigan revealed that some advisors encourage students to enroll in lectures and laboratories concurrently if at all possible. Other advisors, however, do not prioritize concurrent enrollment, and students who do not feel comfortable with their science abilities may be disinclined to concurrently enroll. Understanding that empirical data support a significant increase in retention and final lecture grades could certainly impact both advisors' practices and students' choices, and result (2) substantiates a relatively easy and financially viable route for universities to better assist students who may require more academic support.

Decades of research have been published concerning improving student performance, learning, and attitudes in college-level introductory science courses. Topics include utilizing student response systems (Hall, Collier, Thomas, & Hilgers, 2005), requiring writing assignments (Horton, Fronk, & Walton, 1985), individualized, self-paced instruction (Paul, 1983), and lecturing based on student-generated questions (Teixeira-Dias, Pedrosa de Jesus, & Neri de Souza, 2005), among many other categories of innovation. According to the data presented here, student performance is significantly positively affected by enrolling in the lecture and laboratory during the same term. Similarly, increasing student retention has been found to be affected by implementing cognitive task analyses (Feldon, Timmerman, Stowe, & Showman, 2010), supplemental instruction (Peterfreund, et al., 2007), computer-assisted instruction (Wrensford & Wrensford, 2003), and more appropriate placement strategies (Edwards, Roberts, & Pitter, 2010), among other methods. The data presented here, though, support concurrent enrollment as a method for significantly increasing retention in the lecture. In short, unlike previous studies, these data provide evidence that significant increases in both student performance and retention can be brought about by relatively simple actions on the parts of students and the university.

We argue that the reasons for the observed results, though they are coupled with the issue of "time on task", are related to the design of the laboratory course itself, especially because the sequencing of topics in the lecture and laboratory are unrelated. "Time on task" is truly an important factor in achieving learning gains, but student's problem-solving strategies have been shown to stabilize after a small number of related

problems (Stevens, Soller, Cooper, & Sprang, 2004). Cooper (2008) has also shown that when students problem-solve as a group, they are able to arrive at efficient strategies more quickly than when working individually. Therefore, the design of the learning environment in the laboratory must be considered when interpreting these results. The laboratory course exemplifies some of the principles that purportedly support effective learning environments as outlined in the National Research Council studies *How People Learn: Brain, Mind, Experience, and School* (1999) and *How Students Learn: Science in the Classroom* (2005), that is, the laboratory is knowledge- and community-centered. Specifically, the course is comprised of guided inquiry experiments in which students are not presumed to know the expected results prior to collecting and analyzing their data, and prelabs are not intended to give away the outcomes (Minner, Levy, & Century, 2010; Wilson, Taylor, Kowalski, & Carlson, 2010). Students' resultant confusion facilitates development of their scientific reasoning skills and addresses the ambiguity of the scientific process (Kerner & Penner-Hahn, 2010). Students are encouraged in exploration, organization, and application in each experiment, with the overall goal of deriving concepts and principles from authentic, empirical data and, interestingly, students have access to a bank of many years of prior students' data to aid in pattern discernment. The cumulative curricular design also promotes more cohesive knowledge than a disconnected, traditional curriculum. Finally, this course challenges students with several forms of assessment, very few of which are multiple-choice.

Though the design principles described above contribute to the excellent quality of the laboratory course, we conjecture that the heavy emphasis on collaborative work in the laboratory is the most important causal element related to the outcomes described here. The laboratory is community-centered as the majority of the coursework is done in teams, and productive management of the differences among group members encourages positive learning outcomes (Heller & Hollabaugh, 1992). Team-learning environments have been repeatedly found to be superior to individualized problem solving in terms of student learning, development of interpersonal skills, and promoting student enjoyment of a course (Johnson & Johnson, 1989; Totten, 1991),

perhaps cultivating student interest in learning science. In college-level chemistry courses, many studies have lauded various benefits of collaborative work (Bowen, 2000; Cooper, 1994, 1995; Cooper, et al., 2008; Cooper & Kerns, 2006; Tien, et al., 2002). The collaborative aspects of the specific laboratory studied here are numerous. Most notably, the team lab reports encourage students to come to consensus on all aspects of performing the experiments, and the team discussion presentations require that students confer about the implications of an experiment, including resolving differences of opinion within the group and explaining to the whole class how they did so. Additionally, in the beginning of the term, teams spend time identifying the strengths and previous experiences of their group members with the goal of recognizing skills they may be lacking as a group, and each team member evaluates the contributions of other members to the experiments, team reports, discussion presentations, and team as a whole throughout the semester.

The metacognitive and peer interaction (including argumentation) features of collaborative work may constitute the mechanism that yields the observed results both here and in other studies that explore group work as an intervention. Students engage in metacognitive practices when they must explain their thinking to another group member, and in this laboratory, there are multiple contexts in which students share their ideas with one another, which has been shown to enhance learning by leading to cognitive development (Council, 1999, 2006); these contexts include performing the experiment, writing the team report, and giving oral presentations as a group to the whole class. Sharing and constructing ideas with another student, as well as listening to a student explain something to himself, are metacognitive and peer interaction methods that have been proposed to lead to learning gains (Hausmann, Chi, & Roy, 2004). White and Frederiksen (1998) have also shown that metacognitive activities can specifically help lower-achieving students, which may explain the observed disproportionate effect of concurrent enrollment on final grades that depends on students' placement exam scores. The collaborative design of the laboratory facilitates these metacognitive and peer interaction processes that may lead to the described benefits for concurrently enrolled students.

Despite the large laboratory and lecture courses not being explicitly linked in format or content (other than that they are both general chemistry courses), concurrent enrollment positively impacts student performance and retention in the lecture. These results beg the question as to what outcomes might be observed if the laboratory and lecture were explicitly aligned and taught synergistically, especially in light of studies that have reported advantages of integrated course structures (Bailey, Kingsbury, Kulinowski, Paradis, & Schoonover, 2000; Oliver-Hoyo, et al., 2004). Recall that in the studio-style course, the laboratory and lecture were integrated and aligned in a five-credit course, yet our results indicated no practical benefit in terms of final grades or withdrawal rates over concurrent enrollment in a nonstudio format. This may seem confusing in light of the number of universities that have reported benefits of studio-style courses, but the findings are understandable considering that many pedagogical methods that render studio courses beneficial to students are already present in the laboratory course studied here. It is also possible that the particular metrics employed in this study are not sensitive enough to differentiate between the two student populations given the differences in how studio students were evaluated. In summary, though content alignment is a useful technique, our data indicate that educational benefits can be achieved in unaligned courses as well.

Our survey of large, public universities (Table 3.1) demonstrates that a substantial portion are not requiring concurrent enrollment in introductory-level science lectures and laboratories. The data presented herein indicate that requiring concurrent enrollment may be a viable path for improving student performance and retention in the lecture, and, considering the sheer magnitude of undergraduates who take these introductory science courses, the number of students who could be affected is substantial. Though we focused our attention here on large, public universities, there is potential for similar results to be found at any college or university that does not require concurrent enrollment, regardless of size. Additionally, these results could be extremely influential at the high school level. Consider the potential implications on graduation rates and the scientific pipeline of more students being retained in high school science classes!

Similar results may be found in higher-level courses such as organic chemistry, as well as in disciplines such as physics and biology in which it is evidently fairly common for lectures and laboratories to be offered separately. Comparable effects may also exist across disciplines. For example, based on previous research that has established college math scores as a predictor of good general chemistry scores(Angel & LaLonde, 1998), does a student who enrolls in college algebra and general chemistry do better with regard to some outcome than a comparable student who enrolls in general chemistry but not algebra? The link between general physics and calculus would also be interesting to explore. As is, the results presented here may have impact at the course-level, but similar findings in other disciplines could generate significant impact in pedagogical practice at the college- and university-level; these levels of application are oftentimes neglected in Scholarship of Teaching and Learning research (McKinney, 2007).

Because of the high cost of science laboratories, there is an ever-present need to justify their value, and this is especially true in the face of budget restraints. This research, in summary, supports the laboratory as a valuable method for achieving learning gains and increasing retention in the lecture. The collaborative design of the laboratory provides an important element of practice for metacognitive development and peer interaction, and we surmise that this collaborative nature of the laboratory is the most important feature related to the observed results. We anticipate that this work will be of interest to a broad range of teachers, professors, and educational researchers, especially those involved in course design, as this study is realistically applicable to any discipline that offers a course with separate lecture and laboratory components.

3.7 Conclusions and Future Work

The main findings from this research are that enrolling in an introductory laboratory concurrently with the corresponding lecture course enhances learning gains and retention in comparison to students who enroll in the lecture alone. Specifically, we found that concurrent enrollment in the lecture and laboratory positively impacts (1) the odds of retention in the lecture by 2.2 times on average and (2) final lecture grades by

up to 0.19 grade points on a 4.0 scale for the lowest-scoring students according to university-level mathematics and chemistry placement exam scores. These data provide important results for consideration by curriculum advisors and course planners at universities that do not require concurrent enrollment in general chemistry as well as other science courses. In the face of current budget cuts that threaten to shorten or eliminate laboratory experiences altogether at multiple educational levels, this study demonstrates the value of laboratories in promoting science learning and retention.

Further research in this area is needed as to the particular reasons why the laboratory benefits students' final grades in and withdrawal rates from the lecture. Towards this end, side-by-side courses could be implemented in which one course utilizes more collaborative group work than the other, or another variable of interest could be varied. Additionally, the rationale(s) behind the choice that students make to nonconcurrently enroll should be investigated, as we fully expect that the reasons why students nonconcurrently enroll are nonuniform. This research would provide a basis for understanding whether or not it is practical to encourage all students to concurrently enroll in general chemistry lecture and laboratory, at least in the specific University of Michigan context. Finally, as of now, the majority of students in the cohort studied here have graduated. It would be beneficial to understand whether or not the student's lecture and laboratory grades have any correlation with graduation rates and, more specifically, persistence in a science major.

In order to bring about lasting improvement in STEM education at the national level, change must come from both the top down, as in program funding from federal agencies provided by Congress, and the bottom up, as in reshaping teaching and learning practices across the educational spectrum. This study describes a "bottom up" improvement that may be effective in promoting science learning and retention. Should the efficacy of this practice be verified in other educational contexts, it might soon be the case that concurrent enrollment in introductory science laboratories and lectures will be required and beneficial for student learning.

3.8 Notes

This research was not subject to ongoing Institutional Review Board review per exemption #1 of the Title 45 Code of Federal Regulations, Section 46.101b.

3.9 References

Angel, S. A., & LaLonde, D. E. (1998). Science Success Strategies: An Interdisciplinary Course for Improving Science and Mathematics Education. *Journal of Chemical Education, 75*(11), 1437-1441.

Association of American Universities. (2011). *Five-Year Initiative for Improving Undergraduate STEM Education*. Retrieved from http://www.aau.edu/policy/article.aspx?id=12588.

Bailey, C., Kingsbury, K., Kulinowski, K., Paradis, J., & Schoonover, R. (2000). An integrated lecture-laboratory environment for general chemistry. *Journal of Chemical Education, 77*(2), 195-199.

Baker, N., & Verran, J. (2004). The future of microbiology laboratory classes - wet, dry or in combination? *Nature Reviews Microbiology, 2*(4), 338-342.

Banilower, E. R., Green, S., & Smith, P. S. (2004). *Analysis of data of the 2000 National Survey of Science and Mathematics Education for the Committee on High School Science Laboratories (September)*. Chapel Hill, NC: Horizon Research.

Ben-Zvi, R., Hofstein, A., Samuel, D., & Kempa, R. F. (1976). The attitude of high school students towards the use of filmed experiments. *Journal of Chemical Education, 53*(9), 575-577.

Board, T. C. (2006). *SAT-ACT concordance tables. Retrieved from* http://professionals.collegeboard.com/data-reports-research/sat/sat-act.

Bowen, C. W. (2000). A quantitative literature review of cooperative learning effects on high school and college chemistry achievement. *Journal of Chemical Education, 77*(1), 116-119.

Bransford, J. D., & Schwartz, D. L. (1999). Rethinking transfer: A simple proposal with multiple implications. In A. Iran-Nejad & P. D. Pearson (Eds.), *Review of research in education, no. 24* (pp. 61-100). Washington, D.C.: American Educational Research Association.

Bybee, R. W. (1970). The effectiveness of an individualized approach to a general education earth science laboratory. *Science Education, 54*(2), 157-161.

Carnduff, J., & Reid, N. (2003). *Enhancing undergraduate chemistry laboratories — pre-laboratory and post-laboratory exercises*. London, England: Royal Society of Chemistry.

Cavagnetto, A. R. (2010). Argument to foster scientific literacy: A review of argument interventions in K-12 science contexts. *Review of Educational Research, 80*(3), 336-371.

Cawley, J. J. (1992). Lecture or laboratory: Choosing between two "goods". *Journal of Chemical Education, 69*(8), 642.

Chin, C., & Osborne, J. (2010). Students' questions and discursive interaction: Their impact on argumentation during collaborative group discussions in science. *Journal of Research in Science Teaching, 47*(7), 883-908.

Coletta, V. P., Phillips, J. A., & Steinert, J. J. (2007). Interpreting force concept inventory scores: Normalized gain and SAT scores. *Physical Review Special Topics - Physics Education Research, 3*(1), 010106.

Committee on Prospering in the Global Economy of the 21st Century. (2007). *Rising above the gathering storm: Energizing and employing America for a brighter economic future*. Washington, D.C.: The National Academies Press.

Committee on Prospering in the Global Economy of the 21st Century. (2010). *Rising above the gathering storm, revisited: Rapidly approaching category 5*. Washington, D.C.: The National Academies Press.

Cooper, M. M. (1994). Cooperative chemistry laboratories. *Journal of Chemical Education, 71*(4), 307.

Cooper, M. M. (1995). Cooperative learning: An approach for large enrollment courses. *Journal of Chemical Education, 72*(2), 162-164.

Cooper, M. M., Cox, C. T., Nammouz, M., Case, E., & Stevens, R. (2008). An assessment of the effect of collaborative groups on students' problem-solving strategies and abilities. *Journal of Chemical Education, 85*(6), 866-872.

Cooper, M. M., & Kerns, T. S. (2006). Changing the laboratory: Effects of a laboratory course on students' attitudes and perceptions. *Journal of Chemical Education, 83*(9), 1356-1361.

Council, N. R. (1996). *National science education standards*. National Committee on Science Education Standards and Assessment. Center for Science, Mathematics, and Engineering Education. Washington, D.C.: National Academy Press.

Council, N. R. (1999). *How people learn: Brain, mind, experience, and school*. Committee on Developments in the Science of Learning, J. D. Bransford, A. L. Brown, and R. R. Cocking (Eds.). Washington, D.C.: National Academy Press.

Council, N. R. (2005). *How students learn: Science in the classroom*. Committee on How People Learn: A Targeted Report for Teachers, M. S. Donovan, and J. D. Bransford (Eds.). Washington, D.C.: The National Academies Press.

Council, N. R. (2006). *America's lab report: Investigations in high school science*. Committee on High School Science Laboratories: Role and Vision, S. R. Singer, M. L. Hilton, and H. A. Schweingruber (Eds.). Washington, D.C.: The National Academies Press.

Creswell, J. W. (2008). Analyzing and interpreting quantitative data *Educational research: Planning, conducting, and evaluating quantitative and qualitative research* (3rd ed.). Upper Saddle River, NJ: Pearson Education.

Daugherty, T. K., & Lane, E. J. (1999). A longitudinal study of academic and social predictors of college attrition. *Social Behavior and Personality: An International Journal, 27*(4), 355-361.

DiBiase, W. J., & Wagner, E. P. (2002). Aligning general chemistry laboratory with lecture at a large university. *School Science and Mathematics, 102*(4), 158-171.

Driver, R., Leach, J., Millar, R., & Scott, P. (1996). *Young people's images of science*. Buckingham, England: Open University Press.

Driver, R., Newton, P., & Osborne, J. (2000). Establishing the norms of scientific argumentation in classrooms. *Science Education, 84*(3), 287-312.

Dubravcic, M. F. (1979). Practical alternatives to laboratory in a basic chemistry course. *Journal of Chemical Education, 56*(4), 235-237.

Education, U. S. D. o. (2011). *Digest of education statistics, 2010 (NCES 2011-015), Chapter 3, Tables 199 and 235. Retrieved from* http://nces.ed.gov/programs/digest/d10/ch_3.asp.

Edwards, J., Roberts, S., & Pitter, G. (2010). *A formula for success in general chemistry: Increasing student performance in a barrier course.* Paper presented at the National Symposium on Student Retention, Mobile, AL.

Fayowski, V., & MacMillan, P. D. (2008). An evaluation of the supplemental instruction programme in a first year calculus course. *International Journal of Mathematical Education in Science and Technology, 39*(7), 843-855.

Feldon, D. F., Timmerman, B. C., Stowe, K. A., & Showman, R. (2010). Translating expertise into effective instruction: The impacts of cognitive task analysis (CTA) on lab report quality and student retention in the biological sciences. *Journal of Research in Science Teaching, 47*(10), 1165-1185.

Field, A. P. (2009). *Discovering statistics using SPSS: (and sex, drugs and rock 'n' roll)*. London, England: Sage.

Fincher, C. (1974). Is the SAT worth its salt? An evaluation of the use of the Scholastic Aptitude Test in the university system of Georgia over a thirteen-year period. *Review of Educational Research, 44*(3), 293-305.

Glynn, S. M., Taasoobshirazi, G., & Brickman, P. (2007). Nonscience majors learning science: A theoretical model of motivation. *Journal of Research in Science Teaching, 44*(8), 1088-1107.

Goldstein, M. T., & Perin, D. (2008). Predicting performance in a community college content-area course from academic skill level. *Community College Review, 36*(2), 89-115.

Hall, R. H., Collier, H. L., Thomas, M. L., & Hilgers, M. G. (2005). *A student response system for increasing engagement, motivation, and learning in high enrollment lectures.* Paper presented at the Americas Conference on Information Systems, Omaha, NE.

Hausmann, R. G. M., Chi, M. T. H., & Roy, M. (2004). *Learning from collaborative problem solving: An analysis of three hypothesized mechanisms.* Paper presented at the Proceedings of the 26th Annual Cognitive Science Society, Chicago, IL.

Heller, P., & Hollabaugh, M. (1992). Teaching problem solving through cooperative grouping. Part 2: Designing problems and structuring groups. *American Journal of Physics, 60*(7), 637-644.

Hill, B. W. (1976). Using college chemistry to influence creativity. *Journal of Research in Science Teaching, 13*(1), 71-77.

Hoellwarth, C., Moelter, M. J., & Knight, R. D. (2005). A direct comparison of conceptual learning and problem solving ability in traditional and studio style classrooms. *American Journal of Physics, 73*(5), 459-462.

Hofstein, A., & Lunetta, V. N. (1982). The role of the laboratory in science teaching: Neglected aspects of research. *Review of Educational Research, 52*(2), 201-217.

Hofstein, A., & Lunetta, V. N. (2004). The laboratory in science education: Foundations for the twenty-first century. *Science Education, 88*(1), 28-54.

Hogan, K. (1999). Thinking aloud together: A test of an intervention to foster students' collaborative scientific reasoning. *Journal of Research in Science Teaching, 36*(10), 1085-1109.

Horton, P. B., Fronk, R. H., & Walton, R. W. (1985). The effect of writing assignments on achievement in college general chemistry. *Journal of Research in Science Teaching, 22*(6), 535-541.

Hutcheson, G., & Sofroniou, N. (1999). *The multivariate social scientist: introductory statistics using generalized linear models*. London, England: Sage.

Johnson, D. W., & Johnson, R. T. (1989). *Cooperation and competition: Theory and research*. Edina, MN: Interaction Book.

Kerner, N. K., & Penner-Hahn, J. E. (2010). *Collaborative investigations in general chemistry*. Plymouth, MI: Hayden-McNeil Publishing.

Lederman, N. G. (1992). Students' and teachers' conceptions of the nature of science: A review of the research. *Journal of Research in Science Teaching, 29*(4), 331-359.

Little, R. J. A., & Rubin, D. B. (2002). *Statistical analysis with missing data* (2nd ed.). Hoboken, NJ: Wiley-Interscience.

Long, D. D., McLaughlin, G. W., & Bloom, A. M. (1986). The influence of physics laboratories on student performance in a lecture course. *American Journal of Physics, 54*(2), 122-125.

Lumpe, A. T., & Staver, J. R. (1995). Peer collaboration and concept development: Learning about photosynthesis. *Journal of Research in Science Teaching, 32*(1), 71-98.

Maltese, A. V., & Tai, R. H. (2011). Pipeline persistence: Examining the association of educational experiences with earned degrees in STEM among U.S. students. *Science Education, 95*(5), 877-907.

Marshall, J. A., & Dorward, J. T. (2000). Inquiry experiences as a lecture supplement for preservice elementary teachers and general education students. *American Journal of Physics, 68*(S1), S27-S36.

Martens, E. (2007). Communicating science to the first degree. *ACS Chemical Biology, 2*(8), 501-503.

McKinney, K. (2007). *Enhancing learning through the scholarship of teaching and learning: The challenges and joys of juggling*. Bolton, MA: Anker Publishing.

Meltzer, D. E. (2002). The relationship between mathematics preparation and conceptual learning gains in physics: A possible "hidden variable" in diagnostic pretest scores. *American Journal of Physics, 70*(12), 1259-1268.

Millar, R. (2004). The role of practical work in the teaching and learning of science. Paper prepared for the Committee on High School Science Laboratories: Role and Vision. Available at: http://www7.nationalacademies.org/bose/millar_draftpaper_jun_04.pdf [accessed August 2010].

Minner, D. D., Levy, A. J., & Century, J. (2010). Inquiry-based science instruction—what is it and does it matter? Results from a research synthesis years 1984 to 2002. *Journal of Research in Science Teaching, 47*(4), 474-496.

Nicoll, G., & Francisco, J. S. (2001). An investigation of the factors influencing student performance in physical chemistry. *Journal of Chemical Education, 78*(1), 99-102.

Oliver-Hoyo, M. T., Allen, D., Hunt, W. F., Hutson, J., & Pitts, A. (2004). Effects of an active learning environment: Teaching innovations at a research I institution. *Journal of Chemical Education, 81*(3), 441-448.

Pascarella, E. T., & Terenzini, P. T. (2005). *How college affects students: A third decade of research*. San Francisco, CA: Jossey-Bass.

Paul, A. E. (1983). The comparative effects of teacher-demonstration and self-paced instruction on concept acquisition and problem-solving skills of college level chemistry students. *Journal of Research in Science Teaching, 20*(8), 795-801.

Peterfreund, A. R., Rath, K. A., Xenos, S. P., & Bayliss, F. (2007). The impact of supplemental instruction on students in STEM courses: Results from San Francisco State University. *Journal of College Student Retention, 9*(4), 487-503.

President's Council of Advisors on Science and Technology. (2012). *Engage to Excel: Producing One Million Additional College Graduates With Degrees in Science, Technology, Engineering, and Mathematics*. Retrieved from http://www.whitehouse.gov/sites/default/files/microsites/ostp/pcast-engage-to-excel-final_2-25-12.pdf.

Raghubir, K. P. (1979). Research reports: The laboratory-investigative approach to science instruction. *Journal of Research in Science Teaching, 16*(1), 13-17.

Renner, J. W., & Fix, W. T. (1979). Chemistry and the experiment in the secondary schools. *Journal of Chemical Education, 56*(11), 737-740.

Richmond, G., & Striley, J. (1996). Making meaning in classrooms: Social processes in small-group discourse and scientific knowledge building. *Journal of Research in Science Teaching, 33*(8), 839-858.

Saunders, W. L., & Dickinson, D. H. (1979). A comparison of community college students' achievement and attitude changes in a lecture-only and lecture-laboratory approach to general education biological science courses. *Journal of Research in Science Teaching, 16*(5), 459-464.

Seymour, E., & Hewitt, N. M. (1997). *Talking about leaving: Why undergraduates leave the sciences*. Boulder, CO: Westview Press.

Shavelson, R. J. (1996). Linear regression. In S. W. Wakely (Ed.), *Statistical reasoning for the behavioral sciences* (3rd ed.). Needham Heights, MA: Allyn & Bacon.

Springer, L., Stanne, M. E., & Donovan, S. S. (1999). Effects of small-group learning on undergraduates in science, mathematics, engineering, and technology: A meta-analysis. *Review of Educational Research, 69*(1), 21-51.

Stevens, R., Soller, A., Cooper, M. M., & Sprang, M. (2004). *Modeling the development of problem-solving skills in chemistry with a web-based tutor.* Paper presented at the Seventh International Conference Proceedings, Intelligent Tutoring Systems, Maceió, Alagoas, Brasil.

Strenta, A. C., Elliott, R., Adair, R., Matier, M., & Scott, J. (1994). Choosing and leaving science in highly selective institutions. *Research in Higher Education, 35*(5), 513-547.

Sue, S., & Abe, J. (1988). *Predictors of academic achievement among asian american and white students (College Board Report No. 88-11). Retrieved from The College Board website:* http://professionals.collegeboard.com/profdownload/pdf/RR 88-11.pdf.

Teixeira-Dias, J. J. C., Pedrosa de Jesus, H., & Neri de Souza, F. (2005). Teaching for quality learning in chemistry. *International Journal of Science Education, 27*(9), 1123-1137.

Tien, L. T., Roth, V., & Kampmeier, J. A. (2002). Implementation of a peer-led team learning instructional approach in an undergraduate organic chemistry course. *Journal of Research in Science Teaching, 39*(7), 606-632.

Ting, S.-M. R., & Robinson, T. L. (1998). First-year academic success: A prediction combining cognitive and psychosocial variables for caucasian and african american students. *Journal of College Student Development, 39*(6), 599-610.

Totten, S. (1991). *Cooperative learning: A guide to research*. New York, NY: Garland Publishing.

Walvoord, B. E. (2004). *Assessment clear and simple: A practical guide for institutions, departments, and general education*. San Francisco, CA: Jossey-Bass.

Washam, C. (2007). Where's the lab?: American students miss out on hands-on science. *Chemistry*.

Wheatley, J. H. (1975). Evaluating cognitive learnings in the college science laboratory. *Journal of Research in Science Teaching, 12*(2), 101-109.

White, B. Y., & Frederiksen, J. R. (1998). Inquiry, modeling, and metacognition: Making science accessible to all students. *Cognition and Instruction, 16*(1), 3-118.

Wilson, C. D., Taylor, J. A., Kowalski, S. M., & Carlson, J. (2010). The relative effects and equity of inquiry-based and commonplace science teaching on students' knowledge, reasoning, and argumentation. *Journal of Research in Science Teaching, 47*(3), 276-301.

Wojcik, J. F. (1990). Chemistry service courses: Dispense with the lab? *Journal of Chemical Education, 67*(7), 587-588.

Wolfe, R. N., & Johnson, S. D. (1995). Personality as a predictor of college performance. *Educational and Psychological Measurement, 55*(2), 177-185.

Wrensford, G., & Wrensford, L. (2003). Enhanced student learning of chemistry in a computer assisted environment. *Reaching Through Teaching, 15*, 32-42.

Zimmerman, C. (2000). The development of scientific reasoning skills. *Developmental Review, 20*, 99-149.

3.10 Appendix

Table 3.S1: Impact of Concurrent Enrollment on Final Grades in the Lecture with Placement Exams as Separate Variables

Covariates	*B*	*SE B*	*t*	*p*
Constant	-2.73	0.128	-21.3	< 0.01
(a) High school GPA	0.82	0.029	27.9	< 0.01
(b) Comprehensive SAT score	0.00[a]	0.000	12.2	< 0.01
(c) Chemistry placement exam	0.03	0.002	15.1	< 0.01
(d) Mathematics placement exam	0.04	0.002	26.2	< 0.01
(e) Concurrent or nonconcurrent enrollment	0.25	0.053	4.7	< 0.01
(f) Interaction of (c) and (e)	-0.01	0.003	-2.5	0.01

Note. The chemistry and mathematics placement exam scores are treated as continuous variables. The proportion of variance (R^2) in final grades accounted for by this linear regression model is 0.35. [a]The coefficient B is positive for this covariate but rounds to zero.

Table 3.S2: Average Increase in Final Grade For Concurrently Enrolled Students According to Chemistry Placement Exam Score

Chemistry placement exam score	Δ Grade units
0 to 10	0.22
11 to 20	0.14
21 to 30	0.08
31 to 40	0.01

Note. These data are based on the model in Table 3.S1.

Table 3.S3: Descriptive Statistics of Linear Regression Models Addressing Uncontrolled Variables with Placement Exams as Separate Variables

		N	*Min*	*Max*	*Mean*	*SD*
Concurrent	Average final lecture grade	5538	0.00	4.00	2.95[a]	0.72
	Predicted average final lecture grade with nonconcurrent treatment applied	5061	1.09	4.08	2.85[a]	0.42
Nonconcurrent	Average final lecture grade	3284	0.00	4.00	2.73[b]	0.84
	Predicted average final lecture grade with concurrent treatment applied	2754	1.10	4.11	2.85[b]	0.46

Note. These data are based on the model in Table 3.S1. [a]The difference between the concurrent students' average final lecture grade and the average grade that the concurrent model predicts for nonconcurrent students is 0.10 (0.10 = 2.95 – 2.85). [b]The difference between the nonconcurrent students' average final lecture grade and the average grade that the nonconcurrent model predicts for concurrent students is 0.12 (0.12 = 2.85 – 2.73).

Table 3.S4: Impact of Concurrent Enrollment on Withdrawal Rate from the Lecture with Placement Exams as Separate Variables

Covariates	*B*	*SE B*	*Exp(B)*	*p*
Constant	-6.34	1.03	0.00	< 0.01
(a) High school GPA	0.90	0.26	2.46	< 0.01
(b) Comprehensive SAT score	0.00[a]	0.00	1.00	< 0.01
(c) Chemistry placement exam	0.10	0.02	1.10	< 0.01
(d) Mathematics placement exam	0.12	0.02	1.13	< 0.01
(e) Concurrent or nonconcurrent enrollment	0.77	0.18	2.15	< 0.01

Note. The chemistry and mathematics placement exam scores are treated as continuous variables. The proportion of variance (R^2) in withdrawal rate accounted for by this binary logistic regression model is 0.21. [a]The coefficient B is positive for this covariate but rounds to zero.